MECHANISMS AND KINETICS OF MICROTUBULE PERTURBING AGENTS

by

Brianne S. Raccor

B.S., Indiana University of Pennsylvania, 2001

Submitted to the Graduate Faculty of

Arts and Sciences in partial fulfillment

of the requirements for the degree of

Doctor of Philosophy in Chemistry

University of Pittsburgh

2008

UNIVERSITY OF PITTSBURGH

SCHOOL OF ARTS AND SCIENCES

This dissertation was presented

by

Brianne S. Raccor

It was defended on

September 17, 2008

and approved by

Scott G. Nelson, Associate Professor, Department of Chemistry

Samuel M. Poloyac, Associate Professor, Department of Pharmaceutical Sciences

Stephen G. Weber, Professor, Department of Chemistry

Dissertation Advisor: Billy W. Day, Professor, Department of Chemistry and Department of Pharmaceutical Sciences

Copyright © by Brianne S. Raccor

2008

MECHANISMS AND KINETICS OF MICROTUBULE PERTURBING AGENTS

Brianne S. Raccor, PhD

University of Pittsburgh, 2008

Microtubules are cellular cytoskeletal components that play an integral part in many cell functions. Compounds that bind to microtubules and alter their dynamics are highly sought as a result of the clinical success of paclitaxel and docetaxel. A series of analogues of the microtubule stabilizing dictyostatin were examined to probe biological and biochemical structure-activity relationships. The results were consistent with previous reports showing that 16-normethyldictyostatin and 15*Z*,16-normethyldictyostatin lose potency in pacitaxel-resistant cell lines that have a Phe270-to-Val mutation in the taxoid binding site of β-tubulin. 6-*epi*-Dictyostatin and 7-*epi*-dictyostatin were potent analogues of dictyostatin, and 6-*epi*-dictyostatin was chosen for milligram scale for pre-clinical studies.

The thalidomide analogue 5HPP-33 was identified as an easily synthesized small microtubule perturbing agent, and experiments with isolated tubulin were performed to determine its mechanism of action. Tubulin polymerization was used to determine the effect of 5HPP-33 on normal microtubule formation. In experiments utilizing microtubule associated proteins (MAPs) to induce polymer formation, 5HPP-33 inhibited tubulin polymerization, but under a different set of conditions appeared to form and stabilize microtubules. The polymer was imaged using electron microscopy, which showed that 5HPP-33 caused the formation of spirals and rings. Due to 5HPP-33 failing to compete with known radiolabeled microtubule perturbing agents for their respective binding sites, a tritiated version of 5HPP-33 was synthesized. The

binding experiments performed showed that [^{3}H]5HPP-33 had a slight affinity for isolated MAPs, and this was the reason for the discrepancy between the tubulin polymerization experiments. A binding site for 5HPP-33 could not be determined, making it a possible novel microtubule perturbing agent.

(–)-Pironetin is a microtubule inhibitor that appears to form a covalent linkage to the tubulin heterodimer. Although immunoflourescent images showed (–)-pironetin to work in the same manner as vinblastine, cellular and biochemical experiments proved that (–)-pironetin is mechanistically different from vinblastine.

The tubulysins are known microtubule destabilizers and bind to the vinca domain on β-tubulin. Three analogues of the tubulysins were synthesized and their effects on cell growth and microtubule perturbation experiments were determined. WZY-111-63C (N^{14}-desacetoxytubulysin H) was found to be 50 times more cytotoxic than paclitaxel and vincristine.

TABLE OF CONTENTS

LIST OF TABLES

LIST OF FIGURES

LIST OF SCHEMES

ABBREVIATIONS

ATP	Adenosine 5'-Triphosphate
BSA	Bovine Serum Albumin
ddGTP	2',3'-Dideoxyguanosine-5'-Triphosphate
DEAE	Diethylaminoethyl
DMSO	Dimethyl Sulfoxide
DTT	Dithiothreitol
EDTA	Ethylenediaminetetraacetic Acid
EGTA	Ethyleneglycoltetraacectic Acid
FITC	Fluorescein Isothiocyanate
GFA	Genetic Function Approximation
GTP	Guanosine 5'-Triphosphate
HF	Heat of Formation
MAPs	Microtubule Associated Proteins
MDEC	Minimum Detectable Effective Concentration
MES	*N*-Morpholino Ethane Sulfonate
MR	Molar Refractivity
MSG	Monosodium Glutamate
MTS	3-(4,5-dimethylthiazol-2-yl)-5-(3-carboxy-methoxyphenyl)-2-(4-sulfophenyl)-2*H*-tetrazolium
PBS	Phosphate Buffered Saline
QSAR	Quantitative Structure Activity Relationships
SAR	Structure Activity Relationships
Tris	Tris(hydroxymethyl)aminoethane

PREFACE

I have been incredibly lucky that there have been so many people in my life that have provided me with emotional and intellectual support. First, I would like to thank my advisor Dr. Billy Day for the support and guidance he has provided me with over the years. I have learned much about the fields of medicinal and biological chemistry through his mentorship. I would like to thank my committee members Dr. Steve Weber, Dr. Scott Nelson, and Dr. Sam Poloyac for serving on my committee and helping me to grow as a graduate student.

I would like to Dr. Galina Kirilova for allowing me to work in her lab and providing helpful advice. I would also like to thank Kathleen Hartle for supplying an enjoyable working atmosphere and teaching me experimental techniques. I would like to thank Dr. Sam Poloyac for allowing me to purify my radiolabeled compound in his lab and his helpful discussions. I would also like to thank the Poloyac group for their tips on carrying out my HPLC purification.

The members of Dr. Day's lab have proved invaluable sources for moral and intellectual support. I have learned so much from every member in the group, and I cannot count how many times that they have provided me with important feedback and new ideas. I would like thank all Day lab members both past and present: Drs. Charitha Madiraju, Guangyu Zhu, Raghavan Balachandran, Jelena Janjic, Yun Fan, and Zhe Zhang (Jenny), and Miranda Sarachine, Hikmat Daghestani, Yuanyuan Duan and Yumin Song.

My research projects have been a highly collaborative effort and many people have been involved in the projects on which I have worked. I would like to thank Prof. Dennis Curran and all of the chemists that have worked on the synthesis of dicytostatin and all of the analogues. I would like to thank Prof. Andreas Vogt for his important contributions without which my publication in *Molecular Pharmacology* would not have been possible. He has also provided his vast scientific knowledge to many helpful discussions. I would like to thank Dr. Pui-Kai Li at The Ohio State University for providing the 5HPP-33 project and giving me the chance to work on it. In addition, I would also like to thank the chemists for that worked on the pironetin and tubulysin projects, and Profs. Nelson and Wipf. I would be remiss if I did not thank Dr. Ernest Hamel at the NIH for not only allowing me to work in his lab, but the invaluable scientific information he has provided me with over the years. There is not a time in my graduate career where Dr. Hamel did not provide me with extremely helpful advice when I asked for it.

Finally, I would like to thank my home away from - the School of Pharmacy. If not for their late night moral support I would not be able to write this thesis today. I would like to thank the girls of the 8th floor, Dr. Marci Chew, Nisa Ghonem, Trish Butera and Megan Klamerus. My sincere appreciation is given to the people in the office of Salk 731 for letting me use the computers there, for providing me with delicious food (Shringi Sharma), and engaging in stimulating conversations. Last but certainly not least, I would like to thank my family and fiancé for their unwavering love and support.

1.0 INTRODUCTION

Microtubules play a role in many cellular processes. They provide a means of transportation from the cell periphery to the nucleus, give structural support to the cell as a part of the cytoskeleton, and are the major component of flagella and cilia. Microtubules also play a crucial role in mitosis, serving in the separation of sister chromatids during anaphase and in preparation for the division of the parent cell into two daughter cells. Microtubules are not static structures, rather they interconvert between rapid stages of depolymerization and polymerization. This process is known as dynamic instability. Regulation of dynamic instability is controlled by a number of factors *in vivo*. Agents that can interfere with the normal function of microtubules and arrest cell division are of great importance in cancer treatment.

1.1 MICROTUBULE STRUCTURE, FUNCTION AND REGULATION

1.1.1 Microtubule structure and function

Microtubules are noncovalent polymers formed from the heterdimers of the protein tubulin.[1] The heterodimeric protein is composed of α and β isoforms of similar amino acid sequence, and each isoform has a molecular mass of ~50 kDa.[2] The microtubule is a tube composed of longitudinal strands of heterodimers called protofilaments. These protofilaments, typically 14 of which, interact laterally to form the microtubule, in which the heterodimers are arranged in a left-handed, three-start helix. The interior of the microtubule is known as the lumen. Panel A in Figure 1 shows the tubulin heterodimer, and Panel B provides a diagram of microtubule formation. Microtubules are arranged in a B-type lattice, where lateral interactions occur between adjacent α monomers and adjacent β monomers.[3] These interactions are uniform throughout the helix, except at the seam where the path switches from α to β interactions or *vice versa*.

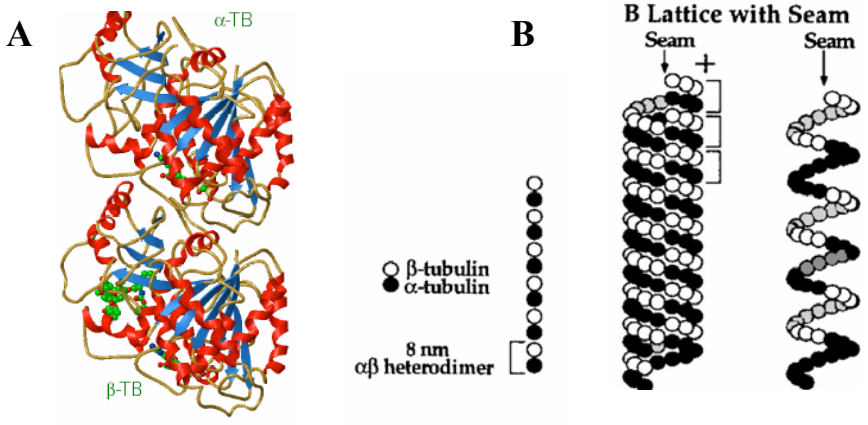

Figure 1. The tubulin heterodimer and diagram of microtubule formation
Panel A shows the quaternary strucuture of the tubulin heteromdimer containing α and β subunits. The monomers share a 50% homology at the amino acid level [adapted from Nogales, E *et al.*, **Nature**, 1998(391): 199[4]]. Panel B shows the formation of protofilaments from head-to-tail interactions of heterodimers. Heterodimers then associate to form the microtubule B lattice. The lateral interactions within the B lattice are between homologous monomers, but there is an exception at the seam of the microtubule [adapted from Desai A and Mitchison T, **Annu. Rev. Cell Dev. Biol.**, 1997(13): 83-117[1]].

Both α and β tubulin contain a binding site for the nucleotide guanosine triphosphate (GTP).[6] The GTP at this site is hydrolyzed after incorporation of the dimer into the microtubule, and remains bound to β tubulin as guanosine diphosphate (GDP). Microtubules have a distinct polarity because of the formation of a layer of newly added GTP containing heterodimers.[5] As the microtubule lengthens, the GTP is hydrolyzed in these heterodimers leaving heterodimers containing GDP in their exchangeable site. The end from which heterodimers contain GDP and readily dissociate from is known as the (–)-negative end, and the end where addition of heterodimers occurs containing a layer of GTP containing heterodimers is known as the (+)-positive end. The subunits containing GDP are released from the (–) end. The released heterodimeric subunits can then actively exchange the bound GDP for GTP, and these subunits can be used in another cycle of microtubule polymerization. The binding site for GTP on α tubulin differs in function from that of the β tubulin monomer. It is known as the non-exchangeable site or N-site due to the lack of exchange for GDP to GTP during microtubule depolymerization and the fact that GTP bound at this site is not hydrolyzed during polymerization.[7]

The process of microtubule formation occurs in three phases termed nucleation, elongation and steady-state.[8] Nucleation is the slow formation of a small microtubule nucleus from soluble tubulin. After formation of this nucleus, elongation of the microtubule rapidly occurs. Elongation is the rapid addition of heterodimers to the (+) end of the microtubule. After a period of elongation, the microtubule reaches a steady state. The steady state occurs when the lengthening and shortening of the microtubule occur at equal rates.

Microtubule polymerization and depolymerization does not usually occur in a continuous manner with equivalent addition and subtraction of subunits at each end.[9, 10] This phenomenon, called treadmilling, does occur, but more often the microtubule never reaches an equilibrium length. Experiments have shown that while a given population of microtubules may have an average length, a single MT rapidly interconverts between depolymerization and polymerization.[11] This rapid change is called dynamic instability and allows for microtubule function within the cell.

Dynamic instability is characterized *in vitro* by four parameters.[12] These parameters are the rate of microtubule growth, the rate of microtubule shortening, the frequency of catastrophes and the frequency of rescues. Catastrophe is the transition of the microtubules from a polymerization state to that of depolymerization and rescue is exactly the opposite process.

GTP hydrolysis powers dynamic instability with the free energy provided by the release of phosphate. The primary role of GTP hydrolysis is destabilization of the microtubule lattice by the formation of weaker lateral interactions within the GDP bound β-tubulin subunits.

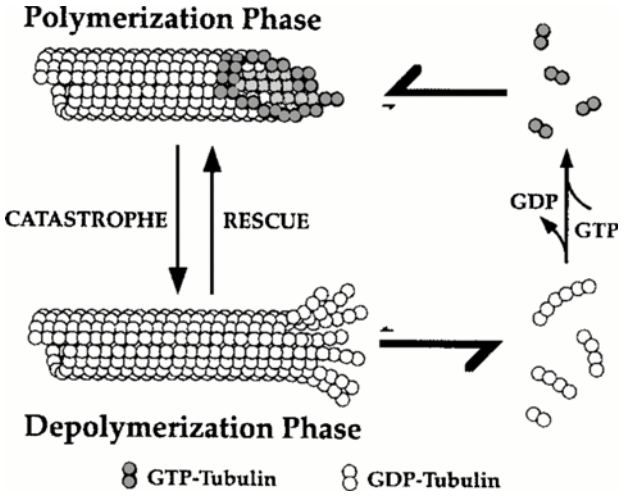

Figure 2. Diagram of microtubule dynamics and the role of GTP [adapted from Desai and Mitchison, **Annu. Rev. Cell Dev. Biol.**, 1997(13): 83-117[1]].

GTP-induced polymerization causes instability. The plus ends of the microtubule contain a small layer of GTP-containing subunits that help to stabilize the microtubule and drive polymerization.[11] The loss of this cap permits rapid depolymerization due to the instability of the GDP-bound tubulin.

1.1.2 Role of microtubules in mitosis

Mitosis is the process by which the nucleus of the cell divides and produces two genetically identical daughter cells from a parent cell.[13] Division of the cytoplasm follows mitosis in a process known as cytokinesis. Mitosis is divided into five stages that occur sequentially, prophase, prometaphase, metaphase and anaphase, with cytokinesis occurring after the last stage.

Microtubules are the main functional component of the mitotic spindle.[14] The bipolar mitotic spindle is made up of the centrosome, which consists of a pair of centrioles, the centrosome matrix and an aster. The attachment of the (–) ends of microtubules to the centrioles produces an array of radiating microtubules known as an aster.[15] The centrosome matrix consists of a number of proteins, which help in the nucleation of the microtubules.

Microtubule dynamics plays a very important role in all stages of mitosis. Figure 3 represents the three phases of mitosis, namely metaphase, anaphase and telophase, in which microtubules are known to play a prominent role.

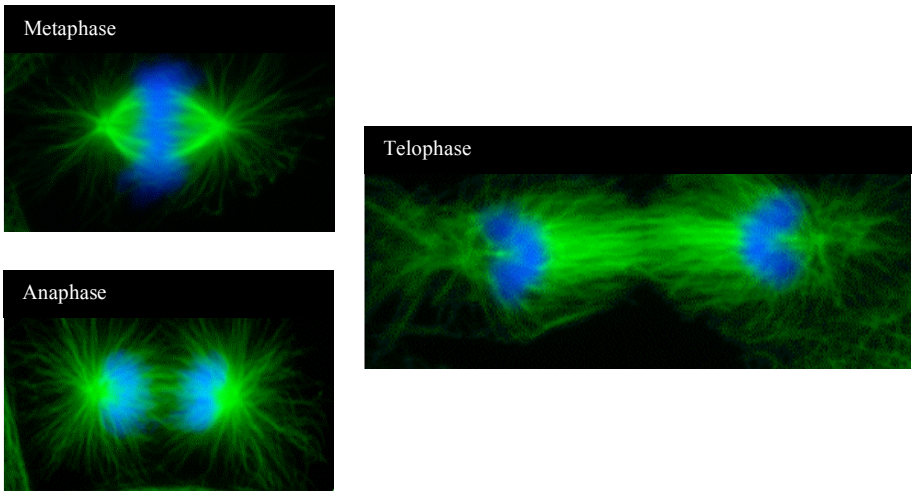

Figure 3. Immunoflourescence images displaying the function of microtubules in three phases of mitosis [adapted from *http:// mitichison.med.harvard.edu/research/microtubules/html*].
The stages of mitosis were visualized using Hoechst to stain chromatin (blue) and a fluorescently labeled secondary antibody to stain microtubules (green).

During metaphase, the microtubules attach to the kinetochores of the sister chromatid pairs, allowing for their correct orientation along the metaphase plate.[16] The cell then enters anaphase where the microtubules function in separating the sister chromatid pairs by, in concert with motor proteins, pulling them to opposite poles of the cell. A membrane forms around the separated chromatin in telophase and prepares for the division of cytoplasm during cytokinesis.[17]

1.1.3 Regulation of microtubule dynamics

The rates of polymerization and catastrophes *in vivo* are both greater than that observed *in vitro* using purified tubulin.[18] This is probably due to the *in vivo* regulation of microtubules through signal transduction pathways, post-translational modifications and binding of regulatory proteins to the microtubule lattice. Cells can alter the expression of proteins that destabilize or stabilize microtubules. Certain proteins that interact with the microtubules are inactive when phosphorylated, and the cell can alter the phosphorylation levels of these proteins.

The most well known microtubule-stabilizing factors *in vivo* are the microtubule-associated proteins (MAPs). MAPs bind to the microtubule and stabilize the lattice by cross-linkage of heterodimers.[19] The crosslinkage functions to stifle heterodimer dissociation, decrease catastrophes and increase rescue.[20] There are four types of well-characterized MAPs: MAP1, MAP2, tau in neurons, and MAP4 in non-neuronal cells. MAP binding in neurons to microtubules is in a ratio or 1:4-10, and binding is primarily through electrostatic interactions with the acidic C-terminal of the microtubule proteins. MAP binding is negatively regulated by phosphorylation, and over-phosphorylation of tau plays a role in the pathogenesis of Alzheimer's disease.[1]

Proteins that increase the rate of catastrophes and decrease rescues include kinesins, stathmin, and microtubule severing proteins.[21-23] Kinesins are motor proteins that move by walking from the (–) to (+) ends of microtubules. It has been shown in *Xenopus* eggs that immunodepletion of kinesin, XKCM1, causes an increase in microtubule length and a decrease in catastrophe frequency.[24]

Stathmin/Op18 is a small protein that binds in a ratio of 1:2 to tubulin heterodimers as determined by electron microscopy.[25] Stathmin not only increases the catastrophe frequency but also lowers the amount of soluble tubulin available. X-ray crystallography studies with the stathmin like domain (SLD) of RB3, a neuron-specific homologue of the stathmin family of proteins, show that binding of the protein to tubulin changes the conformation of the protofilament.[26] As presented in Figure 4, binding of SLD-RB3 to tubulin causes the heterodimer to curve.

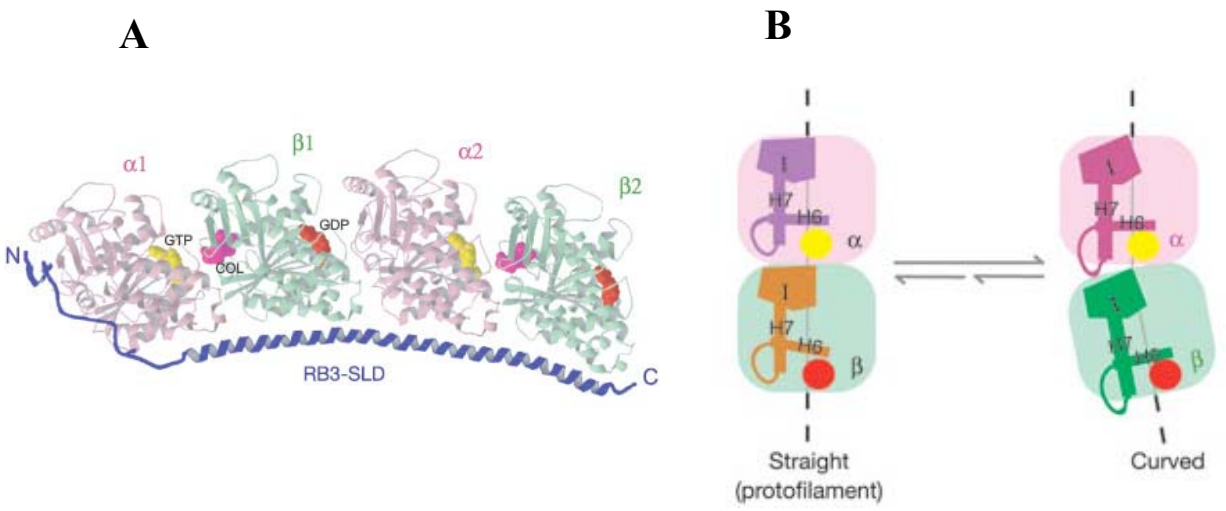

Figure 4. Conformational changes to the tubulin heterodimer associated with SLD-RB3 binding.
A.) The stathmin like binding domain of RB3 bound to two heterodimers. B.) The (🔴) represents the GTP exchangeable site on β tubulin and (🟡) represents the nonexchangeable site on α tubulin. The intermediate domain (I) is rotated toward the nucleotide binding domain in the straight protofilament to allow for lateral interactions to occur [adapted from Ravelli R, **Nature**, 2004(428): 198-202[26]].

The binding of SLD-RB3 is associated with movement in the H6-H7 loops and the intermediate domain in the both the α and β subunits. This movement causes a loss of favorable lateral and longitudinal interactions within and between the protofilaments.

The microtubule severing proteins seem to play multiple roles within the cell. Katanin, a microtubule severing protein in the ciliate protozoa *Tetrahymena,* promotes microtubule assembly in ciliary microtubules, but decreases polymer mass of internal microtubules.[27] Post-translational modifications to tubulin seem to be markers for the severing of the microtubules.

1.2 MICROTUBULE PERTURBING AGENTS

The importance of microtubules to mitosis and the potential to interfere with delicate dynamics of microtubules has lead to the search and development of many microtubule interacting compounds. Microtubule perturbing agents can be roughly classified into two broad groups based upon the mechanism by which they disrupt normal microtubule function. These include agents that stabilize microtubule formation and agents that destabilize or inhibit polymer formation.[28] These agents can further be classified by the location of their binding site to tubulin and/or the microtubule.

1.2.1 Paclitaxel and other known microtubule stabilizers

Paclitaxel was originally isolated from the bark of the yew tree *Taxus brevifolia*.[29] Its ability to stabilize microtubules and increase the polymer mass was recognized in 1979 by Schiff and Horwitz.[30] Paclitaxel was clinically approved in 1995 and has been shown effective for the treatment of breast, ovarian and non-small cell lung carcinomas.[28] The binding of paclitaxel to the microtubule stabilizes the lateral interactions between heterodimers. Paclitaxel binds to the β-tubulin subunit and preferentially binds to polymerized tubulin. Interestingly, high resolution cryoelectron microscopy studies of zinc cation- and paclitaxel-stabilized sheets of tubulin and computational models of microtubules from these sheets strongly suggest that the taxane binding site (*i.e.*, where paclitaxel binds) is in the lumen of the microtubule. Studies with cyclostreptin, a microtubule stabilizer that binds covalently to the taxoid site, have shown that taxane site binding may be a two-step mechanism.[31] Taxane site agents may first bind to an external site on the microtubule surface, and then transfer to an interior site within the lumen.

The great clinical success of paclitaxel has led the search for other microtubule stabilizing agents. Microtubule stabilizers have been identified from a number of sources, such as marine corrals and sponges, soil bacteria and plants. The epothilones, discodermolide, laulimalide, dictyostatin, and peluroside A have been identified to possess the same general mechanism of action as paclitaxel.[32-36] The structures of some of these compounds are presented in Figure 5. This suggests that, and has been proven in competitive binding assays, these drugs bind to the same or only slightly different site on the β-tubulin subunit of the microtubule polymer.

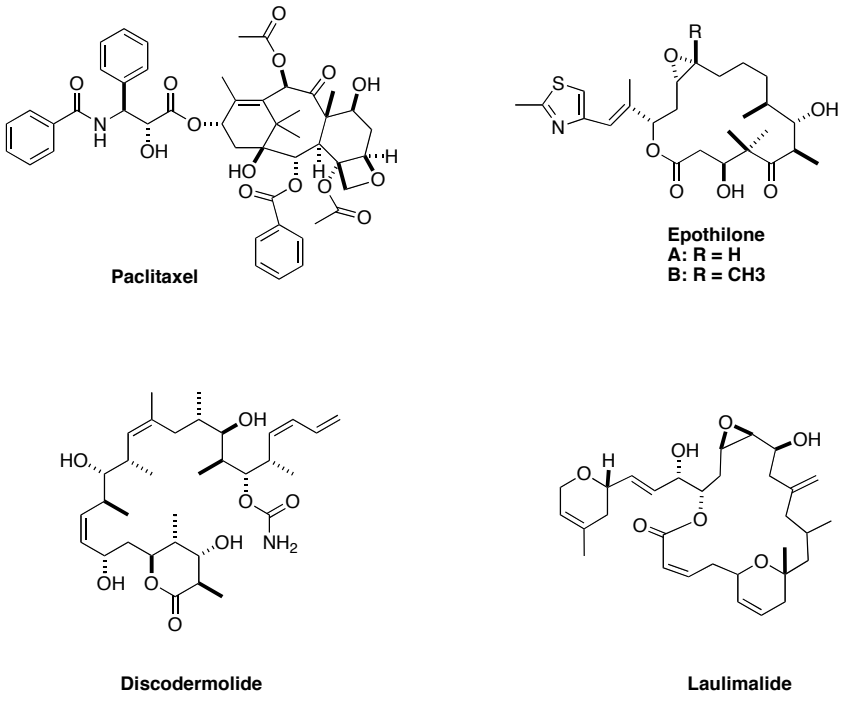

Figure 5. Paclitaxel and other microtubule stabilizers isolated from natural sources.

Laulimalide and peloruside A are the only compounds that bind to a completely different binding site, but this site has yet to be identified.[36, 37]

1.2.2 Microtubule destabilizers: Vinca domain binding agents and colchicine site

Colchicine was the first compound identified possessing tubulin-related antimitotic activity. Radiolabeled colchicine provided the first identification and purification of tubulin from the bovine brain – in fact, tubulin was initially called colchicines-binding protein.[38] Colchicine binds to the β-subunit of tubulin and the kinetics of binding occurs in two phases. The initial phase of colchicine binding to tubulin is relatively fast, but upon further binding it produces a slow conformation change within the protein. Colchicine binds tightly to tubulin and dissociation occurs very slowly. When a colchicine-tubulin complex is incorporated into a microtubule polymer the dynamics of the microtubule are suppressed, and at high colchicine concentrations assembly is completely inhibited.

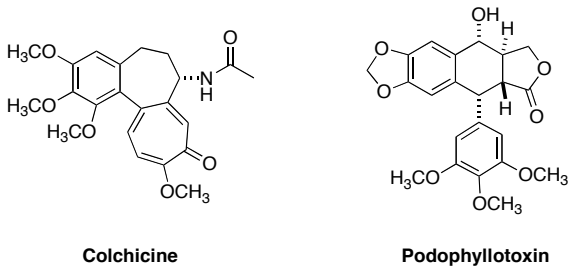

Colchicine **Podophyllotoxin**

Figure 6. Examples of colchicine site binding agents.

Podophyllotoxin and curacin A have been reported to competitively inhibit the binding of colchicine to tubulin, and possess similar antimitotic capablilities.[39, 40] Some examples of colchicine site binding agents are shown in Figure 6.

The vinca alkaloids, vincristine and vinblastine, were first isolated from the leaves of the periwinkle plant *Catharanthus roseus.*[28] Since the 1950s, the vinca alkaloids have been in clinical use for childhood leukemia and adult hematological malignancies. They are characterized as microtubule assembly inhibitors; however, turbidimetric analyses have revealed that these agents cause an aberrant tubulin polymerization reaction.[41, 42] Electron microscopy studies show the aberrant tubulin polymer to be in the form of spirals and rings.

The binding site of vinca alkaloids is located on the β-subunit of the tubulin dimer near the exchangeable nucleotide site and is termed the vinca binding domain.[43] The term "domain" is used instead of "site" due to the discovery of compounds that inhibit vinca alkaloid binding to this part of β-tubulin in a noncompetitive manner. All compounds that bind to this domain share the common characteristics of inhibiting microtubule assembly and preventing GTP hydrolysis.

The competitive inhibitors of the vinca domain are vinca alkaloids, maytansine and rhizoxin.[44] The noncompetitive inhibitors of binding are the peptides/depsipeptides such as dolastatin 10, phomphosin A, cryptophycin, hemiasterlin, and diazonamide A.[45] It is believed that the noncompetitive inhibitors interfere with vinca alkaloid binding by sterically hindering the binding site. This leads to the assumption that the vinca alkaloid binding site overlaps with the binding site of the noncompetitive inhibitors. Some examples of vinca domain binding agents are presented in Figure 7.

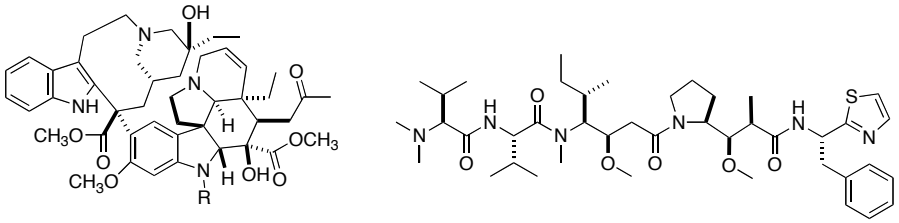

Figure 7. Examples of compounds that bind to the vinca domain on tubulin.

Further evidence for overlapping binding sites is given by the fact that all of the noncompetitive and competitive inhibitors prevent GTP nucleotide exchange on β-tubulin. Vinca alkaloids only weakly block nucleotide exchange.[43]

1.3 MECHANISMS OF RESISTANCE IN ANTIMICROTUBULE CHEMOTHERAPY

Resistance is a major problem associated with most chemotherapy.[46] There are many mechanisms by which the cell combats antimicrotubule therapy. The most common mechanisms are the over expression of the P-glycoprotein pump, overexpression of certain isotypes of tubulin, and mutations which affect the binding of microtubule perturbing agents to their target site. The importance of each of these mechanisms has been determined clinically, and compounds that can overcome this resistance are heavily sought after.

The most common cause of resistance in antimicrotubule therapy is believed to be the over expression of the P-glycoprotein pump in cancer cells, which increases toxin and drug efflux in humans.[46] The *MDR1* (more accurately, *ABCB1*) gene encodes for the P-glycoprotein pump. P-glycoprotein is a membrane bound protein that is part of the adenosine triphosphate binding cassette transporter.[47] The taxanes, both paclitaxel and docetaxel, colchicine, and the vinca alkaloids are well-characterized substrates for this pump.[48, 49] The binding of adenosine triphosphate and hydrolysis of a phosphate group powers the active pumping of drugs out of the cell. Figure 8 shows how the hydrolysis of ATP is used to actively pump drugs out of cancer cells.

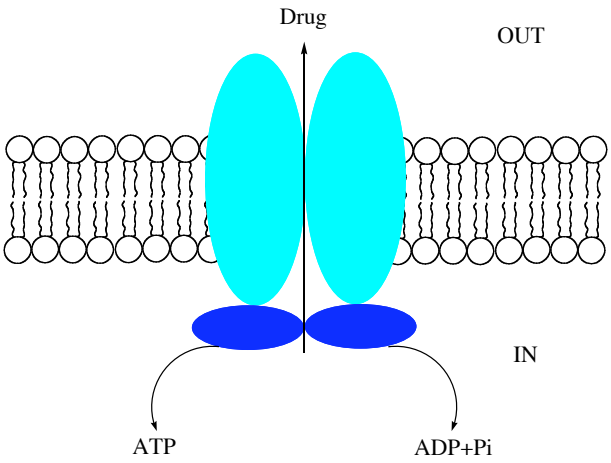

Figure 8. Schematic of the P-glycoprotein pump

There are six different isotypes of β-tubulin that can be found in cells.[50] These isotypes are differentiated into six different classes I, II, III, IVa, IVb, and VI. Class I β-tubulin is the most common type, but recent results indicate that certain isotypes are overexpressed in cancer cells.[50] It is believed that class III β-tubulin incorporation destabilizes microtubules and this overcomes treatment with the microtubule stabilizing agents. A study utilizing 39 patients with recurrent breast cancer notes a high level of correlation between overexpression of class III β-tubulin and failure to respond to treatment with docetaxel.[51]

Cancer cells grown in the presence of paclitaxel and verapamil, a P-glycoprotein pump inhibitor, become resistant to paclitaxel treatment through alterations in the taxane binding site on β-tubulin.[52] Cell lines resistant to epothilone A and B treatment by the same mechanism have also been isolated.[53] Although identification of the mutated amino acids within these cells has provided important information regarding the interactions of these compounds within the binding site, this method of resistance has not been shown to be clinically relevant. A recent study by

Hasegawa *et al.* reports that the frequency of mutations to class I β-tubulin in human breast cancer could be as low as 1.6%.[54]

The importance and clinical success of many microtubule perturbing agents in the treatment of cancer compels further research into agents that overcome these resistance problems. With the FDA approval of ixabepilone, an epothilone analogue, for the treatment of taxane-refractory cancers and the number of microtubule perturbing agents in clinical trial, it is clear that the such research is needed to improve chemotherapeutic treatment.[28] It was therefore hypothesized the the evaluation of potential microtubule perturbing agents for their mechanisms and kinetics will lead to new chemotherapeutic agents that could improve current patient treatment.

Three different projects were undertaken to provide potential chemotherapeutics and to provide more information about the mechanisms of already known microtubule perturbing agents. To gain insight into the structure-activity relationship of the potent microtubule stabilizer dicytostatin, analogues of the parent compound were synthesized and evaluated for their effects on cancer cells and purified tubulin. Then experiments were performed to determine the mechanism by which the small microtubule perturbing agent, 5HPP-33, affected microtubule dynamics. Finally, cell-based and biochemical assays were performed on (–)-pironetin, its analogues, and the tubulysins to compare their microtubule inhibiting abilites to already previously characterized compounds. From this work many novel microtubule perturbing agents were discovered and common mechanisms of action were revealed.

2.0 MATERIALS AND METHODS

2.1 CHEMISTRY

2.1.1 General Information

All reactions were performed in oven-dried glassware under an inert atmosphere of nitrogen unless otherwise stated. Anhydrous THF, CH_2Cl_2 and benzene were obtained from distillation from CaH_2. Melting points for all compounds were performed on a Fisher-Johns melting point apparatus. Infrared spectra were performed on a Perkin Elmer spectrum 100 FT-IR spectrometer. ^{1}H-NMR spectra were recorded on a 400 MHz Varian spectrometer. ^{13}C-NMR spectra were recorded on a Bruker spectrometer equipped with a cyroprobe at 150 MHz or on a Varian spectrometer on a 100 MHz. Spectra were obtained using $CDCl_3$ as the solvent and chemical shifts were reported relative to residual $CHCl_3$ (7.26 ppm) for ^{1}H spectra and $CDCl_3$ (77.0 ppm) for ^{13}C spectra. High resolution mass spectra were obtained an Applied Biosystems 4700 MALDI-TOF-MS. Analytical thin layer chromatography was performed on EM Reagent 0.24 nm silica gel 60-F plates. Flash chromatography was performed as described previously using Aldrich Silica Gel, Merck grade 9385 (230-400 mesh). Analytical gas chromatography was performed on a 5890 Series II gas chromatograph equipped with a Hewlett Packard 5971 Series mass selective detector. Purification of the radiolabeled compound was performed using a

Nova-Pak C18 column (3.9 x 150 mm) on a Waters 2695 separation module equipped with a Waters 2487 dual wavelength absorbance detector. A Packard FlowScintillation analyzer was used to determine the radioactive purity of the compound. Commercial reagents were purchased from Aldrich Chemical Company (Milwaukee, WI).

2.2 EXPERIMENTAL PROCEDURES

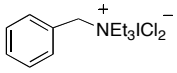

Benzyltriethylammonium dichloroiodate (4):[55] A 250 mL Erlenmeyer flask equipped with a stir bar was charged with water (39 mL), hydrochloric acid (2.0 mmol) and iodine (2.0 mmol). The mixture was stirred for 45 minutes at room temperature, and then chilled to 0 ^{o}C in an ice bath. The mixture was titrated with a solution of 6% NaClO (20 mL) over a period of 4 hours. The endpoint of the reaction was observed when the solution turned yellow. An aqueous solution of 10% NaI was added dropwise to the reaction until a slight orange color was observed. The mixture was then slowly poured into a stirring solution of benzyltriethylammonium chloride (3.0 mmol) in water. The precipitate was collected by vacuum filtration, and washed with water (100 mL 3x). The solid was dried *in vacuo* for 17 hours to obtain a fine yellow powder (8.5 g, 69%): mp 84-88 ^{o}C (lit mp 84-86 ^{o}C); ^{1}H NMR (400 MHz, $CDCl_3$): δ 7.46-7.54, (m, 5H), 4.44, (s, 1H), 3.31, (q, J = 7.2 Hz, 6H), 1.52, (t, J = 7.2 Hz, 9H); ^{13}C NMR (100 MHz, $CDCl_3$): δ 132.60, 131.50, 130.10, 126.30, 61.59, 53.43, 8.70.

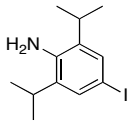

4-Iodo-2,6-diisopropylaniline (5):[56] A 250 mL three neck flask equipped with a stir bar was charged with 2,6-diisopropylaniline(**2**) (11 mmol), CH_2Cl_2 (27 mL), MeOH (27 mL), and $NaHCO_3$ (21 mmol). The mixture was chilled to 0 ^oC, evacuated and backfilled with N_2 (3x). Compound **6** (10.6 mmol) was added to the flask in a solution of CH_2Cl_2 over a period of 15 minutes. The reaction mixture was stirred at 0 ^oC for 5 minutes, then warmed to room temperature. The reaction stirred for an additional 25 minutes and then was poured into $NaHCO_3$ (250 mL). The organic layer was extracted with CH_2Cl_2 and washed with $NaHCO_3$ (2x). The combined organic layers were washed with H_2O (3x), and extracted with CH_2Cl_2. The organic layers were dried over $MgSO_4$, and concentrated *in vacuo.* The crude product was purified by flash chromatography (19:1 hexanes-EtOAc) to yield 2.56 g (80%) of the title compound as brown oil: ^1H NMR (400 MHz $CDCl_3$): δ 7.28 (s, 2H), 3.74 (br s, 2H), 2.84 (septet, J = 6.8 Hz, 4H), 1.24 (d, J = 6.8 Hz, 12H).

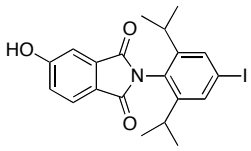

2-(4-Iodo-2,6-diisopropylphenyl)-5-hydroxy-1*H*-isoindole-1,3-dione(6):

A 25 mL flask was equipped with a stir bar, condenser, and 4Å activated molecular sieves. To this flask, 4-hydroxyphthalic acid (**2**) (0.79 mmol), compound **5** (0.66 mmol) and CH_3CO_2H (2 mL) were added. The mixture was heated to 100 ^oC for 2 h, after which it was cooled to room temperature and poured into $NaHCO_3$ (50 mL). The organic layer was extracted with Et_2O and washed with water (3x). The organic layer was dried over $MgSO_4$ and solvent was removed *in vacuo.* The crude product was purified using a small plug of silica gel (3:2 hexanes-EtOAc) to yield 0.12 g (42%) of the title compound as a white crystalline solid: mp 55-59 ^oC; IR: 3365

(hydroxy stretch), 2964 (methyl stretch), 2928 (methyl stretch), 1719 (carbonyl), 1604 (amine), 1467 (aromatic), 1373 (aromatic), 1269 (aromatic), 1097 (aromatic), 854 (aromatic), 755 (ortho substitution pattern); ^{1}H NMR (400 MHz, $CDCl_3$): δ 7.84 (d, J = 8.0 Hz, 1H), 7.56 (s, 1H), 7.36 (d, J = 2.4 Hz), 7.19 (dd, J = 8, 2.4, 1H), 6.09 (br s, 1H), 2.64 (septet, J = 6.8 Hz, 4H), 1.14 (d, J = 6.8, 12H); ^{13}C NMR (150 MHz, ($CDCl_3$): δ 167.67, 167.65, 161.71, 149.77, 134.55, 127.10, 126.13, 123.67, 121.07, 110.97, 97.11, 96.94, 29.25, 23.83, 23.80; HRMS (MALDI-TOF): $[M+H]^+$ calculated for $C_{20}H_{20}INO_3$ *m/z* 449.0488, found 450.0542

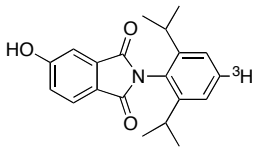

[4-^{3}H]2-(2,6-Diisopropylphenyl)-5-hydroxy-1*H*-isoindole-1,3-dione (**7**):[57]

A 5 mL round bottom flask equipped with a stir bar was charged with compound **6** (0.6 μmol), Et_3N (0.6 μmol), 10% Pd/C (0.6 mg) and MeOH (1 mL) under an inert atmosphere. The flask was degassed by the application of three freeze-pump-thaw cycles. The frozen solution was then covered with an atmosphere of tritium gas supplied by a Trisorber® (IN/US Systems). The mixture was allowed to warm to room temperature and stirred for 1 h. The reaction was filtered to remove the Pd/C and distilled to remove the radioactive solvent *[Note: This is an extremely proficient way to make tritiated methanol; those wishing to perform such reactions should explore other solvents to find those that are not tritiated by this procedure]*. The crude product was purified by HPLC and the total yield was determined using a calibration curve generated using nonradiolabeled compound. An analogue of compound **3** was used as an internal standard. Specific activity was determined from the amount of radioactivity determined by scintillation spectrometry divided by the amount of material (mmol) present.

2.3 BIOLOGY

2.3.1 Materials

Bovine brains were obtained from a local slaughterhouse. *N*-morpholinoethane sulfonate, adenosine 5'-triphosphate (ATP), guanosine 5'-triphosphate (GTP) and 2',3'-dideoxyguanosine-5'-triphosphate (ddGTP) were obtained from USB (Cleveland, OH). Coomassie G250 stain, tris(hydroxymethyl)aminomethane (Tris), glycine and sodium dodecylsulfate were obtained from Bio-Rad Labratories (Hercules, CA). Glycerol was from Invitrogen (Carlsbad, CA). Sodium hydroxide was obtained from Fisher (Pittsburgh, PA). Uranyl acetate and carbon-coated formvar grids were generous gifts from the Center for Biological Imaging at the University of Pittsburgh. The Drug Synthesis and Chemistry Branch, National Cancer Institute, provided normoisotopic and tritiated paclitaxel (16.2 Ci/mmol) and also normoisotopic and tritiated dolastatin 10 (1.96 Ci/mmol). Discodermolide, [^{3}H]discodermolide (specific activity 14.4 Ci/mmol), epothilone B and [^{14}C]epothilone B (specific activity 111 mCi/mmol) were generous gifts from Novartis Pharma AG. Dictyostatin was synthesized as described previously.[59] [^{3}H]Vinblastine (specific activity 8.50 Ci/mmol was obtained from GE Healthcare Bio-sciences (Picataway, NJ). The syntheses of the analogues tested here are reported elsewhere.[59-62] Cell lines (1A9, Ptx10 and Ptx22) were a gift from Drs. Tito Fojo and Paraskevi Giannakakou at the NIH. 5HPP-33 was a generous gift from Dr. Pui-Kai Li at The Ohio State University. MAPs were a generous gift from Dr. Ernest Hamel at the NIH. Rabbit anti-phosphohistone H3 antibody was purchased from Upstate Cell Signaling (Charlottesville, VA). Cy3-labeled donkey anti-rabbit and fluorescein isothiocyanate (FITC)-labeled anti-mouse secondary antibodies were from Jackson

Immunoresearch (West Grove, PA). All other chemicals including mouse anti-alpha tubulin antibody were purchased from Sigma (St. Louis, MO).

2.3.2 Antiproliferative assays

Antiproliferative assays were performed as described previously.[63, 64] Cells were seeded into 96-well plates, allowed to attach and grow for 48 h. One plate of cells was used for a time zero cell number determination (N=16), and cells in other plates were treated for 72 h or 96 h with either DMSO (0.5% v/v; N = 8 for each plate) or a range of concentrations, in quadruplicate, of test agents. Cell number was determined spectrophotometrically at 490 nm minus absorbance at 630 nm after exposure to 3-(4,5-dimethylthiazol-2-yl)-5-(3-carboxymethoxyphenyl)-2-(4-sulfophenyl)-2*H*-tetrazolium (MTS) and *N*-methylphenazine methylsulfate. The fifty percent growth inhibitory concentrations (GI_{50}) of test agents were calculated from the spectrophotometrically determined growth of the control cells over the 72 h period. The antiproliferative assays for the 1A9 cells and its mutants, and the NIH3T3 cells and its transfectants with multidrug resistant pumps (NIH3T3-MDR-G185 and NIH3T3-MDR-V185), were performed as described in the literature.[65]

2.3.3 Flow cytometry

The flow cytometry experiments were performed as described by Li *et al*.[66] Labeling cells with propidium iodide and the mitotic specific antibody, TG3, allowed for quantitation of the amount of 1A9 cells undergoing mitosis. 1A9 cells were trypsinized and washed. They were then

resuspended in 500 µl of RPMI and 500 µl of fetal calf serum and 3 mL of ice-cold 70% ethanol was added dropwise. The cells were kept at 4ºC for at least 30 minutes, centrifuged, resuspended in blocking solution 2% in bovine serum albumin (BSA) in phosphate buffered saline (PBS), and incubated at 4ºC overnight. The cells were then centrifuged, resuspended in blocking solution with TG3 antibody (diluted 1:10, hybridoma cell culture medium), and allowed to incubate for 30 minutes. After washing with blocking solution, the cells were stained with FITC-conjugated goat anti-mouse secondary antibody for 30 minutes. The cells were then centrifuged, resuspended in 450 µl PBS, 450 µl of propidium iodide solution (50 µg/ml in PBS), 50 µl RNase solution (5 mg/ml in PBS), and allowed to incubate for 30 minutes. The suspension was then passed through a nylon mesh filter and analyzed on a FACSort flow cytometer (Becton Dickinson). Fluorescein-5-isothiocyanate (FITC) fluorescence was monitored with a 525 nm bandpass filter and propidium iodide with a 585 bandpass filter.

2.3.4 Purification of tubulin from bovine brain

Tubulin was extracted from two freshly-obtained bovine brains using a modified version of Hamel's procedure.[67] Previous to the morning of the experiment, two extraction buffers, labeled Solution A and Solution B, were prepared. Solution A was 0.1 M MES, pH 6.4, containing 1 mM ethyleneglycoltetraacetic acid (EGTA), 4 M glycerol, 1 mM $MgCl_2$, 1 mM 2-mercaptoethanol, 0.1 mM ethylenediaminetetraacetic acid (EDTA) and 0.1 mM GTP. Solution B was the same as Solution A but without 4 M glycerol.

All centrifugations were performed in a Beckman-Coulter Ti 45 rotor. Bovine brains were homogenized in a blender with 0.75 mL/g of Solution A at 0 ^{o}C. The homogenate was clarified by spinning at 6,000 rpm for 15 min at 0 ^{o}C. The homogenate was transferred to

Beckman centrifuge tubes and centrifuged at 0 °C at 28,000 rpm for 44 min. The supernatant was collected in a clean autoclaved beaker and ATP and GTP were added to make the final concentration in the supernatant 1 mM and 0.3 mM, respectively. The supernatant was divided into six aliquots and incubated at 37 °C for 40 min. The aliquots were transferred to centrifuge tubes and centrifuged at 37 °C at 28,000 rpm for 44 min. The supernatant was discarded and the pellet was resuspended in 10 mL/ brain of Solution B. The pellet was incubated on ice for 30 min. The solution was transferred to centrifuge tubes and centrifuged at 24,000 rpm for 30 min at 0 °C. The amount of supernatant was determined. Each 1 mL of the supernatant was treated with 0.553 g of glycerol (to give a final concentration of 4 M) and 50 μL of a solution containing MES, pH 6.4, with EGTA, $MgCl_2$, 2-mercaptoethanol and EDTA to give concentrations of these components as per solution Solution A were added. ATP and GTP were added to give final concentrations of 1 mM and 0.3 mM, respectively. The mixture was incubated at 37 ^{o}C for 1 h and centrifuged at 37 ^{o}C at 28,000 rpm for 44 min. The supernatant was discarded and the pellet was homogenized in 6.25 mL/brain of Solution B. The rehomogenized pellet was incubated on ice for 30 min and centrifuged at 24,000 rpm for 30 min. The concentration of protein was determined using the Bradford method, and adjusted (if needed) to a concentration of 27.5 mg/mL with Solution B.[68] The High-MES pellet was formed using 0.5 mg/mL 2 M lyophilized MES at pH 6.9 for a final concentration of 1.6 M. GTP and dithiothreitol (DTT) (final concentrations of 1 mM and 2 mM, respectively) were then added and the mixture was incubated for 45 min at 37 ^{o}C. The mixture was transferred to centrifuge tubes and centrifuged for 44 min at 28,000 rpm. The pellet was homogenized in 8-10 mL of cold 1 M MSG, pH 6.6. The rehomogenized pellet was incubated for 2 h on ice and centrifuged at 24,000 rpm at 0°C for 30 min. The next cycle of polymerization was induced by the addition of 1 mM GTP to the

supernatant and incubation for 1 h at 37 ^{o}C. The mixture was centrifuged at 40,000 rpm at 37 ^{o}C for 40 min, and then the pellet was homogenized in 8-10 mL of 1 M MSG and incubated on ice for 1 h. A final centrifugation was performed at 0 ^{o}C at 40,000 rpm for 40 min. The electrophoretic homogeneity of the protein was determined by SDS-PAGE gel electrophoresis, and protein concentration was determined by the method of Lowry.[69]

2.3.5 High-content analysis of mitotic arrest

Detailed conditions for the high-content analysis of microtubule perturbing agents using a cell based immunoflourescence assay have been described previously.[70] Briefly, HeLa cells were plated at a cell density of 8000 cells per well in coolagen-1 coated 384-well microplates. Cells were allowed to attach and spread for 3-8 h and treated with either vehicle dimethyl sulfoxide (DMSO) or ten two-fold concentrations gradients of test agents and incubated for an additional 20 h at 37 ^{o}C. After the incubation, cells were fixed with formaldehyde containing 10 μg/mL Hoechst 33342 to stain nuclei/chromatin, permeabilized with Triton X-100 and simultaneously immunostained with antibodies against α-tubulin (mouse monoclonal, 1:2500 dilution) and phosphohistone H3 (rabbit polyclonal, 1:1000 dilution) followed by FITC–labeled donkey anti-mouse IgG (1:250). Each well was imaged on an ArrayScanII (Cellomics Inc.) using an Omega XF93 filter set at excitation/emission wavelengths of 350/461 nm (Hoechst), 494/519 nm (FITC) and 556/573 nm (Cy3). Images were analyzed with the Target Activation Bioapplication (Cellomics, Inc.). The algorithm provided quantitative measurements of nuclear FITC and Cy3 intensity, cell density, and of mean and total nuclear Hoechst 33342 intensities. Microtubule mass was defined as the average FITC intensity in an area defined by the Hoechst-stained nuclei. To estimate the percentage of cells with elevated phosphohistone H3 levels and with condensed

chromatin, thresholds were defined as the average intensity plus one standard deviation of Hoechst or Cy3 intensities in anti-phosphohistone H3- or Hoechst 33342-stained cells, respectively, using a minimum of 1000 vehicle-treated cells per well. Cells were classified as positive if their average intensities in the Hoechst or Cy3 channel exceeded these thresholds. The EC_{50} was the effective concentration of drug that decreased cell growth by 50% compared to vehicle treated with control.

2.3.6 Tubulin assembly *in vitro*

Assessing the ability of agents to inhibit tubulin polymerization in monosodium glutamate

The ability of agents to inhibit tubulin assembly was assessed in a standard assay utilizing MSG.[71] Electrophoretically homogeneous bovine brain tubulin (final concentration 10 μM; 1 mg/mL) was preincubated with test agents dissolved in DMSO (4% *v*/*v* final concentration) and monosodium glutamate (0.8 M final concentration, pH 6.6) for 15 min at 30 ^{o}C. The reaction mixture was cooled to 0 ^{o}C and GTP (0.4 mM final concentration) was added. Reaction mixtures were transferred to cuvettes held at 2.5 ^{o}C in a Beckmann 7400 multichannel spectrophotometer reading absorbance (turbidity) at 350 nm in each cuvette every 15 sec. Baselines were established and temperature was quickly raised to 30 ^{o}C (in approximately 1 min). After 20 min, the temperature was returned to 2.5 ^{o}C. The change in absorbance 20 min after samples reached 30 ^{o}C was used to calculate extent of polymerization. The change in absorbance at this time point for vehicle plus no GTP was considered 100% assembly inhibition (negative control), while the change in absorbance for GTP plus vehicle was taken as 0 % inhibition (positive control).

Percent inhibition was calculated by:

((absorbance of positive control at 20 min – absorbance of compound at 20 min)/absorbance of positive control at 20 min) * 100

A linear curve of concentration versus percent inhibition was used to extrapolate a value for the IC_{50}, the concentration at which 50 % of tubulin assembly was inhibited.

Assessing the effects of agents on induction of tubulin assembly in monosodium glutamate

Tubulin assembly was monitored by turbidity development at 350 nm as described previously.[72] Reaction mixtures (0.25 mL final volume) contained tubulin (1 mg/mL; 10 μM), MSG (0.8 M from a stock solution adjusted to pH 6.6 with HCl), DMSO (final volume 4% *v/v*), and test agent (10 μM). If GTP was added, it was at concentration of 0.1 or 0.4 mM. Reaction mixtures without test agent were cooled to 0 °C and added to quartz cuvettes held at 0.25–0.5 °C a temperature-controlled (via a Peltier unit), 6-sample Beckman DU 7400 spectrophotometer (Beckman Coulter). Test agent in DMSO was then rapidly mixed into the reaction mixture. Absorbance at 350 nm was monitored in each cuvette every 15 sec. Each 6-sample run contained one positive control (paclitaxel, 10 μM final concentration) and one negative control (DMSO only). Baselines were established at 0.25–2.5 °C and temperature was rapidly raised to 30 °C (in approximately 1 min) and held there for 20 min. The temperature was then rapidly lowered back to 0.25–2.5 °C. The change in absorbance 20 min after samples reached 30 °C was used to calculate the extent of polymerization.

Tubulin polymerization in the complete system

The effect of 5HPP-33 on tubulin polymerization was determined using microtubule associated proteins (MAPs) to induce assembly. Assembly was monitored at 350 nm on a 250 Gilford spectrophotometer equipped with a Peltier temperature controller and a mechanical multicuvette system as described previously.[63] Reaction mixtures contained 1.0 mg/mL tubulin purified from bovine brain, 0.75 mg/mL MAPs, 400 μM GTP, 0.1 M MES pH 6.9, various concentrations of test agent, and 4% DMSO. If Mg^{2+} was included in the assay, it was via addition of 0.5 mM $MgCl_2$ to determine the effects of Mg^{2+} on the activity of 5HPP-33. Reaction mixtures without test agent were cooled to 0 ^{o}C and added to precooled cuvettes at the same temperature. The four-sample run contained various concentrations of 5HPP-33 in DMSO and 4% DMSO without test agent as a positive control. Samples were held at 0 ^{o}C for 5 min to establish a baseline and then the temperature was the rapidly raised to 30 ^{o}C for 30 min. To assess 5HPP-33 full effects on microtubule polymerization the temperature was again decreased to 0 ^{o}C and held for 15 min. The IC_{50} for 5HPP-33 was determined using the change in absorbance of vehicle at 30 ^{o}C as 100% assembly and comparing that to baseline (0% assembly).

2.3.7 Radioligand displacement studies

Saturation Binding Experiments with [^{14}C]Epothilone B

Determination of the equilibrium binding constant (K_d) for epothilone B was determined as described previously.[63, 72] An 80 μM stock solution of [^{14}C]epothilone B was prepared in 50% DMSO. Samples of [^{14}C]epothilone B at 0.005-2 μM were prepared in 4:1 (*v/v*) 0.75 M MSG/DMSO (total volume 50 μL) and warmed to 37 °C. Microtubules were preformed in separate tubes by incubating 2.5 μM tubulin and 25 μM ddGTP in 0.75 M for 30 min at 37 °C.

Equal volumes (50 μL each) of the radiolabeled compound mixtures and microtubule solutions were mixed and incubated for 30 min at 37 °C. Reaction mixtures were then centrifuged in a Beckman Allegra TM 64R at 14,000 rpm for 30 min at room temperature. The amount of radiolabel in the supernatant was determined by scintillation spectrometry in a LS6500 Beckman multi-propose scintillation counter. Non-specific radiolabel binding was determined from competition experiments with 8 μM discodermolide and processing as described above.

Saturation binding data for [^{14}C]epothilone B and was analyzed using a modified version of Swillens' equation that accounts for ligand depletion:[73,74]

$$\text{Total Binding} = \{((B_{max} \times ([L]_T - [L]_B))/(K_D + (([L]_T - [L]_B))\} + ([L]_T - [L]_B) \times NS$$

B_{max} = Number of binding sites

$[L]_T$ = Amount of radioligand added

$[L]_B$ = Amount of ligand bound to tubulin polymer

NS = Fraction of radioligand bound to nonspecific sites

Non-linear regression analysis was performed using GraphPad Prism software that allows for the simultaneous fitting of nonspecific and total binding data.

Determination of K_i values for dictyostatin analogues utilizing [^{14}C]Epothilone B

Inhibitors in 4:1 (v/v) 0.75 M MSG/DMSO were pre-incubated with radiolabeled compound in a final volume of 50 μL for 10 min at 37 °C. To this mixture, 50 μL of microtubules that were formed as described above were added and the resulting mixture was incubated for 30 min at 37 °C. Reaction mixtures were centrifuged as described above, and a 50 μL aliquot of supernatant

was analyzed by scintillation spectrometry. The equilibrium inhibition constant (K_i) values for dictyostatin and its analogues were determined using a modified Hanes analysis:[75]

$$[S]/\nu = K_d \times (1 + [I]/K_i) + [S]$$

[S] = Free concentration of [^{14}C]epothilone B

ν = Fractional saturation of microtubule sites by epothilone B and inhibitor.

GraphPad Prism was used for linear regression, providing the $-K_d$ value as the x-intercept in the absence of inhibitor. The x-intercept in the presence of inhibitor, $-K_d(1+[I]/K_i)$, was used to calculate the K_i values.

Saturation Binding Experiments with [^{3}H]Discodermolide

Determination of the K_d for discodermolide was determined as described above for epothilone B. A stock solution of 50 μM [^{3}H]discodermolide was prepared in 50% DMSO. Samples of [^{3}H]discodermolide at 8 – 0.025 μM were prepared in 4:1 (*v/v*) 0.75 M MSG/DMSO (total volume 50 μL), and incubated with 0.2 mg/mL preformed microtubules. Samples were processed and analyzed as described above for [^{14}C]epothilone B. A K_i value was determined for 6-*epi*-dictyostatin in the presence of [^{3}H]discodermolide using the method described above for competitive studies utilizing [^{14}C]epothilone B.

Saturation Binding Experiments with [^{3}H]5HPP-33 in the tubulin only system

Determination of the K_d value for 5HPP-33 in the tubulin only system was performed as described previously.[76] A stock solution of 45 mM [^{3}H]5HPP-33 in DMSO was prepared and

from this samples of [^{3}H]5HPP-33 between concentrations of 200-1 μM were prepared in DMSO. Reaction mixtures (total volume 0.32 mL) contained indicated concentration of [^{3}H]5HPP-33, 1.0 mg/mL tubulin, 1% DMSO, and a buffer containing 0.1 M MES, pH 6.9, and 0.5 mM $MgCl_2$. Reaction mixtures were incubated for 30 min at 0 ^oC, and 0.15 mL aliquots were applied in duplicate to Microcon centrifugal filtration units equipped with an Ultracel YM-30 regenerated cellulose membranes. The samples were spun at 14,000 x *g* for 12 min at 4 ^oC, and 80 mL of the filtrate was used to determine concentration of free ligand by scintillation spectrometry. The amount of non-specific binding was determined from samples prepared in the absence of tubulin and processed as described above. Data was analyzed using the Hill equation that describes biphasic dose response:

$$\text{Bound} = ((B_{max1} \times [S]^{n1})/(K_{d1} + [S]^{n1})) + ((B_{max2} \times [S]^{n2})/(K_{d2} + [S]^{n2}))$$

Determination of [^{3}H]5HPP-33 Binding to MAPs

The binding of 5HPP-33 to MAPs was determined as described for the binding in the tubulin only system. Samples of [^{3}H]5HPP-33 were prepared at concentrations ranging from 50-200 μM in DMSO. The 0.32 mL reaction mixtures contained indicated concentrations of [^{3}H]5HPP-33, 2.0 mg/mL of MAPs, 1-3% DMSO, and 0.1 M MES, pH 6.9, containing 0.5 mM $MgCl_2$. The mixtures were incubated for 30 min at room temperature, and processed in duplicate at room temperature as described above. The binding of the compound to MAPs was determined from the amount of bound ligand in the presence of MAPs subtracted from the amount of bound ligand in the absence of MAPs.

Saturation Binding Experiment with [^{3}H]5HPP-33 in the tubulin plus MAPs system

The determination of a K_d value for 5HPP-33 in the presence of tubulin and MAPs was performed as described above. Samples of [^{3}H]5HPP-33 were prepared between concentrations of 200 - 1 μM in DMSO from a 50 mM stock solution. The 0.32 mL reaction mixture contained the indicated concentrations of [^{3}H]5HPP-33, 1.0 mg/mL tubulin, 0.75 mg/mL MAPs, 1% DMSO and 0.1 M MES, pH 6.9, containing 0.5 mM $MgCl_2$. The reaction mixture was incubated for 30 min at 0^{o}C and processed as described above. The data was analyzed using the Hill equation:

$$\text{Bound} = (B_{max} \times [S]^n)/(K_d + [S]^n)$$

[^{3}H]Paclitaxel Competitive Inhibition Binding Assay

The competitive inhibition assay was performed as described previously.[77] To determine the ability of 5HPP-33 to displace paclitaxel from its binding site on the microtubule, a solution of 8 μM [^{3}H]paclitaxel solution was prepared in 0.75M MSG, pH 6.6. HPP-33 was prepared in 25% (v/v) DMSO and diluted into 0.75M MSG to give final concentrations of 4 μM and 20 μM. Discodermolide (4 μM) was prepared in the same mixture of DMSO and MSG and used as a positive control. The test agents (25 μL) were mixed with the [^{3}H]paclitaxel (25 μL) and warmed to 37 °C. Microtubules were preformed by incubating 0.75 M MSG, 0.2 mg/mL tubulin and 40 μM ddGTP at 37 °C for 30 min. The preformed microtubules (50 μL) were added to the mixture of test agents and tracer, then incubated at 37 °C for 30 min. The reaction mixture was centrifuged at 14,000 rpm for 20 min at room temperature. A 50 μL aliquot of supernatant was carefully removed and the amount of free [^{3}H]paclitaxel was obtained using scintillation

spectrometry. Bound [^{3}H]paclitaxel was calculated from the amount of total [^{3}H]paclitaxel minus the amount of [^{3}H]paclitaxel found in the supernatant. Percent inhibition was calculated from bound values normalized to controls:

% Inhibition = {[1-(bound test agents/bound control)]*100}

[^{3}H]Colchicine Percent Inhibition Binding Assay

The [^{3}H]colchicine percent inhibition binding assay was performed as described previously.[71] To determine the ability of 5HPP-33 to displace colchicine from its binding site, a reaction mixture containing 1 μM tubulin in 1M MSG, pH 6.6, containing 0.1 M glucose-1-phosphate, 1 mM $MgCl_2$, 1 mM GTP and 0.5 mg/mL bovine serum albumin was prepared. The reaction mixture was incubated with 5 μM [^{3}H]colchicine and test agent at 37 °C for 10 min. Podophyllotoxin at 5 μM was used as a positive control. After incubation, the solution was filtered through two stacks of diethylaminoethyl (DEAE)-cellulose filters. The filters trapped [^{3}H]colchicine bound to the protein. Each set of filters was immersed in scintillation cocktail and the radioactive counts determined using scintillation spectrometry. Percent inhibition was calculated from the bound values normalized to the control values (with no inhibitor added).

Radiolabeled Vinca Domain Binding and [^{3}H]5HPP-33 Competitive Binding Assay

The binding of radiolabeled ligand to tubulin was measured by centrifugal gel filtration as described by Bai *et al.* on 2 mL columns of sephadex G-50 (superfine).[78] Each 0.32 mL reaction mixture contained 1.0 mg/mL (1.5 mg/mL for [^{3}H]5HPP-33 binding assay) bovine brain tubulin in 0.1 M MES, pH 6.9, containing 0.5 mM $MgCl_2$ that was treated with 5 μM inhibitor and 10 μM [^{3}H]vinblastine, [^{3}H]dolastatin 10, or [^{3}H]5HPP-33 predissolved in DMSO (final

concentration 1%, v/v). The mixture was incubated for 30 min at room temperature. Aliquots (0.15 mL) of the reaction mixture were applied in duplicate to 2 mL Sephadex G-50 (superfine) columns preswollen with 0.1 M MES, pH 6.9, containing 0.5 mM $MgCl_2$ and 1% DMSO. The columns were centrifuged at 800x*g* for 4 min and the protein concentration in the effluent was determined using the bicinchoninic acid assay. The amount of radiolabeled ligand bound to tubulin was determined using scintillation spectrometry. Each value represents the mean $\pm$ SD of four determinations. The average stoichiometry of binding in the control reaction mixture was 0.63 mole of [^{3}H]vinblastine or [^{3}H]dolastatin 10 per mole of tubulin. The average stoichiometry of binding in the control reaction mixture was 0.011 mole of [^{3}H]5HPP-33 per mole of tubulin. Inhibition was calculated as the percent difference relative to that of the control incubation with DMSO (*i.e.*, without test agent -- assigned as 0% inhibition).

2.3.8 Quantitative structure-activity relationships analyses

Molecular modeling and quantitative structure activity relationships (QSAR) analyses were performed with the Cerius^2 suite of programs (v. 4.05, Accelrys, Inc., San Diego, CA) utilizing the Merck Molecular Force Field/CHARMM, the adopted-basis Newton-Raphson approach to molecular mechanics minimizations in a dielectric field = 1, rigid body superimpositions based on atom similarities, the MOPAC93 suite of semi-empirical molecular orbital algorithms, and the genetic function approximation as previously described.[40]

3.0 CELL-BASED AND BIOCHEMICAL STRUCTURE ACTIVITY ANALYSES OF ANALOGUES OF THE MICROTUBULE STABILIZER DICTYOSTATIN

3.1 ANALOGUES MADE PRIOR TO IDENTIFICATION OF THE ACTUAL STRUCTURE OF DICTYOSTATIN

Prior to the elucidation of the exact structure of dictyostatin, the Curran group synthesized hybrids of discodermolide and dictyostatin.[64] At this point, the only template for the structure of dicytostatin was Pettit's partially assigned configuration as shown in Figure 9.[79] The design of these early hybrids focused on constraining the discodermolide structure by hypothetical condensation of the lactone carbonyl with the amine. Removal of the C6, C7, and C9 hydroxyl groups to form the analogue 6,7,9-deshydroxy-2,3,4,5,-tetrahydro-15*Z*,16-normethyldicytostatin was based on previous structure-activity relationship (SAR) data for discodermolide, which indicated that the omitted groups are not important for biological activity.[64] SAR studies are applied to search for the minimum structural elements that in this case contribute to biological activity, cytotoxicity and retention of affinity to the taxoid site.[80] 7-*epi*-9-Deshydroxy-15*Z*,16-normethyldictyostatin was biologically active with GI_{50} values, the amount of compound needed to inhibit growth inhibition by 50% as compared to control, of 1 μM in the breast and ovarian cancer cell lines tested. The analogues possessed a modest ability to compete with [^{3}H]paclitaxel for its binding site.

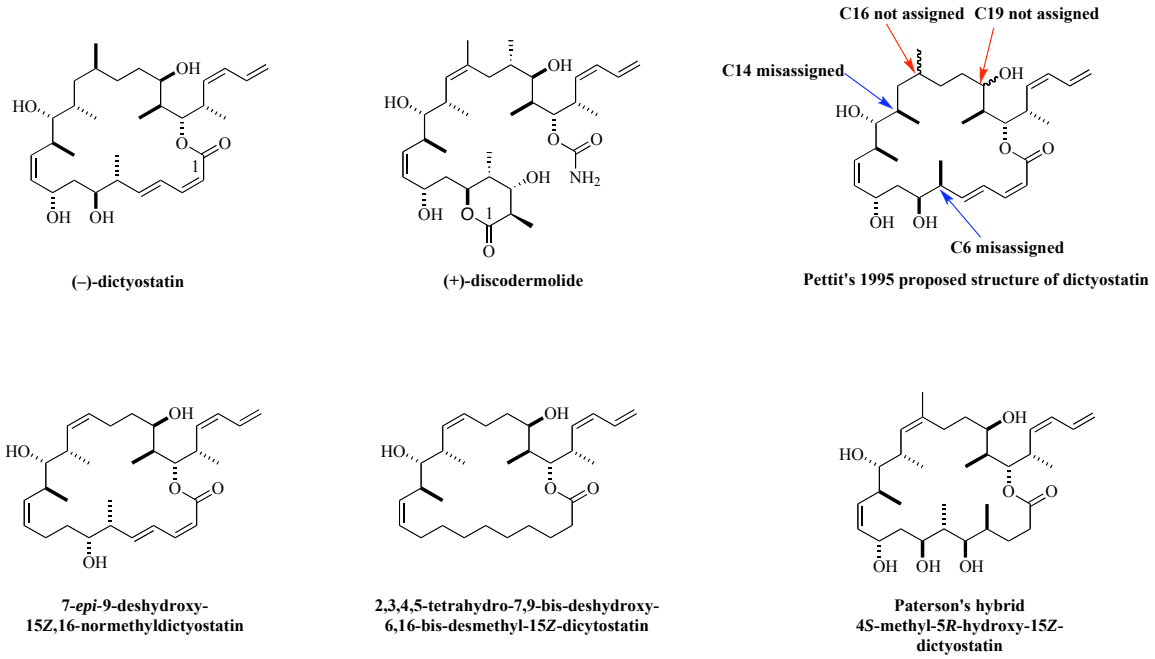

Figure 9. Dictyostatin/discodermolide hybrids before and after the elucidation of the structure of (–)-dictyostatin.

In 2007, Paterson *et al.* expanded on Curran's work by synthesizing a dictyostatin/discodermolide hybrid containing the full linear sequence (C2-C24) of discodermolide.[81] Its three-dimensional structure nicely superimposes with that of discodermolide, but it does have GI_{50} values seven times higher than that of discodermolide in the cancer cell lines tested.

Based on Pettit's structure, the Curran's group next step was to synthesize analogues to elucidate the structure of dictyostatin through the evaluation of biological activity.[62] These analogues were 6,16-bis-*epi*-dictyostatin, 2*E*,6,14-bis-*epi*-dictyostatin, 6,14,19-tris-*epi*-dicytostatin, and 2*E*,6,14,19-tris-*epi*-dicytostatin. These analogues are shown in Figure 10.

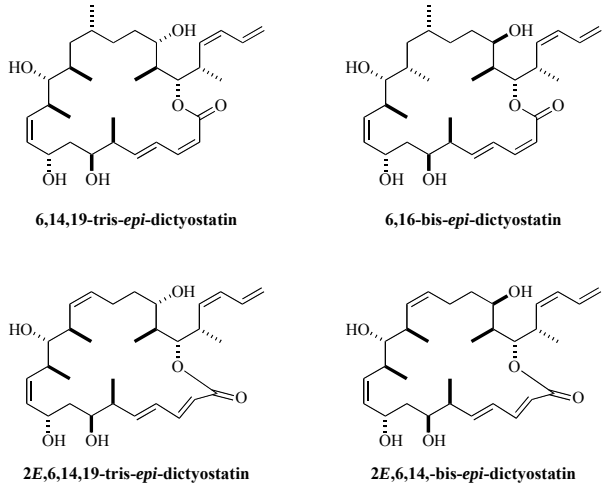

Figure 10. First generation analogues of dictyostatin based on Pettit's proposed structure.

These analogues were then tested to determine their biology and their potential as microtubule stabilizers. Agents were tested in the ovarian cancer cell line 1A9 and in mutants of these cells that are resistant to paclitaxel. The cell lines 1A9/Ptx10 (Phe270 to Val) and 1A9/Ptx22 (Ala364 to Thr) contain mutations within the paclitaxel binding site on β-tubulin.[52] 2*E*,6,14-*epi*-dictyostatin is the only analogue that had any significant biological activity with GI_{50} values under 1 μM in all cell lines tested. Tubulin polymerization assays were performed in the presence and absence of MAPs to determine if the analogues induce polymerization and form cold stable polymer. All of the analogues were inactive in this assay when compared to discodermolide and paclitaxel. A competitive inhibition assay revealed that the analogues did not possess any ability to compete with [^{3}H]paclitaxel for its binding site on β-tubulin.

3.2 SYNTHESIS OF DICTYOSTATIN ANALOGUES FOR STRUCTURE-ACTIVITY RELATIONSHIP STUDIES

After the elucidation of the structure, synthesis and biological characterization of dictyostatin, the Curran and Paterson groups synthesized a number of analogues to provide clues into the SAR of dictyostatin.[59-62, 64, 72, 82-84]

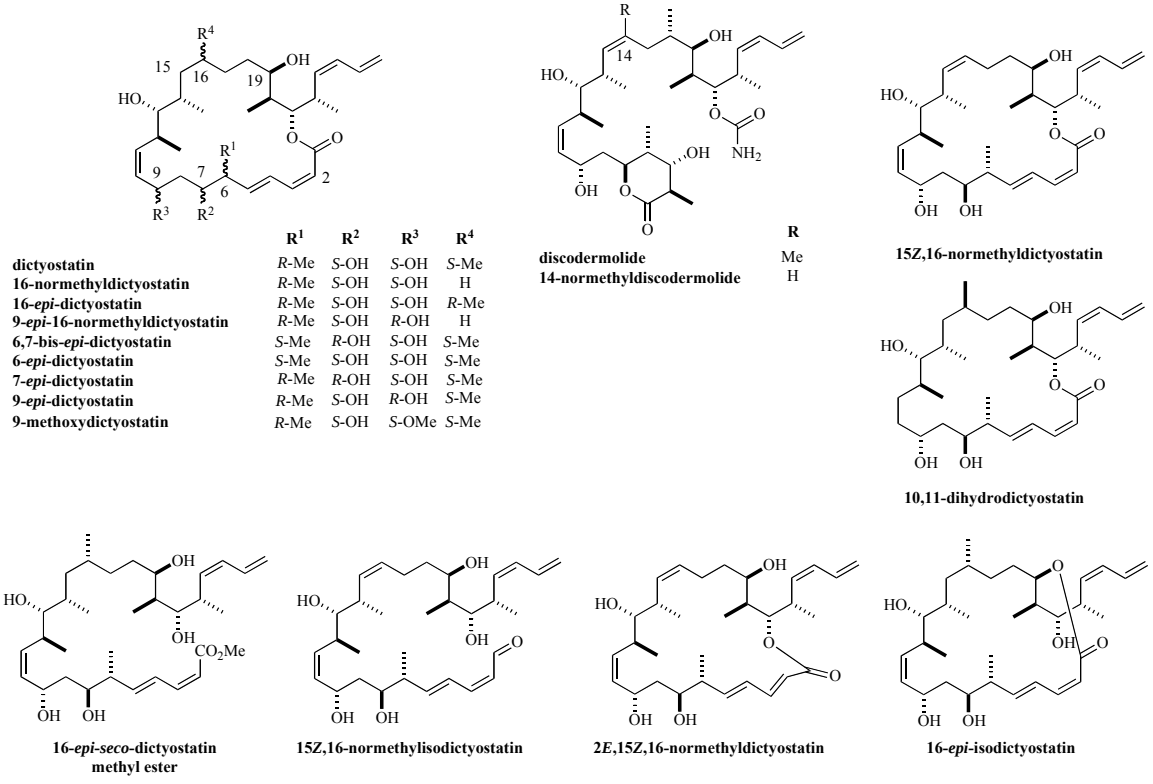

Figure 11. Dictyostatin analogues generated for use in SAR studies.

The obvious way to begin the SAR studies of dictyostatin was to employ what was already known about discodermolide, due to the wealth of research done on its SAR, and exploit the key differences between the two compounds. It is well known that changes to the C7 hydroxyl group of discodermolide do not change the cytotoxic behavior of the molecule, and that some modifications actually enhance activity.[85, 86] C9 is the corresponding stereocenter in dictyostatin,

and Paterson *et al*. synthesized three analogues containing modifications there: 9-*epi*-dictyostatin, 9-methoxydictyostatin and 9-normethyldicytostatin.[87] Inversion of the stereocenter at C9 causes a significant drop in cytotoxicity in the cancer cell lines tested, which suggests that the C9 configuration is important to maintain biological activity. The C9 methoxy analogue is almost as active as dictyostatin, with GI_{50} values in the low nanomolar range. This analogue is active in the paclitaxel-resistant cell line NCI/ADR, which overexpresses the P-glycoprotein pump.

From the SAR studies of discodermolide, it is known that the alkene at C13-14 is necessary for retention of biological activity, but reduction of the C8-C9 double bond produces a compound that retains activity.[88] Using this information, Paterson *et al.* designed 10,11-dihydrodictyostatin, hypothesizing that this simplification would not alter biological activity.[84] This analogue is more active than discodermolide in the pancreatic and colon cancer cell lines tested, but does not retain activity in the NCI/ADR cell line. This suggests that the C10-C11 alkene is necessary for dictyostatin to avoid becoming a substrate for the P-gylcoprotein pump.

The C1-C9 chain is one of the main structural differences between the two natural products, and dictyostatin analogues designed to examine this region were epimers at C6, C7 and C9, and C2:3 geometric isomers. From discodermolide SAR studies, it is has been established that removal of the C14 methyl group does not decrease cytotoxicity in the cancer cell lines tested. When the 14-normethyldiscodermolide was tested in paclitaxel resistant cell lines, however, cytotoxicity was greatly decreased (IC_{50} values in the micromolar range).[89] From this finding, the Curran and Paterson groups were prompted to synthesize 16-normethydictyostatin (Paterson's group refers to this compound as 16-desmethydictyostatin.[83,87] Curran's group expanded on this work with the synthesis of a series of C16 analogues. Since discodermolide is

an open chain analogue of the macrolactone of discodermolide, a 16-*epi* open chain methyl ester analogue was also synthesized. Discodermolide possesses a C13:14 *Z*-alkene, which is missing in dictyostatin, and an analogue was synthesized containing a C15:16 *Z*-alkene. In theses syntheses, two analogues with dictyostatin's macrolactone contracted to 20 members were also made (the isodicytostatins).[61]

Due to the loss in cytoxic activity of 14-normethyldicodermolide analogue in 1A9 cell containing the Phe270 mutation to Val, it can be hypothesized that changes to the C16 region of dictyostatin would also be lead to a loss in cytotoxicity. Although changes to the C9 stereocenter of dictyostatin had already been investigated changes to the C6 and C7 stereocenters had not. It can be hypothesized that changes to this region will not affect the biological activity because signication changes to the lactone region of discodermolide are well tolerated as long as the lactone remains intact.[88] To examine in detail the effects of these targeted structural modifications on biological activity and the interaction with the proposed target, quantitative multiparameter immunofluorescence assays were used to measure mitotic arrest and nuclear morphology in conjunction with *in vitro* tubulin assembly and displacement studies using the taxoid site-binding agents epothilone B and discodermolide. During this evaluation, the saturation binding kinetics of epothilone B and discodermolide were also characterized. Quantitative structure-activity relationship (QSAR) and molecular modeling studies were employed to gain insight into the correlation between the structure of dictyostatin and its analogues to their cytotoxic effects.

3.3 CELLULAR EFFECTS OF DICTYOSTATIN AND ITS ANALOGUES DETERMINED BY MULTIPARAMETER IMMUNOFLOURESCENCE MICROSCOPY

Multiparameter high content analyses, a tool to acquire, manage and retrieve information from multiparametric experiments to yield information about the activity and spatial regulation of multiple targets in cells, were used to characterize the responses of tumor cells to the agents.[61] This work was performed in Dr. Andreas Vogt's lab in the Department of Pharmacology, School of Medicine at the University of Pittsburgh. This assay provided information on the effects of such agents on microtubule mass, histone H3 phosphorylation and nuclear morphology. The procedure is described in detail in Chapter 2. In short, HeLa cells were grown in 384-well microtiter plates and were treated with each compound for 21 h. The cells were fixed, their nuclei stained with Hoechst 33342, permeabilized, microtubules and phosphohistone H3 were immunostained, and FITC- and Cy3-conjugated secondary antibodies were added. From the Hoechst staining, a nuclear mask was generated defining the area used to determine microtubule mass and percentage of histone H3 phosphorylation. Microtubule mass was determined from the cells average (FITC) pixel intensity in cells. The percentage of histone H3 phoshorylation was determined from the number of cells with a higher pixel intensity for Cy3 than the average plus one standard deviation seen within vehicle-treated cells. Using a range of concentration of test agents, the minimum detectable effective concentration (MDEC) was determined. The MDEC value is the minimum concentration at which each agent causes a response in excess of vehicle-treated control cells.[70] The MDECs for nuclear condensation, histone H3 phosphorylation, and changes in microtubule morphology for dictyostatin and its analogues are shown in Table 1. As a measure of toxicity, cell densities were measured as Hoechst 33342-stained nuclei per imaging field. The toxicity measurements in HeLa cells were consistent with those reported for other

human cancer cell lines examined with the 3-(4,5-dimethylthiazol-2-yl)-5-(3-carboxymethoxy-phenyl)-2-(4-sulfophenyl)-2*H*-tetrazolium (MTS) assay, where the decrease in absorbance at 490 nm was seen after cells treated with drug were exposed to the mitochondrially-activated dye MTS along with the electron acceptor *N*-methylphenazine.[61, 62]

Toxicity measurements and the MDEC values generated from this initial screen allowed for the quick assessment of the analogues' abilities to increase histone H3 phosphorylation, cause cell death, and increase microtubule mass. Increases in the levels of histone H3 phosphorylation and microtubule mass are indicators of more cells undergoing mitosis compared to control, and are fundamental markers of microtubule perturbing agents. As shown from the values in Table 1, The *S* configuration of the C16 methyl group, C2:3*Z* geometry, and a 22-membered ring were essential for retention of biological activity.[61] From this data, the four most potent analogues were chosen for further evaluation: 6-*epi*-dictyostatin, 7-*epi*-dictyostatin, 16-normethyldictyostatin and 15*Z*,16-normethyldictyostatin.

Table 1. Potency of dictyostatin and its analogues against HeLa cells using multiparameter fluorescence microscopy.

	EC_{50} (nM)		**MDEC (nM)**	
Compound	**Cell Density**	**Nuclear Conden-sation**	**Mitotic Index**	**Micro-tubule Mass**
Paclitaxel	10.4 ± 1.9	3.9 ± 2.0	3.5 ± 1.2	5.2 ± 0.4
Dictyostatin	9.2 ± 6.6	3.9 ± 1.0	5.8 ± 1.5	5.4 ± 1.9
16-*epi*-dictyostatin	1872 ± 449	1132 ± 66	1032 ± 173	1278 ± 181
16-*epi*-open chain dictyostatin	>5000	>5000	>5000	>5000
16-*epi*-isodictyostatin	>5000	>5000	>5000	>5000
16-normethyldictyostatin	34.7 ± 6.2	23.7 ± 8.8	24.1 ± 5.4	25.0 ± 9.0
7-*epi*-dictyostatin	17.5 ± 1.9	7.7 ± 2.1	8.5 ± 3.9	8.0 ± 3.2
6-*epi*-dictyostatin	8.9 ± 2.7	4.5 ± 1.9	3.8 ± 2.8	4.0 ± 0.9
2*E*,3,15*Z*,16-normethyldictyostatin	896 ± 135	738 ± 214	520 ± 95	647 ± 106
15*Z*,16-normethyldictyostatin	23.9 ± 15.5	12.6 ± 5.2	9.3 ± 0.2	11.7 ± 1.7
9-*epi*-15*Z*,16-normethyldictyostatin	>5000	>5000	>5000	>5000
15*Z*,16-normethylisodictyostatin	>5000	>5000	>5000	>5000

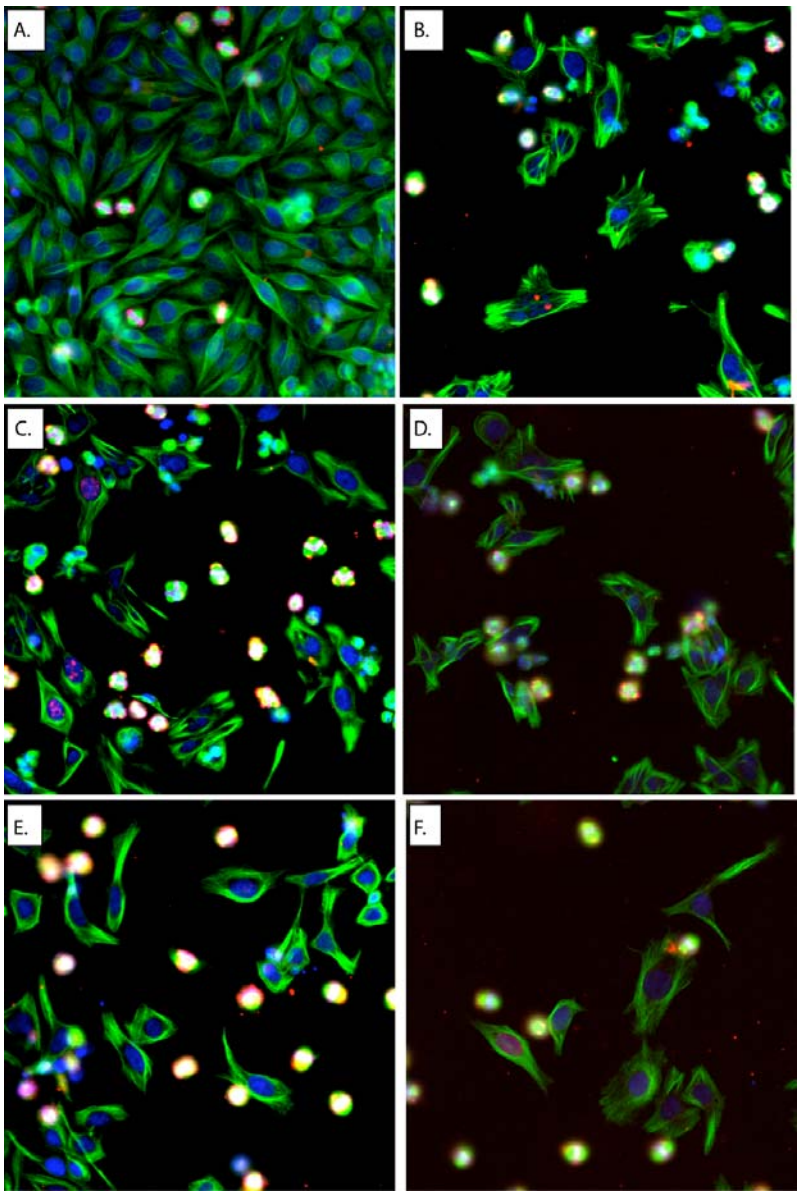

Figure 12. Immunofluorescence images of HeLa cells treated with dictyostatin and analogues. HeLa cells were treated with vehicle (A) or equipotent concentrations of dictyostatin (B), 6-*epi*-dictyostatin(C), 7-*epi*-dictyostatin (D), 15*Z*,16-normethyldictyostatin (E), or 16-normethyldictyostatin (F). The nucleus was stained with Hoechst (blue) and microtubules (green), and phosphohistone H3 (red) were stained with fluorescently labeled secondary antibodies

Figure 12 illustrates the mitotic phenotype observed after treatment of cells with the four test agents. Equipotent concentrations were picked to illustrate similar phenotypes for each test agent as compared to control cells (treated with DMSO only). Cells were immunostained for α-tubulin (green) and phospho-histone H3, and the nuclei were stained with Hoechst (blue).

Vehicle-treated cells had highly organized microtubules and a low percentage of mitotic cells. All compounds tested caused a heterogenous response of microtubule disorganization, increased numbers of phospho-histone H3 positive cells, enhanced chromatin condensation and nuclear fragmentation. Images shown are representative from a single experiment that was repeated twice with each experiment yielding similar results.

Cells treated with dictyostatin (2B, 31 nM) showed microtubule bundling and abnormal spindle formation, characteristic of cells treated with a microtubule stabilizer. Panels C-F represent the images obtained when HeLa cells were treated with 6-*epi*-dictyostatin (2C 7.8 nM), 7-*epi*-dictyostatin (2D, 15.6 nM), 15*Z*,16-normethyldictyostatin (2E, 19.5 nM) or 16-normethyldictyostatin (2F, 31 nM). All compounds produced microtubule bundling and abnormal spindle formation. These compounds caused increased mitotic indices, condensed nuclei, an increased microtubule mass, and a loss of cell density at nanomolar concentrations. 6-*epi*-Dictyostatin and 7-*epi*-dictyostatin affected all parameters at concentrations comparable to dictyostatin, whereas the 16-normethyl derivatives had less activity. It was a surprise to find that 15Z,16-normethyldictyostatin was more potent in all aspects than 16-normethyldictyostatin, because both compounds had a loss at C16 of the methyl group. Thus, high-content analysis provided a rapid and efficient means to generate cellular SAR data on mitotic arrest, microtubule morphology, and cytotoxicity. It demonstrated that structural modifications in the 6, 7, 15, and 16 positions did not significantly reduce compound activity in cells.

3.4 DETERMINATION OF THE ABILITY OF DICTYOSTATIN AND ITS ANALOGS TO INDUCE TUBULIN ASSEMBLY AND FORM COLD STABLE POLYMER

Under the hypothesis that the potent analoges would retain the ability to hypernucleate and stabilize polymer a microtubule polymerization assay was performed. *In vitro* tubulin assembly assays were performed with the agents under conditions in which polymerization does not occur in the absence of test agents and compared their activities to that of paclitaxel (△) as shown in Figure 13. Tubulin polymerization assays register microtubule formation as a change in absorbance, which is a consequence of the polymer scattering light as it is formed.

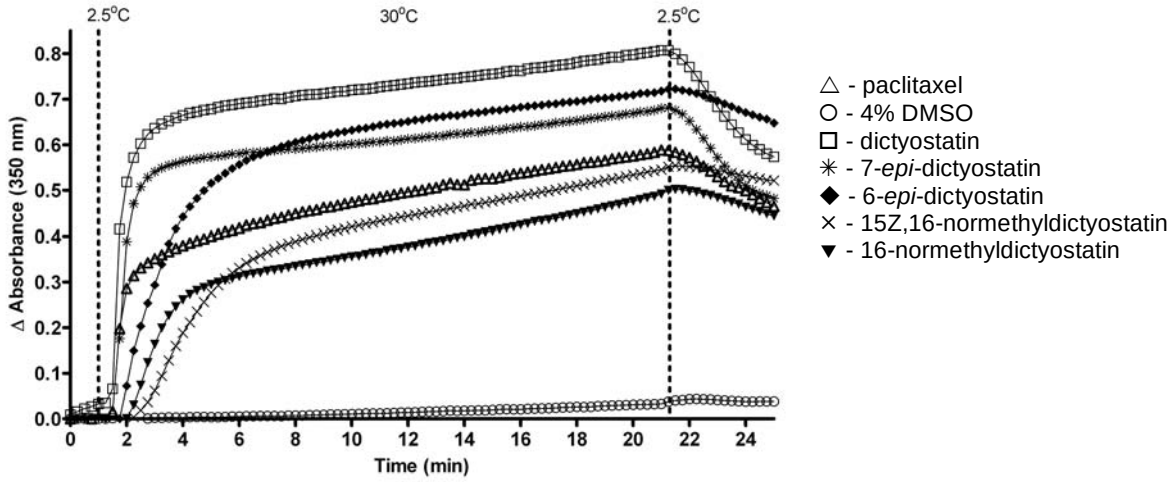

Figure 13. Tubulin polymerization assay to determine effects of dictyostatin and its analogues on tubulin assembly.

In a temperature-controlled spectrophotometer reading absorbance at 350 nm every 15 sec, isolated bovine brain tubulin was cooled to 2.5 °C and test agents were added at time zero to a final concentration of 10 μM. The test agent-containing tubulin solutions were rapidly warmed to 30 °C to induce assembly and, after 20 min at 30 °C, cooled back to 2.5 °C. To ensure that

polymer was formed only in the presence of test agents, 4% DMSO (○) was used as a negative control. Three agents were more active than the positive control paclitaxel (△). Dictyostatin (□) was the most potent compound in terms of nucleating and polymerizing ability, closely followed by 7-*epi*-dictyostatin (✳) and 6-*epi*-dictyostatin (◆). There were some slight differences between the C6 and C7 epimers. 7-*epi*-Dictyostatin caused polymer to form more rapidly than did 6-*epi*-dictyostatin, but the extent of polymerization caused by 6-*epi*-dictyostatin was greater. The polymer formed with 6-*epi*-dictyostatin appeared more stable against cold depolymerization than the polymer from 7-*epi*-dictyostatin or dictyostatin itself. The nucleating and polymerizing activities of 15Z,16-normethyldictyostatin (×) and 16-normethyldictyostatin (▼) were reduced, but still comparable to those of paclitaxel. Polymer formed in the presence of these two compounds was cold stable.

From this study it was concluded that 6-*epi* and 7-*epi*-dictyostatin retain microtubule stabilizing and hypernucleating abilities. There was a slight loss in these ablities with the C16 analogues but there activity was still comparable to paclitaxel. This data provides evidence that the analogues of dictyostatin are working in the same manner as the parent compound.

3.5 CHARACTERIZATION OF [^{14}C]EPOTHILONE B SATURATION BINDING TO MICROTUBULES

As discussed in the introduction, dictyostatin and the four analogues have the ability to displace radiolabeled paclitaxel from preformed microtubules *in vitro*. [63] It was hypothesized that based on previous evidence that epothilone B can competively compete with [^{3}H]paclitaxel for its site, dictyostatin and its analogues should competitively compete with epothilone B. These preliminary observations were expanded upon by performing detailed binding kinetics using [^{14}C]epothilone B.

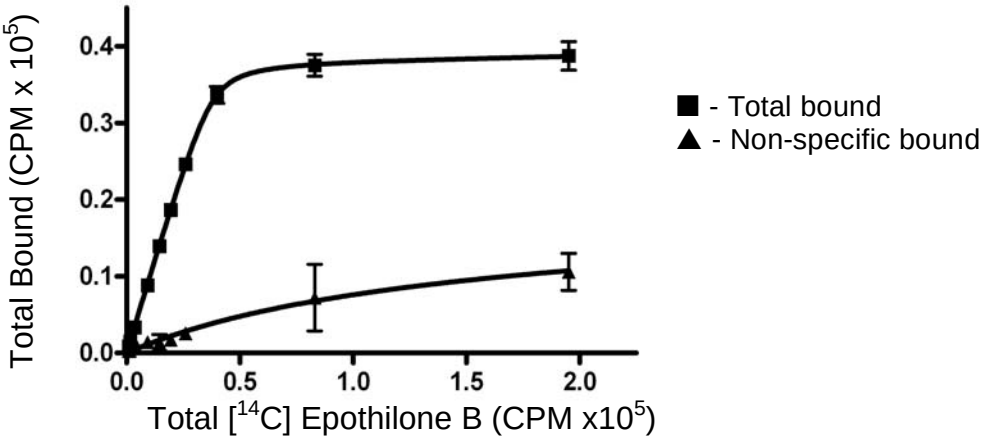

Figure 14. Saturation binding data for the binding of [^{14}C]epothilone B to microtubules.

Epothilone B has an even higher affinity to the taxoid site on tubulin than does paclitaxel.[91] The saturation binding kinetics of [^{14}C]epothilone B has not been reported. Isolated tubulin was incubated with radiolabeled [^{14}C]epothilone B and the amount of protein-bound radioactivity quantified as described in Chapter 2. A version of the saturation binding equation that was

modified to account for ligand depletion, known as Swillen's equation, was employed to determine the K_d value for the binding of [^{14}C]epothilone B to microtubules. As shown in Figure 14, fitting the data using Swillen's modified equation, which simultaneously fits total binding and nonspecific binding, yielded a K_d value for epothilone B of 36.04 $\pm$ 1.58 nM. The x-axis shows the total [^{14}C]epothilone B added and the y-axis the amount of ligand bound. Nine concentrations in the range of 5 nM to 2 μM of the radiolabeled compound epothilone B (■) were used to determine the K_d value. Nonspecific binding was determined by competition with 8 μM discodermolide (▲). Each data point shown is the mean of three independent experiments ± S.D. The extent of non-specific binding was estimated by measuring the amount of [^{14}C]epothilone B bound to microtubules in the presence of 8 μM discodermolide. As the K_d value of paclitaxel is reported to be between 0.06-0.1 μM and since the relative affinities of agents for the taxoid site follows the order paclitaxel < epothilone B < discodermolide, the K_d value obtained in these experiments for epothilone B was considered reasonable and acceptable.[80]

3.6 DETERMINATION OF INHIBITION CONSTANTS FOR DICTYOSTATIN AND ITS ANALOGUES UTILIZING [^{14}C]EPOTHILONE B IN COMPETITION EXPERIMENTS

The K_i values for dictyostatin and its analogues were determined using the modified Hanes analysis method of Edler *et al*.[75] The method uses the free concentration of radioligand instead of the total concentration, and also accounts for the free inhibitor concentrations. Concentrations used ranged from 0.25-12 μM for the inhibitors dictyostatin, 6-*epi*-dictyostatin, and 7-*epi*-dictyostatin. For the less potent inhibitors, concentrations ranged from 1-50 μM. [^{14}C]Epothilone B concentrations were 1, 2, 2.5 and 3 μM for all experiments. As shown in Figure 15, plots of free concentration of [^{14}C]epothilone B versus free substrate divided the fractional saturation (instead of enzyme velocity) for 6-*epi*-dictyostatin yielded plots of parallel lines with slopes close to 1.

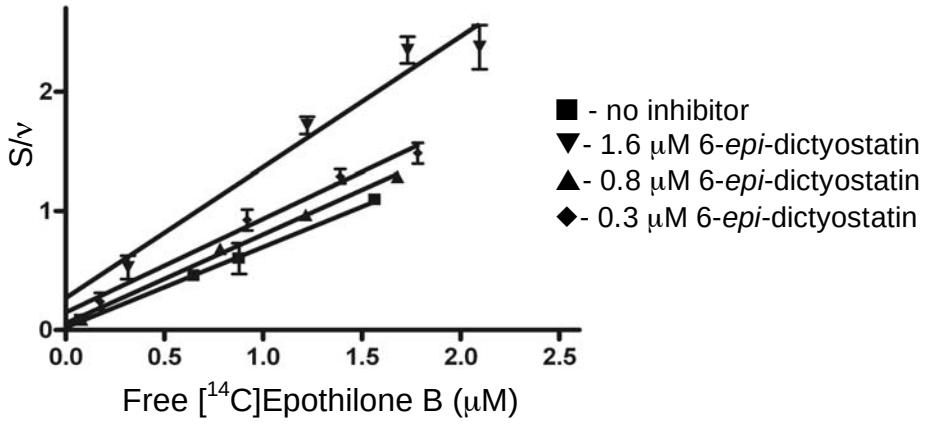

Figure 15. Hanes plot of the inhibition of binding of [^{14}C]epothilone B to microtubules by 6-*epi*-dictyostatin.

The fractional saturation was calculated from the total amount of tracer added minus the free concentration of tracer counted. Experiments were performed as described in Chapter 2. K_is were determined from the x-intercept equal to $-(K_d(1+[I]/K_i)$. The legend is as follows: (■), no inhibitor μM; (▼), 1.6 μM 6-*epi*-dictyostatin; (▲), 0.8 μM 6-epi-dictyostatin; and (◆), 0.3 μM 6-*epi*-dictyostatin. The K_d value for [^{14}C]epothilone B, determined from the negative intercept on the x-axis, was 50 ± 20 nM, close to the value obtained from the saturation experiments. As shown in Table 2, 16-normethyldictyostatin and 15*Z*,16-normethyldictyostatin gave the highest K_i values, reflecting their reduced binding affinity.

Table 2. Equilibrium inhibition constants for dicytostatin and its analogues calculated from Hanes analysis of [^{14}C]epothilone B competition experiments.

Compound	**Ki (μM)**
15*Z*,16-normethyldictyostatin	4.47 ± 0.28
16-normethyldictyostatin	4.55 ± 0.41
6-*epi*-dictyostatin	0.48 ± 0.07
7-*epi*-dictyostatin	0.93 ± 0.31
dictyostatin	0.07 ± 0.02

The K_i value for 15*Z*,16-normethyldictyostatin was 4.47 ± 0.28 μM and the value for 16-normethyldictyostatin was 4.55 ± 0.41. This data correlates with the tubulin polymerization data, which showed that 16-normethydictyostatin and 15*Z*,16-normethyldictyostatin were the least potent of the compounds in nucleation and microtubule stabilization. Dictyostatin, as expected, showed the highest affinity for the taxoid site with a K_i value of 70 ± 20 nM. Surprisingly although 6-*epi* and 7-*epi* dictyostatin were either as good or better in the high content screening assay, these compounds had substantially lower affinities with K_i values of 480 ± 70 nM and 930 ± 310 nM, respectively. It was concluded, that dictyostatin was a potent competitive inhibitor of [^{14}C]epothilone B binding to β-tubulin. As seen by their slightly lower

K_i values, the 6-*epi*-and 7-*epi*-dictyostatin analogues retained their affinity for the taxoid site. The C16 analogues showed a loss in affinity for binding to isolated tubulin and this was in concordance with the tubulin polymerization study. All analogues showed a competitive nature to the inhibition of [^{14}C]epothilone binding and the slopes of the parallel lines indicated one site competition.

3.7 CHARACTERIZATION OF [^{3}H]DISCODERMOLIDE SATURATION BINDING TO MICROTUBULES

An attempt was made to elucidate the binding of [^{3}H]discodermolide to microtubules. Dictyostatin is the structural cousin of discodermolide and the kinetics of dicytostatin binding to the microtubule might be analogous to those of discodermolide. The saturation binding kinetics of [^{3}H]discodermolide has not been previously determined. As described in Chapter 2, 8 μM-25 nM of [^{3}H]discodermolide were incubated with 0.2 mg/mL preformed microtubules for 30 min, centrifuged for 30 min, and then supernatant removed for scintillation spectrometry. The concentration of free ligand was calculated from the amount of radioactivity in the supernatant, and from this value the total amount of [^{3}H]discodermolide bound could be determined. The modified Swillen's equation was employed to determine the K_d value for discodermolide binding to microtubules as shown in Figure 16.

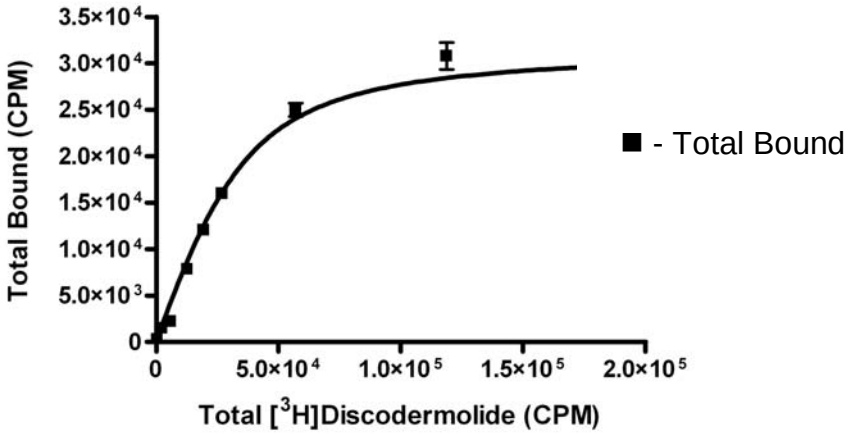

Figure 16. Saturation binding data for the binding of [^{3}H]discodermolide to microtubules.

A K_d value of 0.207 $\pm$ 0.088 μM was obtained, but this value does not accurately reflect what is reported in the literature. This value is higher than obtained for both paclitaxel and epothilone B. From the competitive binding experiments performed in the Day lab and in the literature, it is generally agreed that affinity for the taxoid site goes in the order discodermolide > epothilone B > paclitaxel.[63] One reason for the discrepancy in the K_d value for [^{3}H]discodermolide stems from the inablility to determine its non-specific binding. Non-specific binding is the amount of radioligand bound to sites other than of the specific site of interest. It is usually determined by adding a high concentration (~100 times the K_d) of a known competitor to completely saturate any potential binding sites.[73] Bound radioligand is measured under these conditions for each concentration, and is substracted from the total bound to give the amount of specifically bound to the site of interest. Unfortunately, discodermolide has such a high affinity for the taxoid site that I could not find an inhibitor with enough solubility and affinity to appreciably alter the binding of this radioligand. It is thus not possible with the current supply of inhibitors to accurately determine non-specific binding for [^{3}H]discodermolide.

Although there was not a non-specific binding determination, it is possible that the K_d value obtained could be close to the actual value for [^{3}H]discodermolide binding. The data from competitive binding assays indicates that there is not a known agent that can effectively displace [^{3}H]discodermolide from its binding site.[92,93] There is a possibility that discodermolide's binding to β-tubulin produces a conformational change within the protein that either reduces or prevents the binding of other taxoid site agents. It is possible then that the competitors' ineffectiveness in displacing [^{3}H]discodermolide from its binding site is due to this conformational change and not to a higher affinity for the taxoid site.

3.8 DETERMINATION OF AN INHIBITION CONSTANT FOR 6-*EPI*-DICTYOSTATIN UTILIZING [^{3}H]DISCODERMOLIDE

Although accurate an accurate K_d value could not be determined for discodermolide in the previous binding experiments, Hanes analyses were still employed to determine an inhibition constant for 6-*epi*-dictyostatin as a competitive inhibitor of [^{3}H]discodermolide binding. As shown by the almost parallel lines in Figure 17, 6-*epi*-dictyostatin was a competitive inhibitor of [^{3}H]discodermolide binding to the microtubule with slopes close to 1. The concentrations of 6-*epi*-dictyostatin used in this experiment ranged from 0.25-12 μM and the concentrations of [^{3}H]discodermolide were 0.25 μM, 0.5 μM, 1.0 μM and 2.0 μM.

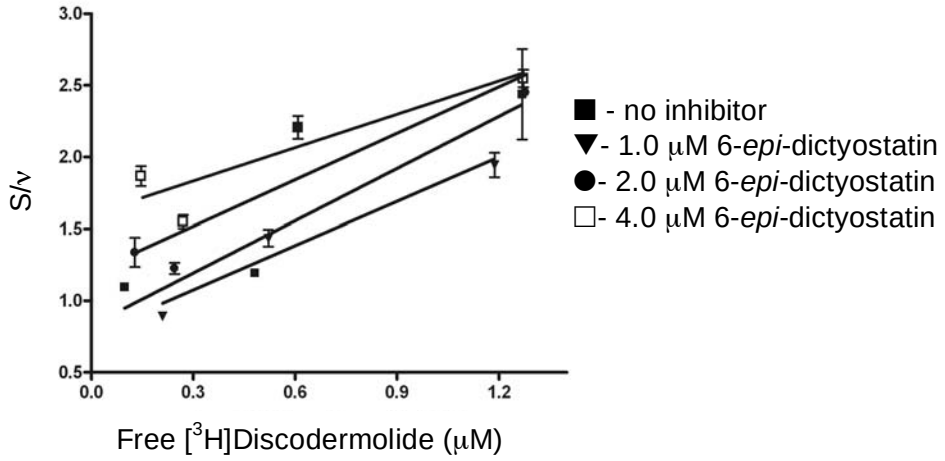

Figure 17. Hanes plot of the inhibition of binding of [^{3}H]discodermolide to microtubules by 6-*epi*-dictyostatin.

Unlike the competitive binding experiments with [^{14}C]epothilone B, there was not significant depletion of the inhibitor, 6-*epi*-dictyostatin, because the concentrations of 6-*epi*-dictyostatin used in this assay did not significantly inhibit the binding of discodermolide. The fractional saturation was calculated from the total amount of tracer added minus the free concentration of tracer counted. A K_i value was determined from the x-intercept equal to $-(K_d(1+[I]/K_i)$. The

legend is as follows: (■), no inhibitor μM; (▼), 1.0 μM 6-*epi*-dictyostatin; (●), 2.0 μM 6-epi-dictyostatin; and (□), 4.0 μM 6-*epi*-dictyostatin. The K_i value for 6-*epi*-dictyostatin was calculated to be 2.38 $\pm$ 0.13 μM. The K_d value for [^{3}H]discodermolide, determined from the negative intercept on the x-axis, was 68 nM.

3.9 QUANTITATIVE STRUCTURE-ACTIVITY ANALYSES

Using the NMR-derived solution structure of discodermolide as a template, molecular models of dictyostatin, its analogues, discodermolide, and 14-normethyldiscodermolide were built.[94] This work was performed in the Day lab by Ms. Kia Montgomery. The lowest energy conformers of the models were found by exhaustive molecular mechanics minimization, and all models were superimposed onto that of discodermolide. The only structures that did not superimpose well were 2*E*,15*Z*,16-normethyldictyostatin and the 20-member iso analogues as shown in Figure 18. A large number of thermodynamic, electronic, steric, and linear free energy descriptors were then calculated for each model.

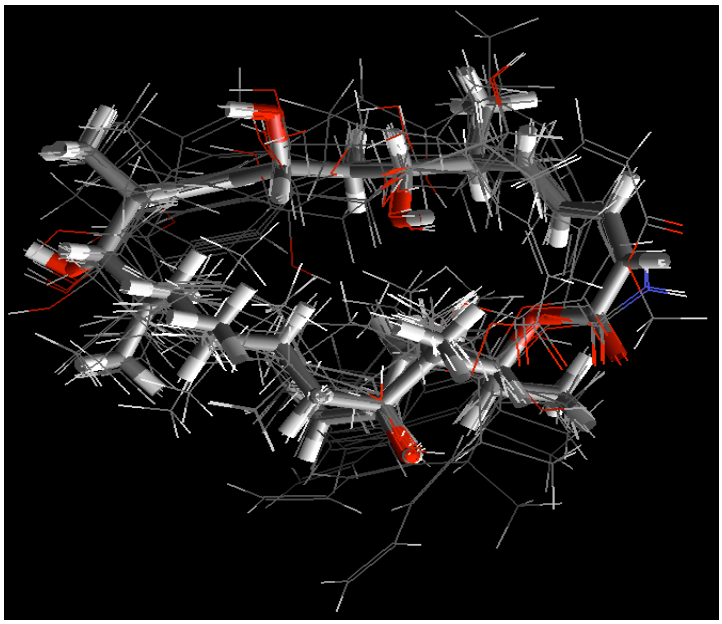

Figure 18. Image generated by superimposing the structures of dictyostatin, the 12 analogues of dictyostatin, and 14-normethydiscodermolide (sticks) onto the solution NMR structure of discodermolide (bars).

At this point a decision was made as to the biological metric to use for the "activity" portion of the QSAR. The 50% growth inhibitory concentrations (GI_{50}) of the compounds against human ovarian carcinoma 1A9 cells, which express wild type β-tubulins, were chosen for this purpose. Because the number of descriptors far exceeded the number of compounds studied, the genetic function approximation (GFA) was used to fit the smallest number of descriptors. In the GFA approach, a random population of equations of given length is generated, their fitness is determined by a number of statistical metrics (in particular Friedman's lack-of-fit and R^2), and the equations are "evolved" by inclusions of combinations from two of the best equations (parents).[39] This process is reiterated (each iteration is termed a "generation") with a given frequency of "mutation" (random descriptor loss or use) incorporated into each iteration until the best descriptors and QSAR equations with the best statistical metrics are found. The five best equations were:

(1) $-(\log GI_{50}) = -0.017328 - 0.41287(\text{rotable bonds}) + 0.091723\,(HF_M OPAC) - 0.223325(HF) + 0.0611096(\text{dipoleMAG})$

(2) $-(\log GI_{50}) = -26.5019 + 0.03692(\text{area}) - 0.328785(\text{rotable bonds}) - 0.04374(HF) + 0.924229(\text{dipoleMOPAC})$

(3) $-(\log GI_{50}) = -26.3842 + 0.1088(\text{area}) + 1.31599\,(\text{dipoleMOPAC}) - 0.353032(MR) + 0.654779(\log P)$

(4) $-(\log GI_{50}) = 1.694349 - 0.305704(\text{rotable bonds}) - 0.135425(HF) + 0.605182(\text{dipoleMOPAC}) - 0.053736(\text{HFMOPAC})$

(5) $-(\log GI_{50}) = -48.6935 + 0.200571(MR) - 0.270041(\text{rotable bonds}) + 1.27617(\text{dipoleMOPAC}) + 0.117247(\text{area})$

where rotable bonds is the number of single bonds contained within the molecule, HF is the heat of formation (the change in enthalpy for forming a molecule from its constituent atoms) calculated with MNDO or with PM3 in MOPAC, log P is the calculated octanol-water partition coefficient, MR is molar refractivity, area describes the Van der Waals area of a molecule, and dipole is the dipole moment of the molecule.

The most significant descriptors in each equation were determined using a "leave-one (descriptor)-out" exercise.[39] This entailed calculating the activity with one of the descriptors set to zero, and then calculating the deviation of the resulting value from the predicted activity when all descriptors were used. From this exercise, the contribution of each descriptor was determined. For equations 2, 3 and 5, the most important contributors to activity were area and molar refractivity. For equations 1 and 4, the most important descriptor was the heat of formation.

The predicted activity values generated from these equations were plotted versus the actual activity in 1A9 ovarian cancer cells to determine the correlations. As shown in Figure 19, a plot of the predicted values generated from equation 1 versus actual values lead to a correlation coefficient (R^2) of 0.943. Values for the R^2 of the other four equations were also >0.93.

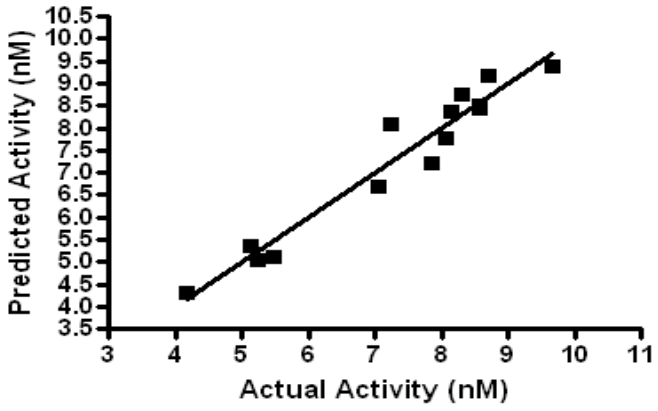

Figure 19. Graph of predicted activity from QSAR analyses versus actual values for dictyostatin, its analogues, and 14-normethyldiscodermolide.

3.10 DISCUSSION

Several conclusions were reached about the SAR for dictyostatin based on the compounds' effects on HeLa cell proliferation, histone H3 histone phosphorylation, microtubule mass, and nuclear morphology. The importance of the 22-membered ring was proven by the inactivity of the 20-membered analogues 16-*epi*-isodictyostatin and 15*Z*,16-normethylisodictyostatin. If the C16 methyl group is present, it must be in the *S*-configuration, which is seen by the complete loss in activity of the 16-*epi*-analogue. C2:3*Z* geometry is also necessary. The most potent analogues from this screen were 6-*epi*-dictyostatin, 7-*epi*-dictyostatin, 15*Z*,16-normethyldictyostatin and 16-normethyldictyostatin. Only minor differences in the compounds' cellular activities were observed, although 6-*epi*-dictyostatin and the parent compound were the most active agents in all experiments. From these and previous experiments performed in the Day lab, and in conjunction with Paterson's work, a rather complete picture of dictyostatin's SAR can be depicted as shown in Figure 20.

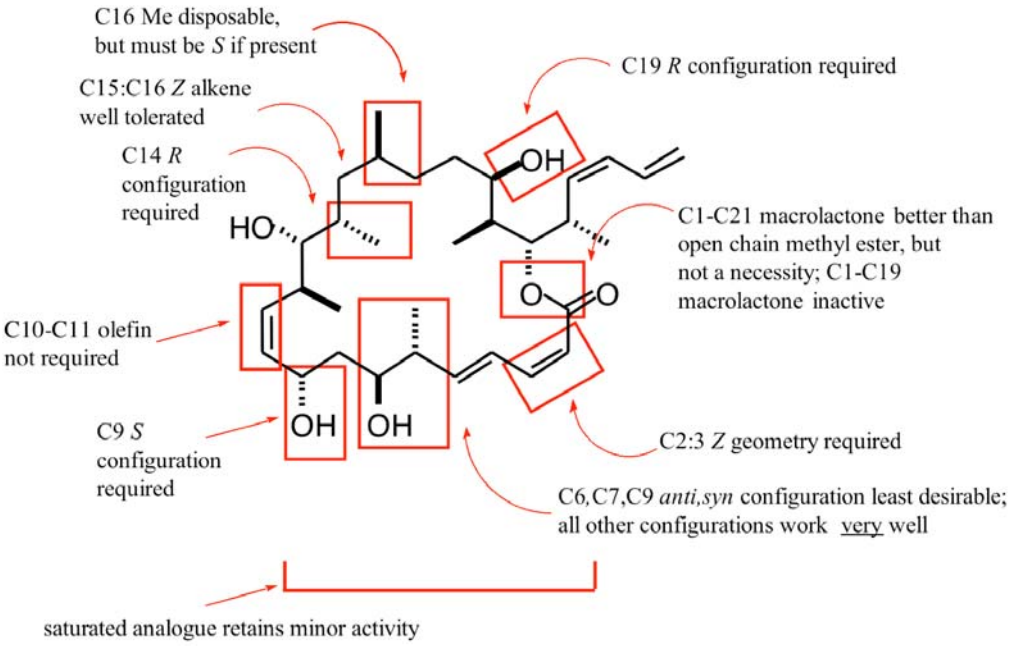

Figure 20. SAR for dictyostatin.

Although qualitatively the rank order of cellular activities correlated with the *in vitro* activities, there were some differences in the compounds' abilities to cause *in vitro* tubulin assembly and binding site affinity studies. It is noteworthy that the 16-normethyl derivatives 15*Z*,16-normethyldictyostatin and 16-normethyldictyostatin had an almost 5-fold higher K_i values compared with the C6 and C7 epimers. This is consistent with the hypothesis that the C16 methyl group is important in binding to the taxoid site through a key interaction with Phe270 on β-tubulin. 16-Normethyldictyostatin has a reduced potency in the paclitaxel-resistant 1A9/PTX10 ovarian cancer cell line, which has a Phe270 to Val point mutation in the taxoid binding site. This is consistent the binding data, where the lower affinity observed in competition experiments with 15*Z*,16-normethyldictyostatin and 16-normethyldictyostatin can be attributed to the loss of the favorable interaction of the C16 methyl group of dictyostatin with the Phe270 in β-tubulin.

As observed from a similar loss in potency in 1A9/PTX10 lines, the interaction between the benzoyloxy group of paclitaxel and Phe270 of β-tubulin is important for activity. [52, 83] The importance of the interaction between Phe270 and methyl substituents in dictyostatin, epothilone B and discodermolide is now becoming well established. Molecular modeling studies performed by Xia *et al*. show the C14 methyl group of discodermolide could be positioned in a favorable interaction with Phe270 in the hydrophobic binding pocket of the taxoid site.[92] The importance of this interaction has been confirmed by in the decrease of nucleating ability in tubulin polymerization assays with 14-normethyldictyostatin performed in our laboratory (data not shown). Reese *et al*. have recently reported on the NMR-derived binding mode of epothilone A to the tubulin heterodimer.[95] A two dimensional NMR-derived binding model of epothilone A to

the tubulin heterodimer suggests that the increased potency of epothilone B over epothilone A is due to the interaction of the C12 methyl with Phe270.

As shown by the QSAR studies, the size of the molecule (area and molar refractivity) is the most significant contributor to cytostatic activity against 1A9 ovarian cancer cells. A loss of a methyl substituent would certainly lead to a decrease in the van der Waals area of the molecule and according to calculations, lead to a decrease in activity. Molar refractivity is a measure of the volume occupied by the molecule. It is dependent on a number of factors such as molecular weight, refractive index and density. This descriptor relates to the London dispersive forces that act in the drug-receptor interaction.[96] Again, 16-normethyldictyostatin and 15*Z*,16-normethyldictyostatin would be expected to have molar refractivities differing from those of dictyostatin and its C6 epimer, whose molar refractivities are identical.

Canales *et al.* recently published a report on the bound conformation of both dictyostatin and discodermolide to microtubules polymerized in the presence of the nucleotide analogue, guanosine 5'-α,β-methylenetriphosphate (GMPCPP).[97] This model predicts both discodermolide and dictyostatin to overlap with almost the entire paclitaxel skeleton except for the phenylisoserine side chain. This model does explain the ability of discodermolide and dictyostatin to stabilize microtubules by binding to the M loop on β-tubulin and enhance the lateral contacts between protofilaments.

There is a problem with this model of discodermolide and dictyostatin binding to β-tubulin. The first is the observation that GMPCPP forms different microtubule structures under different buffer conditions.[98] This could account for differences in the orientation of these compounds in the microtubules formed in the presence of this compounds and those within cells.

Changes to the C6 and C7 stereocenters of dictyostatin were explored because they are present in the structure of discodermolide as its C4 and C5 carbons; part of its delta lactone ring. The multiparameter immunofluourescence studies with 6-*epi*-dictyostatin and 7-*epi*-dictyostatin showed that these analogues produced microtubule bundling and abnormal spindle formation at nanomolar concentrations. Their ability to produce these various cellular responses was observed at lower concentrations than that required with dictyostatin. Although there was a slight loss in nucleation ability in tubulin polymerization assays, these compounds retained their ability to induce assembly of microtubules and to form cold stable polymer. In addition, both compounds still had a high affinity for the taxoid site on β-tubulin with the K_i values obtained in competition experiments with [^{14}C]epothilone B of 480 nM and 930 nM for 6-*epi*-dictyostatin and 7-*epi*-dictyostatin, respectively. From these experiments, it can be said that changes to this area is not only well tolerated, but lead to no loss in potency *in vivo*.

The saturation binding kinetics of epothilone B were characterized. One important assumption that is made to ease calculations in equilibrium binding is that only a small amount of substrate binds to its target leaving the relative amount of free substrate concentration unchanged. Ligand depletion occurs if more than 10% of the substrate binds to the protein.[73] When ligand depletion occurs, this assumption is invalidated and can, if not taken into account, cause errors in data analysis. Ligand depletion is a common problem in the centrifugation assay commonly used to determine the binding kinetics of microtubule stabilizing agents. For this reason, the saturation binding data were analyzed using the modified Swillen's equation as described in Chapter 2, which not only accounts for ligand depletion but also fits total binding and nonspecific binding simultaneously. Fitting the nonspecific and total binding data simultaneously allows for calculation of free ligand, and defines nonspecific binding as a

constant fraction of the free ligand concentration. The K_d value obtained using this analysis was reasonable using previous competitive inhibition studies as a measure of the affinity of epothilone B for the taxoid site.[35, 63]

The binding kinetics of dictyostatin and its analogues were determined with radiolabeled epothilone B. Epothilones are competitive inhibitors of paclitaxel binding, and the epothilones retain activity against almost all known paclitaxel resistant cell lines; the exception is the 1A9/A8 line, which possesses a mutation of Arg 282 to Gln in β-tubulin and is resistant to both paclitaxel and epothilone B.[53] All of the agents tested here were found to be competitive inhibitors of epothilone B's binding site on tubulin polymer, implying that dictyostatin and epothilone B share a common binding site on microtubules. As in the saturation binding experiments with with [^{14}C]epothilone B, significant ligand depletion was observed in the competition experiments. The modified Hanes analysis was employed as described in Chapter 2 and accounts for the free concentration of radiolabeled tracer and that of the free inhibitor.

QSAR modeling led to a number of equations that will be useful in predicting the activity of new analogues of dictyostatin in cells. The four descriptors employed in these equations are all variables that can be easily manipulated by a synthetic chemist.

It is not surprising that the structures of dicytostatin and a number of its analogues superimposed well on the NMR-determined solution structure of discodermolide (which, in fact, closely matches the structure determined by X-ray crystallography).[99] In fact, Sanchez-Pedregal recently published a superimposition of the U-shaped configuration of discodermolide bound to tubulin onto that of dictyostatin and noted that they are superimposable.[100] As can be correlated with its significant decrease in activity, 2*E*,3,15*Z*,16-normethyldictyostatin did not superimpose well onto the structure of dictyostatin.

In conclusion, a number of potent analogues of the microtubule stabilizer dictyostatin have been tested to determine the cellular responses they evoke, their effects on tubulin polymerization, and their ability to inhibit binding of [^{14}C]epothilone B to microtubules. During this process, the saturation binding kinetics of epothilone B was characterized, and epothilone B demonstrated great affinity for the taxoid site. Dictytostatin and its analogues are all competitive inhibitors of [^{14}C]epothilone B binding as demonstrated by Hanes analysis. These experiments have further led to the conclusio that dictyostatin, discodermolide, epothilone B, and paclitaxel have favorable interactions with Phe270 within the taxoid binding site on β-tubulin. A change to the configuration of the stereocenter at C6 or C7 of dictyostatin is well tolerated. From this work, it can be conjectured that for good efficacy against cancer cell lines, all future analogues of dictyostatin must retain the ability to interact with Phe270 on β-tubulin, and that this interaction is important to the efficacy of many other taxoid site-binding, microtubule-stabilizing compounds. The characterization of the 6-*epi*-dictyostatin analogue as a potent microtubule-stabilizing agent has motive the gram scale synthesis for use in preclinical studies. Our QSAR analyses led to a number of equations that will be useful in guiding the production of and predicting the cellular activity of new, more potent dictyostatin analogues. The four descriptors employed in these equations are all variables that can be easily be manipulated by a medicinal chemist.

4.0 GENERATION OF A RADIOLABELED VERSION OF A THALIDOMIDE ANALOGUE TO DETERMINE THE KINETICS OF A NEW MICROTUBULE PERTURBING AGENT

4.1 AN ANALOGUE OF THALIDOMIDE, 5HPP-33 (2-(2,6-DIISOPROPYLPHENYL)-5-HYDROXY-1*H*-ISOINDOLE-1,3-DIONE)

Thalidomide was first prescribed to pregnant women in the 1950s as a sedative and antiemetic.[101, 102] It was quickly withdrawn from the market in 1961 due to reports of limb growth defects in babies of mothers who were given thalidomide during pregnancy. Interest in thalidomide was renewed due to the fact that it is useful in the treatment of various dermatological and inflammatory conditions.[103] It was approved in the United States for the treatment of a serious dermatological reaction associated with leprosy. Folkman *et al*. found that thalidomide prevents angiogenesis, elucidating the underlying cause of the limb growth defects.[104] Angiogenesis is the formation of new blood vessels and is important in the growth and metastasis of tumor cells *in vivo*.[105] This revelation has led to the prospect of thalidomide as a potential chemotherapeutic agent.

Thalidomide has been found to be effective in the treatment of multiple myeloma. Multiple myeloma is a devasting cancer of the bone marrow and results in the malignancy of the plasma cells and B cells.[104] Thalidomide's efficacy against this disease stems from a number of

mechanisms. Thalidomide is a potent inhibitor of the cytokine TNF-α.[106] TNF-α is one of the major cytokines involved in the mediation of innate immune responses. The most important role of TNF-α is its function in stimulating inflammatory and immune responses to a variety of foreign bodies (*e.g.*, microbial infections). The inhibition of TNF-α expression within the bone marrow decreases the growth and formation of new blood vessels that nurture the malignant cells. Thalidomide is also known to increase T-cell proliferation, thereby causing the release of certain cytokines.[107] These cytokines activate natural killer cells, which attack and lyse the cancerous cells. Reports also suggest that thalidomide decreases the expression of vascular endothelial growth factor (VEGF), a pro-angiogenic growth factor.[108]

The multiple actions of thalidomide have inspired many researchers to design analogues of the drug with hopes of creating a compound with enhanced activity. The focus of most of these evaluations of the analogues has been on the immunomodulatory functions of thalidomide.[109, 110] Hashimoto *et al.* originally designed thalidomide analogues in an attempt to enhance the regulatory mechanism of TNF-α production.[111] Replacement of the glutaramide ring of thalidomide with an aromatic ring led to the production of active analogues.[112, 113]

4.2 5HPP-33 AS A MICROTUBULE PERTURBING AGENT

Inatsuki *et al*. reported on a readily synthesizable thalidomide analogue containing a 5C-hydroxy group and an isopropylphenylpthalimide structure as a potent antiproliferative agent with an IC_{50} of 5 μM against human leukemia cells.[114] The authors named this compound 5HPP-33. The authors provided evidence for the mechanism by which proliferation is inhibited. Evidence suggested that the compound inhibits the formation of microtubules and binds to tubulin dimers rather than to microtubule polymer. It was not clear at this time where the compound binds on the dimer or the mechanism of the inhibition of polymerization.

The characterization of this small molecule as a potential microtubule perturbing agent prompted its synthesis in Dr. Pui-Kai Li's lab at The Ohio State University.[66] The synthesis is shown in Scheme 1. 5HPP-33 [94] was prepared by the condensation of 2,6-diisopropylaniline (**1**) with 5-hydroxyphthalic acid (**2**).

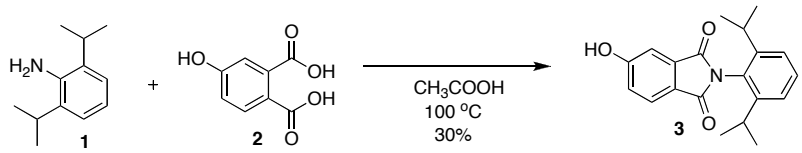

Scheme 1. Synthesis of 5HPP-33

The objectives of this study were to fully characterize 5HPP-33 as a microtubule perturbing agent and potential chemotherapeutic agent. A number of biochemical and cellular studies were performed to reach this goal. The antiproliferative effects of 5HPP-33 were determined in a number of cancer cell lines. Flow cytometry experiments were performed to determine the effects of 5HPP-33 on cell cycle progression. Tubulin polymerization assays were performed in the presence and absence of microtubule associated proteins (MAPs) to determine the effects of 5HPP-33 on polymer formation. Electron microscopy pictures were taken to visualize the

phenotype of polymer formed in the presence of 5HPP-33. Competitive inhibition experiments were performed to determine if 5HPP-33 could compete for known microtubule perturbing agents at their respective binding sites on the tubulin heterodimer. Finally, a radiolabeled analogue of 5HPP-33 was synthesized and the kinetics of its interaction with tubulin were determined to establish a K_d value in the presence and absence of MAPs.

4.3 EVALUATION OF THE EFFECTS OF 5HPP-33 ON CELLULAR PROLIFERATION AND THE CELL CYCLE

4.3.1 5HPP-33 is a potent antiproliferative agent against many tumor cell lines *in vitro*

Li *et al*. have shown 5HPP-33 to have antiproliferative activity against many different cell lines, with GI_{50} concentrations as shown in Table 3.[66] 5HPP-33 inhibits the proliferation of estrogen-dependent (MCF-7), estrogen-independent (MDA-MB231) breast cancer cells, colon cancer cells (HT-29), bladder cancer cells (TCCSUP), ovarian carcinoma cells (1A9), and androgen-dependent (LNCaP) as well as androgen-independent prostate cancer cells (DU-145 and PC-3). The GI_{50} values represent the means of three experiments with triplicate determinations. The GI_{50} values of the agent were in the low micromolar range against every cell line tested. Thalidomide was not nearly as active as 5HPP-33 and exhibited GI_{50} values of > 300 μM.

Table 3. Determination of 50% growth inhibition concentrations of 5HPP-33 and thalidomide against various cancer cell lines.

Cell Type	5HPP-33 (GI_{50}) (μM)	Thalidomide (μM)
MCF-7	6.2 ± 0.41	>300
MDA-MB231	5.2 ± 0.32	>300
HT-29	5.09 ± 1.41	>300
TCCSUP	6.52 ± 0.97	>300
LNCaP	1.65 ± 0.21	>300
DU-145	5.74 ± 0.23	>300
PC-3	8.28 ± 0.81	>300
1A9	2.1 ± 0.1	Not Tested

5HPP-33 also maintains its activity against cell lines expressing the P-glycoprotein pump and containing mutations within the binding site of paclitaxel on β-tubulin as shown in Tables 4 and 5. The P-glycoprotein pump confers resistance to multiple cell types through overexpression of

the *ABCB1* (a.k.a. *MDR1* = multidrug resistance) gene.[115] The cell lines used were transfected with retroviral vectors expressing either of two forms of P-glycoprotein pump: wild type (G185) or a point mutant (V185) that alters the selectivity of the pump. Values given are the average of two separate experiments. RR is relative resistance (ratio of the GI_{50} of transfected cells/ GI_{50} of the non-transfected cells). Paclitaxel is a known substrate of the P-glycoprotein pump and this is seen by the 57-fold decrease in its potency within the cell line expressing the wild type pump (Table 4).[116] Colchicine and 5HPP-33 retain their respective potencies in these cell lines and with only a 6.7-fold and 1.2-fold decrease, respectively, in GI_{50} values. When the compounds were tested in the NIH 3T3 cell line expressing the mutated P-glycoprotein pump, 5HPP-33 is the only drug that retains potency in this cell line. This is compared to paclitaxel and colchicine, where potency is dramatically reduced.

Table 4. Effects of 5HPP-33, paclitaxel, and colchicine on the NIH 3T3 cell lines.

Drug	**NIH 3T3**		**NIH3T3G185**		**NIH3T3V185**	
	GI_{50} (μM)	**RR**	**GI_{50} (μM)**	**RR**	**GI_{50} (μM)**	**RR**
5HPP-33	3	1	3.6	1.2	4.5	1.5
Paclitaxel	0.04	1	2.28	57	1	25
Colchicine	0.06	1	0.4	6.7	5.2	87

Table 5. Effect of 5HPP-33 in 1A9 ovarian carcinoma cells.

Drug	**1A9 Parental**		**PTX10 (F270V)**	**PTX22 (A364T)**
	GI_{50} (μM)	**RR**	**Relative Resistance**	**Relative Resistance**
5HPP-33	2.1 $\pm$ 0.1	1	1.1	0.7
Paclitaxel	0.002*	1	24	24
Vinblastine	0.0035*	1	0.5	0.4

The effects of 5HPP-33 in 1A9 ovarian carcinoma cells and derived lines were tested. 1A9PTX10 contains a mutation at nucleotide 810, which replaces the phenylalanine at position

270 with valine on the β-tubulin subunit within the paclitaxel binding site.[52] 1A9PTX22 contains a mutation at nucleotide 1092, which changes the alanine at position 364 to threonine. Values for the GI_{50}s of paclitaxel and vinblastine were taken from Giannakakou *et al.*[52] Paclitaxel has a GI_{50} value in the low nanomolar range in the parental cell line, but this value increases 24-fold in the resistant cell lines. Vinblastine retains activity in both the parental and resistant cell lines. These results are not surprising because vinblastine binds to a site on the tubulin heterodimer different from that of paclitaxel.[28] 5HPP-33 retains potency in all cell lines tested suggesting that its binding site is not identical to that of paclitaxel.

4.3.2 The effect of 5HPP-33 on the cell cycle.

Flow cytometry is used to detect and measure the fluorescence or absorbance signals of cells as they flow in a liquid stream through a beam of light.[117] Li *et al.* used flow cytometry to quantitate the number of 1A9 cells in the G_1, S and G_2/M phases of the cell cycle.[66] The cells were stained with the DNA intercalating agent propidium iodide, which provides a way of determining DNA content. The cells were also treated with the mitosis-specific antibody TG3. This provided a means of determining the amount of cells in the M phase over the G_2 phase[118]. The results of this study are shown in Figure 21.

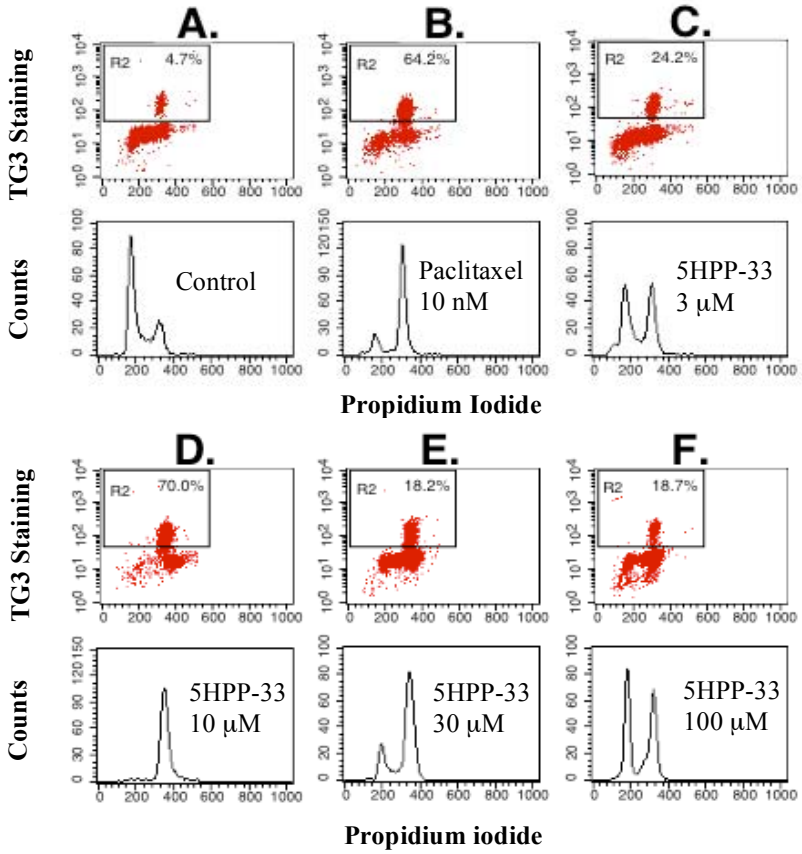

Figure 21. Flow cytometric analysis of 1AP cells treated with the indicated concentrations of 5HPP-33 and paclitaxel.

The bottom graphs in Figure 21 are histograms of the number of cells counted versus fluorescent intensity of propidium iodide staining. These provide easy visualization of the proportion of cells in each phase upon drug treatment at the various concentrations indicated compared to the control. The upper graphs are the two-parameter analyses of fluorescence intensity of TG3 staining versus fluorescence intensity of propidium iodide. These graphs allow for the calculation of the percentage cells in M phase. The percentage of cells in each phase after the indicated treatment of drug is presented in Table 6. After treatment with of 1A9 cells with 10 nM paclitaxel, 81% of cells are in the G_2/M phase and 64% are in M phase. A comparison can be made to the 10 µM 5HPP-33 treatment, where 96% of cells are in G_2/M phase and 70% are in

M phase. It can now be hypothesized that the antiproliferative activity of 10 μM 5HPP-33 can be attributed to the agent's ability to block cells in the G_2/M phase. At very high concentrations of 5HPP-33, this effect is lessened, likely due to death (and disappearance from the analysis) of the cells blocked in G_2/M, and apparent appearance of a greater number of cells in G_1 and S.

Table 6. Calculation of percentage of 1A9 cells in the G_2/M and M phase from two-parameter flow cytometric analysis.

Compound	**% G_2/M**	**% M phase**
Control	13.5	4.7
10 nM Paclitaxel	81	64
3 μM 5HPP-33	38	24
10 μM 5HPP-33	96	70
30 μM 5HPP-33	68	18
100 μM 5HPP-33	47	19

4.4 EFFECTS OF 5HPP-33 ON TUBULIN POLYMERIZATION AND VISUALIZATION OF POLYMER FORMED USING ELECTRON MICROSCOPY

4.4.1 Tubulin polymerization assays

Tubulin polymerization *in vitro* is stimulated under different conditions and can be quantified using a spectrophotometer that measures polymerization as a change in turbidity, which is measured as a change in absorbance at λ = 350 nm.[63] Due to the large amount of tubulin found in the mammalian brain, tubulin can be purified from fresh bovine brain in high yield.[67] Tubulin polymerization assays are performed under a variety of conditions to gain insight into the interactions of potential antimitotic agents with purified tubulin.[119] The two most common conditions to monitor tubulin assembly are the glutamate system and the microtubule-associated proteins (MAPs) system. Microtubule associated proteins bind to the microtubule lattice and help to stabilize the heterodimer interactions.[1] Polymerization can be simulated *in vitro* with the mixture of MAPs, purified tubulin and GTP in a buffer warmed to 37 ^{o}C in a cuvette.[120] High concentrations of glutamate salts can induce tubulin assembly, take the place of MAPs, and act as a buffer. Although GTP is still necessary to induce polymerization, the glutamate system is easier to use over the MAPs system because the need for an additional purified protein is negated. Potent inducers of microtubule polymerization, such as discodermolide and dictyostatin, can induce formation of microtubules without the addition of MAPs or GTP.[63] Also the glutamate system alleviates the possibility of the compound binding to MAPs. A major limitation to the spectrophotometrically-quantified tubulin polymerization assays is that the exact structure of the polymer formed cannot be directly determined. There are antimitotic compounds

that form aberrant polymer, but this is registered on the spectrophotometer no differently from microtubule formation.[78]

4.4.2 The effects of 5HPP-33 on tubulin polymerization in the MAPs system

The tubulin polymerization assay was first performed in 0.1 M MES, pH 6.9, containing 1.0 mg/mL tubulin, 0.75 mg/mL MAPs and 400 μM GTP, and the indicated concentrations of 5HPP-33 in vehicle. The temperature of the cuvettes was tightly controlled throughout this experiment from 0 – 30 ^{o}C as shown in Figure 22.

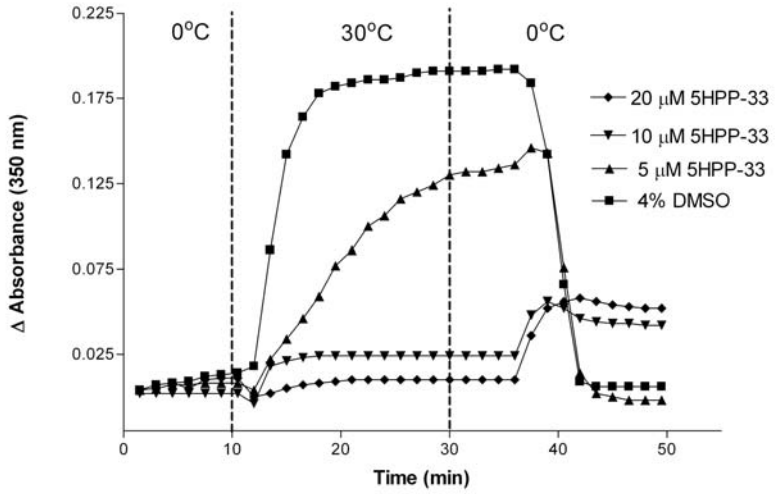

Figure 22. Tubulin polymerization assay to determine the effects of 5HPP-33 on tubulin assembly in the MAPs system.

5HPP-33 completely inhibited tubulin polymerization at 10 μM. The concentration at which 5HPP-33 inhibited tubulin polymerization by 50% as compared to control (IC_{50}) was calculated to be 6.77 μM.

The addition of exogenous Mg^{2+} to tubulin polymerization assays enhances tubulin assembly; 0.05 M $MgCl_2$ was therefore added to the MAPs system. Magnesium cation binds to tubulin in a 1:1 ratio and has been shown to improve GTP's ability to bind to the exchangeable site.[121] The results of the experiment are shown in Figure 23.

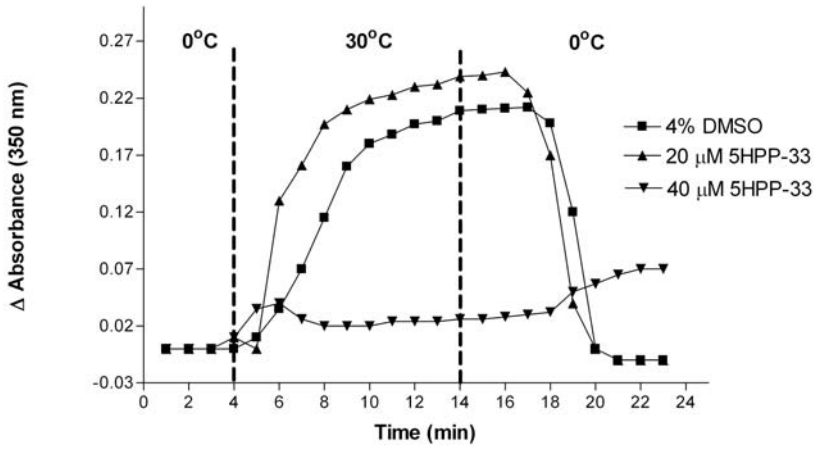

Figure 23. Effect of 5HPP-33 on tubulin polymerization in the MAPs system with addition of 0.05 M $MgCl_2$.

The presence of magnesium cation decreased the ability of 5HPP-33 to inhibit polymerization. As shown in Figure 23 in the MAP's system without exogenously added Mg^{2+}, a concentration of 20 μM 5HPP-33 completely inhibited tubulin polymerization. At 20 μM, 5HPP-33 in the system containing Mg^{2+} tubulin polymerization was still able to occur, but almost complete inhibition of the reaction did occur at 40 μM 5HPP-33. It was concluded from this experiment, that the addition of Mg^{2+} was overcoming 5HPP-33's ability to inhibit microtubule

polymerization. This experiment provided further evidence that 5HPP-33 is a microtubule inhibitor.

4.4.3 The effects of 5HPP-33 on tubulin polymerization in the glutamate system

It was first noted by Hamel *et al*. that organic anions, such as monosodium glutamate (MSG), could be used to induce tubulin polymerization.[122] MSG is the buffer preferred for the long-term storage of purified tubulin.[67] For assembly to occur with purified tubulin in MSG, the temperature must be above 20 ^{o}C and GTP must be added. A standard protocol is usually performed in MSG to assess potential tubulin polymerization inhibitory activity. The method for the assay is described in the Materials and Methods section. Briefly, tubulin, MSG, and indicated drug concentrations in 4% DMSO are pre-incubated for 15 min, then placed into cuvettes cooled to ~0 ^{o}C, and 400 μM GTP is added. As shown in Figure 24, 5HPP-33 did not inhibit polymerization at 5 μM but seemed to induce it.

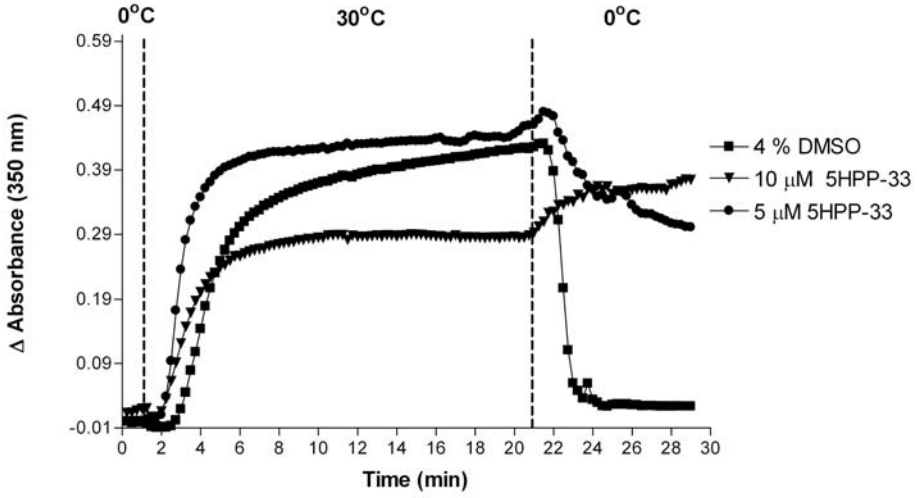

Figure 24. Effect of 5HPP-33 on tubulin assembly in the MSG system.

At a concentration of 10 μM, 5HPP-33 increased the extent of assembly, which is the last turbidity reading at 30 ^{o}C, and forms cold stable polymer. This formation of cold stable polymer is also seen at 5 μM 5HPP-33, but the extent of assembly and reaction rate was reduced at this concentration.

In an attempt to determine an IC_{50} for 5HPP-33 in the MSG system, the concentration of GTP was lowered from 400 μM to 100 μM. As shown in Figure 25, 2.5 μM 5HPP-33 inhibits tubulin assembly by 41 %.

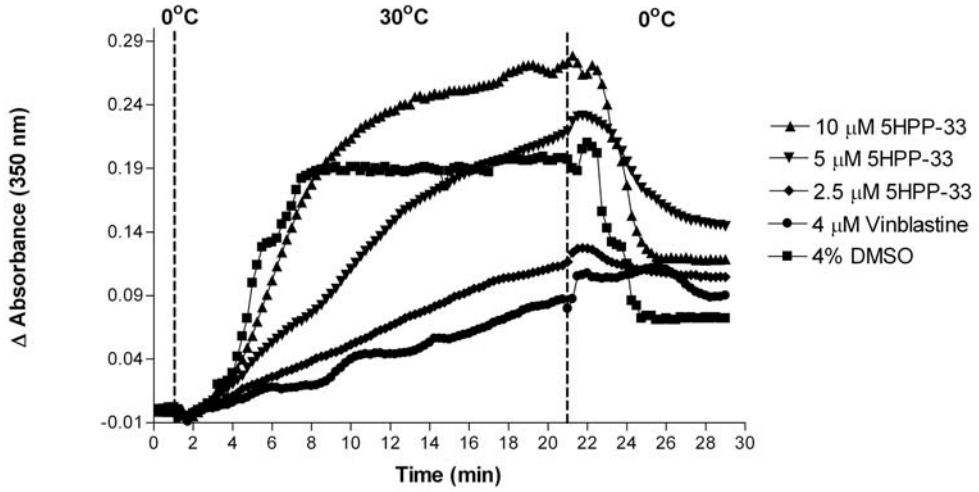

Figure 25. Effect of 5HPP-33 on tubulin assembly in the MSG system containing 100 μM GTP.

Although the reaction rate was decreased as compared to vehicle only control, there was polymer formed in the presence of 5μM 5HPP-33. This extent of polymer formation was even greater in the presence of 10 μM 5HPP-33. The polymer formed appeared to be stable to cold disassembly. Examination of these tubulin polymerization graphs shows it is unlikely that 5HPP-33 was causing the formation of tubulin polymer. The inhibition of assembly indicates that microtubules are likely not forming in either system, but that an aberrant polymer formation

with a concentration dependent increase in the MSG system was occurring. The only true test of this was to visualize the polymer formed using electron microscopy.

4.4.4 Electron microscopy analysis of the effects of 5HPP-33 on tubulin assembly

Electron microscopy has made it possible to visualize particular structures within the cell and is commonly utilized to display the effect of microtubule perturbing agents on tubulin assembly. Transmission electron microscopy, where the images are generated from the absorbance of electrons, is typically used to visualize microtubule.[123] Specimens are prepared by taking sample directly out of the cuvettes used in the tubulin polymerizations assays, placing a 1 μL drop on a copper grid, and staining with a heavy metal salt. The heavy metal is needed to visualize the image because the greater the atomic number in the specimen, the larger the percentage of electrons scattered, and the greater the resolution.[124]

With compounds that stabilize and promote microtubule formation such as paclitaxel and discodermolide, microtubule lengths measured from electron micrographs give an estimate of the nucleating ability of the compound.[63] For compounds that inhibit microtubule formation, aberrant polymer formation can be visualized with electron microscopy. Such is the case with the vinca domain/depsipeptide site binding agent dolastatin 10, which causes the formation of rings and tightly coiled spiral aggregates.[125] The formation of these structures causes a change in turbidity in tubulin polymerization assays.

The polymer formed in the presence of 5HPP-33 in the two systems was visualized by taking aliquots from the polymerization assays at 30 ^{o}C. A concentration of 5HPP-33 of 20 μM was chosen for the evaluation of the polymer because this is the temperature and concentration at

which 5HPP-33 completely inhibited polymerization in the MAPs system. Figure 26 shows the electron micrographs of polymer obtained at 30 ^{o}C in the MSG system.

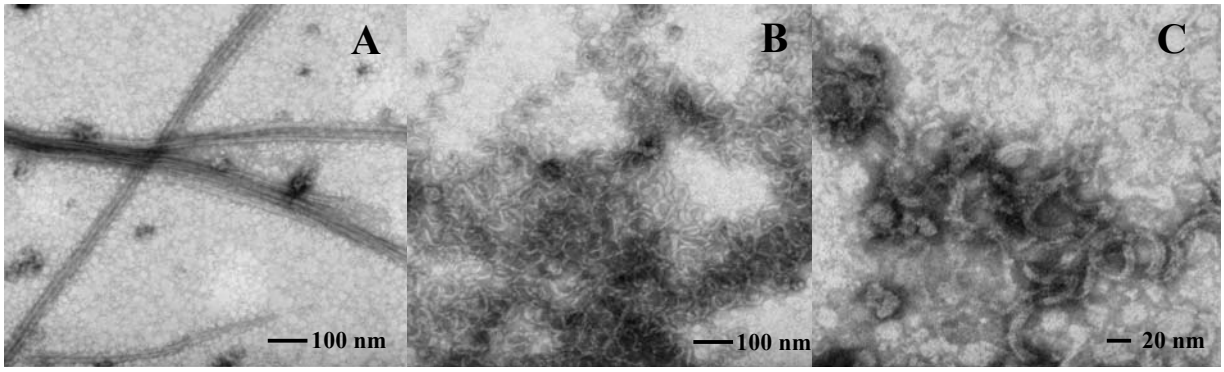

Figure 26. Electron microscopy images of the effects of 5HPP-33 on tubulin polymerizaiton in the MSG system.

Panel A is the negative control that shows normal microtubule formation in the presence of no drug. The protofilaments that make up the microtubule can be visualized at 20000x magnification. It is clear from Panel B that at 30 °C microtubule formation did not occur. 5HPP-33 in the MSG system appeared to induce tubulin to form aggregates of spirals and rings, which is the cause of the turbidity development in the cuvettes during the polymerization assay. The average ring outer diameter of the rings was 35.8 $\pm$ 6.7 nm. Panel C shows a 60000x magnification of the aberrant polymer that was formed.

The electron micrographs obtained from the MSG system showed no signs of microtubule formation in the presence of this modifier, and the reason for the increase in turbidity during the polymerization assay. Electron micrographs were also taken from experiments done with the MAPs system at 30 ^{o}C and are shown in Figure 27.

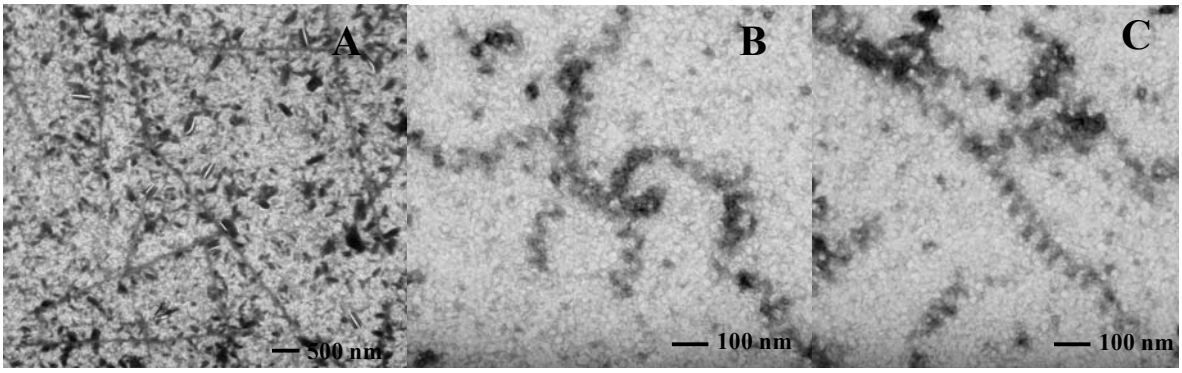

Figure 27. Electron microscopy images of the effects of 5HPP-33 on tubulin polymerization in the MAPs system.

Panels B and C show that an aberrant polymer was still formed, but was mostly in the form of small rings instead of the large aggregated polymer that was observed in the MSG system. This could account for the difference in the results for the tubulin polymerization reactions between the two systems. The diameter of the rings could not be measured from the reactions with 20 μM 5HPP-33 in the MAPs due to poor resolution. In the MSG system, the aggregation reaction seemed to be much more aggressive than in the MAPs system. This phenomenon has been seen before with other microtubule perturbing agents such as dolastatin 10, where there is a major change in morphology and aggregation in different systems.[44] Unlike 5HPP-33, the turbidity and morphology change with dolastatin 10 occurs in the MAPs system and not the MSG system.

From the images obtained by electron microscopy in both systems, it is clear that the major mechanism by which 5HPP-33 perturbs microtubules is by inhibition of polymer formation. The next step was to determine where on the tubulin heterodimer 5HPP-33 might bind, and if it competes with other known microtubule perturbing agents.

4.5 EFFECTS OF 5HPP-33 ON THE BINDING OF RADIOLABELED MICROTUBULE PERTURBING AGENTS TO TUBULIN OR TUBULIN POLYMER

Percent inhibition of radiolabeled ligand by a normoisotopic competitor are used to quickly determine if compounds of interest can compete, either competitively or non-competively, for the binding site of a previously characterized microtubule perturbing agent. [63] These assay provides a quick method to assess the ability of new agents and analogues to bind to tubulin or tubulin polymer, and to determine if further analyses are needed.

4.5.1 Effect of 5HPP-33 on the binding of [^{3}H]paclitaxel to tubulin polymer

Paclitaxel binds to the β subunit of tubulin when in the form of the microtubule, and stabilizes the lateral interactions between heterodimers. To determine if 5HPP-33 can compete with [^{3}H]paclitaxel for its binding site on the microtubule, a competition assay was performed as described in the Materials and Methods section. Briefly, 2 μM [^{3}H]paclitaxel, inhibitor, and 0.2 mg/mL preformed microtubules in 0.75 M MSG, pH 6.9, were incubated for 30 min at 37 ^{o}C, centrifuged for 30 min, and the amount of free [^{3}H]paclitaxel in the supernatant determined. Discodermolide was used as the positive control because of its known ability to compete for the taxoid binding site.[63, 77]

Table 7. Percent inhibition by 5HPP-33 of the binding of [^{3}H]paclitaxel to tubulin polymer.

Compound	Concentration (μM)	% Inhibition ± S.D.
5HPP-33	4	−10 ± 0.4%
5HPP-33	20	−10 ± 0.5%
Discodermolide	4	86 ± 3%

The percent inhibition values are the average of three separate experiments. As shown in Table 7, at 5HPP-33 concentrations of 2- and 10- fold higher than [^{3}H]paclitaxel, no competition for the taxoid binding site on the microtubule was observed. This is in contrast to 4 μM discodermolide, which completely inhibited binding of 2 μM [^{3}H]paclitaxel.

4.5.2 Effect of 5HPP-33 on the binding of [^{3}H]colchicine to tubulin

The colchicine binding site is located on β-tubulin near the α/β heterodimer interface.[26] Colchicine binds to tubulin and causes a slow conformational change, which inhibits the polymerization of microtubules.[28] To see if 5HPP-33 binds to the same site as colchicine and other related agents, a percent inhibition assay was performed. In this assay, one separates bound tubulin from free competitor by filtration through diethylaminoethyl (DEAE) cellulose filters. The binding of colchicine to tubulin is stabilized in this assay by the addition of exogenous salts and organics acids.[126]

Table 8. Effects of 5HPP-33 on [^{3}H]colchicine binding to tubulin

Compound	**% Inhibition ± S.D.**
5 μM 5HPP-33	–10 ± 7
25 μM 5HPP-33	–64 ± 1
5 μM Podophyllotoxin	75 ± 18

As shown in Table 8, 5HPP-33 actually enhanced the binding of [^{3}H]colchicine to tubulin instead of inhibiting it. The percent inhibition values listed are the average of duplicate experiments ± S.D. This is compared to the positive control, podophyllotoxin, which inhibited the binding of [^{3}H]colchicine by 75%.

4.5.3 Effects of 5HPP-33 on the binding of vinca domain and peptide/depsipeptide site agents to tubulin

The microtubule perturbing agents that bind to the vinca domain and the closely associated peptide/depsipeptide site on β tubulin are inhibitors of polymerization and can inhibit GTP hydrolysis.[44] These binding sites are near the exchangeable nucleotide site on the protein and, when bound, cause a block in the longitudinal interactions between tubulin heterodimers. Dolastatin 10 and the vinca alkaloids cause aberrant polymer formation at superstoichiometric concentrations in polymerization assays in the MAPs system. As shown above, 5HPP-33 also causes aberrant polymer formation, which was visualized by electron microscopy. Percent inhibition assays were performed with [^{3}H]dolastatin 10 and [^{3}H]vinblastine to determine if 5HPP-33 binds to the peptide/depsipeptide site or the vinca domain. These two compounds were chosen because they are known to be non-competitive for each other's respective binding sites.

The results from the [^{3}H]dolastatin 10 competition assay are presented in Table 9. The percent inhibition values represent the average $\pm$ S.D. of two independent experiments. 5HPP-33 did not compete for [^{3}H]dolastatin 10's binding site at any concentration tested.

Table 9. Effect of 5HPP-33 on [^{3}H]dolastatin 10 binding to tubulin.

Compound	**% Inhibition $\pm$ S.D.**
5 μM 5HPP-33	-7 ± 4
50 μM 5HPP-33	-1 ± 5
5 μM Vincristine	17 ± 5
5 μM Colchicine	-11 ± 10

5HPP-33 also did not show any appreciable inhibition of [^{3}H]vinblastine binding to its site on β-tubulin as shown in Table 10. Vincristine, an analogue of vinblastine, was used as a positive control, and it inhibited binding of the radiotracer by 62%.

Table 10. Effect of 5HPP-33 on [^{3}H]vinblastine binding to tubulin

Compound	**% Inhibition**
5 μM 5HPP-33	10 ± 7
100 μM 5HPP-33	3 ± 3
5 μM Vincristine	62 ± 2
5 μM Colchicine	–3 ± 4

4.6 SYNTHESIS AND PURIFICATION OF A RADIOLABELED ANALOGUE OF 5HPP-33

The competitive percent inhibition data suggested that 5HPP-33 may bind to a novel site on the tubulin heterodimer. To gain further insight into the binding site of 5HPP-33 and its kinetics, a radiolabeled analogue was synthesized. The synthesis was performed in three steps, which are shown in Scheme 2.

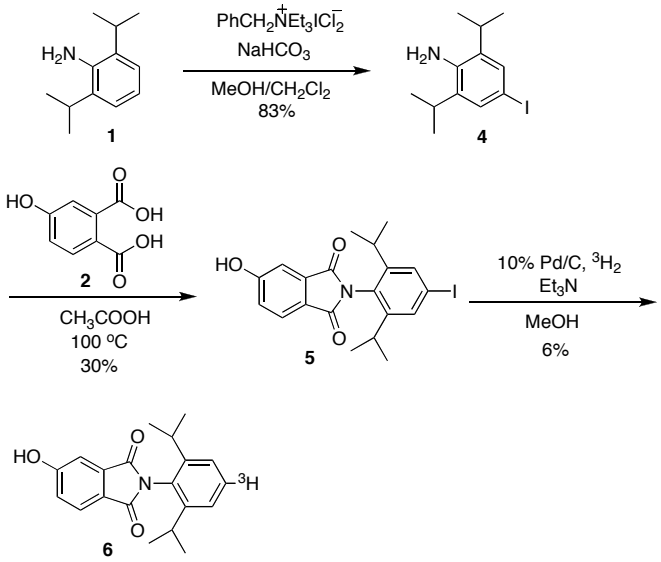

Scheme 2. Radiosynthesis of [^{3}H]5HPP-33

In the first step, benzyltriethylammonium dichloroiodate was utilized to selectively iodinate the *para* position of 2,6-diisopropylaniline **1**. Condensation of 4-hydroxyphthalic acid **2** and the aryl iodide **4** yielded iodo-5HPP-33 **5** ,which was hydrogenolyzed using 10% Pd/C as the catalyst and tritium gas to form [^{3}H]5HPP-33 **6**. Tritium gas was supplied by a Trisorber® tritiation manifold. This method allows for a measured amount of tritium to be released, and subsequent uptake of any unused gas without release into the surroundings of the experiment. The total radioactivity yielded was 1.20 mCi.

The determination of chemical and radioactive purity of the compound was performed by HPLC analysis with both UV and scintillation detection as detailed in the Materials and Methods section. The specific activity of [^{3}H]5HPP-33 from this procedure was 26.78 Ci/mmol.

4.7 BINDING OF [^{3}H]5HPP-33 TO TUBULIN AND COMPETITIVE INHIBITION ANALYSES

4.7.1 Interactions of [^{3}H]5HPP-33 with purified tubulin

To determine the mechanism by which [^{3}H]5HPP-33 interacts with purified bovine brain tubulin, concentrations between 1-200 μM were incubated with 1.0 mg/mL tubulin at 0 ^{o}C for 30 min. Bound ligand was separated from free using a Millipore ultrafiltration apparatus, and the filtrate was used for scintillation spectrometry. The results of this experiment are presented in Figure 29, and each data point is the average of two experiments ± S.D. [^{3}H]5HPP-33 did not exhibit normal saturation binding kinetics, and attempts to fit the data using a non linear equation that fits one site or two- site binding yielded no results. As previously described in Chapter 2, K_d values were calculated using the Hill equation to fit the observed biphasic sigmoidal kinetics shown in Figure 28.

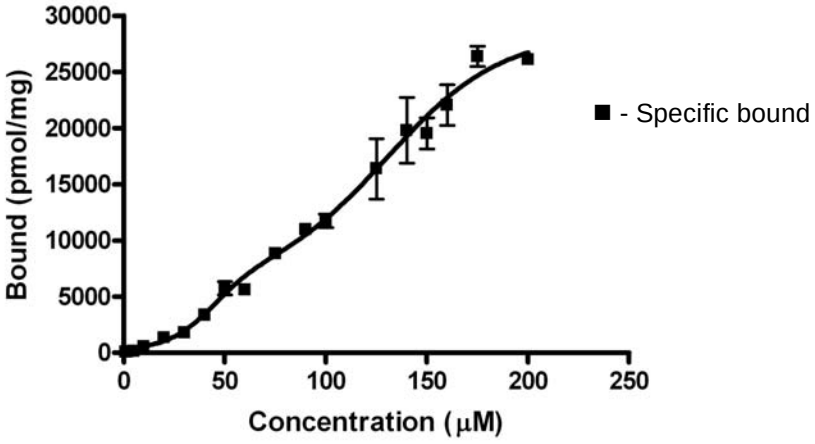

Figure 28. Determination of [^{3}H]5HPP-33 binding to tubulin.

Two K_d values were obtained, 78.6 $\pm$ 3.5 μM and 137.5 $\pm$ 10.5 μM for a high and a low affinity site, respectively. The Hill slopes were calculated to be ~2 and ~6 for the high and low affinity K_d values, respectively. As shown in Figure 29, the Scatchard plot for [^{3}H]5HPP-33 binding to tubulin exhibited a downward curvature. Such a curvature is reminiscent of enzyme systems displaying positive cooperativity. The plot appears to be two downward facing curves, which could indicate two binding sites.

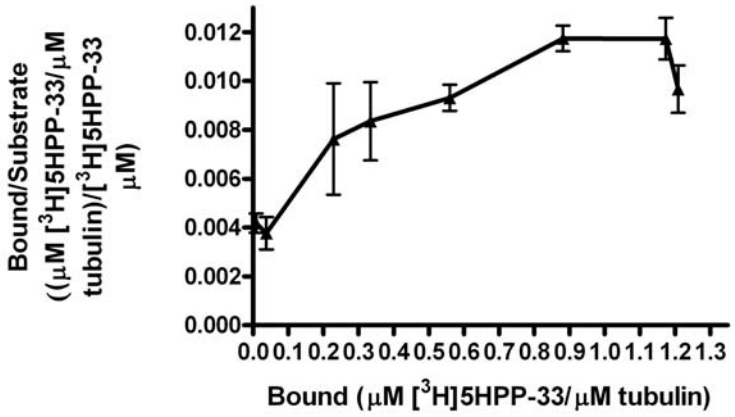

Figure 29. Scatchard plot of [^{3}H]5HPP-33 binding to tubulin

4.7.2 Interactions of [^{3}H]5HPP-33 with Microtubule Associated Proteins

The possibility that 5HPP-33 interacts with MAPs and diminishes the aggregation reaction of tubulin dimmers was tested by incubating 2.0 mg/mL of MAPs with various concentrations of [^{3}H]5HPP-33. Figure 30 shows the results of this experiment using three concentrations of [^{3}H]5HPP-33. Higher concentrations could not be tested because of solubility issues with

[^{3}H]5HPP-33 (insoluble in the assay conditions at concentrations $\geq$ 200 μM), which prevented the determination of a K_d value.

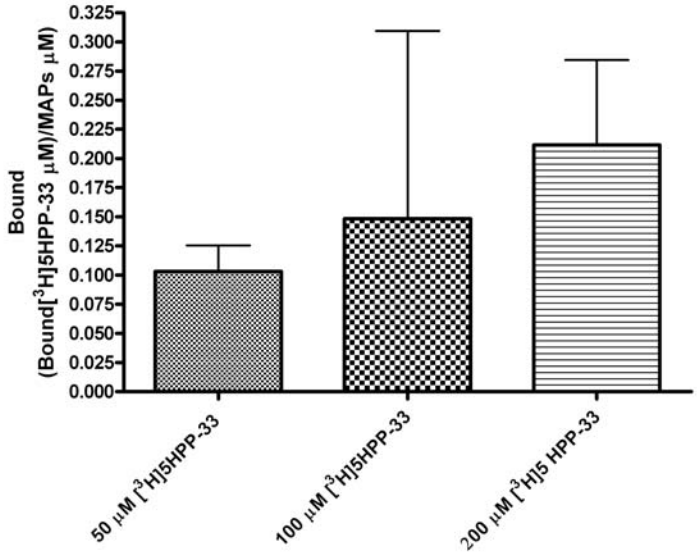

Figure 30. [^{3}H]5HPP-33 binding to 2.0 mg/mL MAPs

The values reported are the average of two experiments ± S.D. At a concentration of 50 μM, [^{3}H]5HPP-33 binding to 2.0 mg/mL MAPs could be detected, and binding increased in a concentration dependent manner.

4.7.3 Effect of MAPs on [^{3}H]5HPP-33 binding to the tubulin heterodimer

The conditions performed in the tubulin polymerization assay were simulated in the binding assay to test the effects of the presence of MAPs on [^{3}H]5HPP-33 binding to tubulin heterodimer. Briefly, various concentrations of [^{3}H]5HPP-33 were incubated with 0.75 mg/mL MAPs and 1.0 mg/mL tubulin at 0^{o}C for 30 min. The reaction mixture was then transferred to the ultrafiltration apparatus and the amount of free [^{3}H]5HPP-33 was determined by scintillation

spectrometry. The results of this experiment are presented in Figure 31. The binding data was analyzed as described previously for the tubulin only data set. The high affinity K_d value for the MAPs plus tubulin binding set, was not significantly different from that obtained in the tubulin only system, yielding a value of 67.5 $\pm$ 12.4 μM, but a low affinity K_d value could not be determined. The Hill slope was calculated to be ~3 using GraphPad Prism.

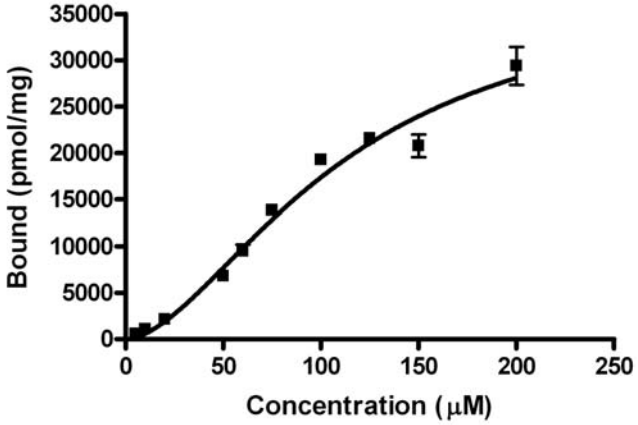

Figure 31. Saturation binding data for [^{3}H]5HPP-33 in the MAPs plus tubulin system

The Scatchard plot for this binding data is presented in Figure 32. This plot is a downward parabola that is characteristic of both self-associating and positive cooperativity systems. This plot does not have the two downward curves that were seen in the tubulin only system in Figure 30.

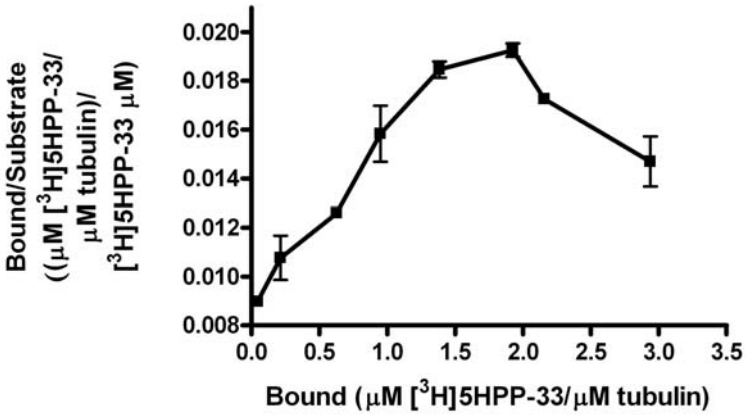

Figure 32. Scatchard plot of binding data in tubulin plus MAPs system

4.7.4 Competitive inhibition assays with [^{3}H]5HPP-33

It is conceivable that 5HPP-33 competes with known microtubule perturbing agents, even though this could not be detected in any of the previous binding experiments. There are two possible explanations for this phenomenon. One is that the low affinity of 5HPP-33 for the tubulin heterodimer made it impossible to detect any significant competition, or the wrong form of tubulin was used in the competition assay (*i.e.*, soluble tubulin versus preformed microtubules). To determine if this was the case, a competitive inhibition assay utilizing gel filtration to separate bound ligand from free was utilized. Table 11 presents the results of this assay, in which 10 μM [^{3}H]5HPP-33, 1.5 mg/mL tubulin and various concentrations of inhibitor were used.

Table 11. Competitive inhibition experiments with [^{3}H]5HPP-33

Compound	**% Inhibition ± S.D.**
5 μM Vinblastine	–6 ± 10
5 μM Colcemid	–15 ± 11
50 μM Colcemid	–42 ± 8
5 μM Paclitaxel	0 ± 3
50 μM Paclitaxel	18 ± 7

Colcemid, an colchicine analogue, failed to inhibit binding of [^{3}H]5HPP-33 at all concentrations tested.[127] There was not any appreciable inhibition of binding using 5 μM vinblastine. Paclitaxel at a concentration of 50 μM inhibited the binding of [^{3}H]5HPP-33 by 18%. This inhibition is probably due to the formation of microtubules in the presence of paclitaxel, which causes the loss of the soluble tubulin. It was reported by Inatsuki *et al*. that 5HPP-33 binds to soluble tubulin over microtubules.[114]

4.8 DISCUSSION

5HPP-33 is a small, structurally simple molecule, with antiproliferative activity in the low micromolar range against a number of cancer cell lines. Flow cytometric analyses show that 10 μM 5HPP-33 blocks cells in the G_2/M phase of the cell cycle.[66] Tubulin polymerization assays showed 5HPP-33 to have mixed effects on microtubule polymerization dynamics. In the tubulin polymerization system utilizing MSG, 5HPP-33 appeared to induce polymerization and stabilize polymer against cold depolymerization. In the MAPs system, 5HPP-33 produced the opposite effect, and at a concentration of 10 μM completely inhibited microtubule polymerization. To unravel this discrepancy, electron microscropy was used to characterize the polymer formed in both systems. The electron microscopy pictures explained the differences between the tubulin polymerization assays. From the images obtained, it is clear that microtubules are not being formed in either system and that 5HPP-33 causes an aberrant polymer formation. This polymer was an aggregation of rings and spirals, and aggregation was lessened in the MAPs system. The lessened aggregation explains the appearance of the tubulin polymerization graph. At this point in time, the exact mechanism for the heightened aggregation in the presence of MSG was not known.

The rings and spirals formed in the presence of 5HPP-33 is reminiscent of the vinca domain binding agents, such as dolastatin 10 and the vinca alkaloids.[44] Numerous percent inhibition assays with radiolabeled vinca domain binding compounds were performed, but 5HPP-33 failed to compete with any of these agents. 5HPP-33 failed to compete with [^{3}H]colchicine and [^{3}H]paclitaxel for their respective binding sites on tubulin heterodimer. A five-fold excess of paclitaxel seems to compete for the 5HPP-33 binding site on the tubulin

dimer. This inhibition is probably due to the formation of microtubules in the presence of paclitaxel but not to actual competition between the two compounds.

The inability of 5HPP-33 to compete for the binding site of many known microtubule perturbing agents, and the lessening of aggregation seen in the MAPs system tubulin polymerization graphs prompted the radiosynthesis of [^{3}H]5HPP-33. It is possible that the loss in aggregation observed in the MAPs system is due to the binding of 5HPP-33 to MAPs, and this hypothesis was tested using [^{3}H]5HPP-33. Three condition under which saturation binding kinetics were devised, which were binding in the presence of tubulin only, binding in the presence of MAPs only, and binding in the presence of tubulin + MAPs. The concentrations of tubulin and MAPs were identical to that of the tubulin polymerization assay.

Saturation kinetic data from the tubulin only system showed that there are two possible mechanisms for [^{3}H]5HPP-33 binding to tubulin. In one possible scenario, 5HPP-33 has two binding sites on the microtubule, which upon binding to either site on the tubulin dimer can cause aberrant polymer formation can occur. The other possible mechanism is that there is binding only to one site on the tubulin dimer, and that the aggregation reaction just exhibits itself as two site binding, which is common with the vinca domain binding compounds.[44]

The Hill slopes were calculated to be ~2 and ~6 for the high and low affinity K_d values respectively. The Hill slope coefficient supplies information about the nature of the interaction between ligand and protein.[73] A Hill slope deviation from unity indicates cooperativity, which occurs when the binding of one ligand causes a conformational change in the protein-binding site that leads to activation or inhibition of the binding of a second ligand molecule. Cooperativity can be negative or positive, as well as homotropic or heterotropic. If the Hill slope is > 1, this indicates positive cooperativity and that the binding of one ligand increases the affinity of the

binding of a second. If the Hill slope is < 1, negative cooperativity is occurring and the binding of one ligand decreases the affinity of a second binding. Homotropic cooperativity involves the same substrate and heterotropic cooperativity is between different substrates.[128] The Hill slope for [^{3}H]5HPP-33 binding deviated from unity, but unfortunately this does not necessarily mean that cooperativity is occurring. The deviation from unity in the Hill slope is most likely due to the self-association of tubulin dimers in the presence of [^{3}H]5HPP-33 as witnessed in the electron microscropy analyses.[125] This association does not have to occur with conformational change to the binding site.

The K_d values determined in both systems are not true determinations of the values, but probably represent a mixture of the relative K_d values for each individual step in the aggregation reactions. Further studies involving ultracentrifugation reactions to determine sedimentation coefficients and extent of aggregation are needed to determine reaction rates, and the type of self-association occuring.[129, 130]

The binding of [^{3}H]5HPP-33 to MAPs was observed at concentrations above 50 μM, and the binding occurred in a concentration dependent manner. Unfortunately, a K_d value could not be determined for this interaction because of solubility issues.

The saturation binding graph generated from the tubulin + MAPs system was different from the plot obtained in the tubulin only system. This graph showed only one binding site for [^{3}H]5HPP-33, and the transformation of the this data into a scatchard plot showed only one downward curve.

It is now plausible to say from the combined data from all three systems that 5HPP-33 probably does not bind to two sites on the tubulin heterodimer, but the aggregation reaction disguises itself as two binding sites. The binding to the second site was not observed in the

tubulin + MAPs at the concentrations used in the tubulin only system. From the tubulin polymerization assays it is known that the aggregation reaction caused by 5HPP-33 is lessened in the presence of MAPs. This is due to the competition between MAPs and tubulin for 5HPP-33.

The small molecule estramustine is known to compete with paclitaxel in a non-competitive manner for its binding site, and binds to two sites on the tubulin dimer.[131] It has also been reported that estramustine has an affinity for binding to MAPs.[132, 133]

Cemadotin, a synthetic analogue of dolastatin 15, shares many common characteristics with 5HPP-33. Cemadotin does not inhibit the binding of any know microtubule agents, appears to have two binding sites on tubulin, and has an IC_{50} value for the inhibition of tubulin assembly 20 times lower than its K_d.

In conclusion, 5HPP-33 is a small, easily synthesized, potential chemotherapeutic agent, which blocks cells in the G_2/M phase and exerts it activity by perturbing microtubule dynamics. The kinetics of binding of this agent were characterized, and it seems to have a novel mechanism through which it inhibits microtubule polymerization. Further analysis of this compound might lead to a useful new set of microtubule perturbing agents.

5.0 EVALUATION OF POTENTIAL MICROTUBULE INHIBITORS

5.1 THE MICROTUBULE DESTABILIZER (–)-PIRONETIN

(–)-Pironetin is a small natural product that contains an α,β-unsaturated lactone, six stereocenters and an alkyl chain. Originally described as a potent inhibitor of plant growth, it was isolated from the bacterial broth of *Streptomyces* sp. NK10958.[134] It was later recognized that (–)-pironetin arrests cancer cells in G_2/M phase and is a potent inhibitor of microtubule assembly. It is also retains its activity against multi-drug resistant cell lines. It has been suggested that (–)-pironetin forms a covalent bond to Lys352 on α-tubulin, which is found near the interface of the heterodimers.[135] This places (–)-pironetin in proximity to the nucleotide exchangeable site on β-tubulin, the site at which the vinca alkaloids bind.[44]

Recently, Shen *et al.* reported on the total synthesis of (–)-pironetin using their novel alkaloid catalyzed acyl halide (ACC) methodology.[136] Using this methodology, four compounds were synthesized, (–)-pironetin in two-steps with a 56% yield, the optical antipode (+)-pironetin, 3-hydroxypironetin, and pironetin-2,4-dione. The structures of these compounds are shown in Figure 33.

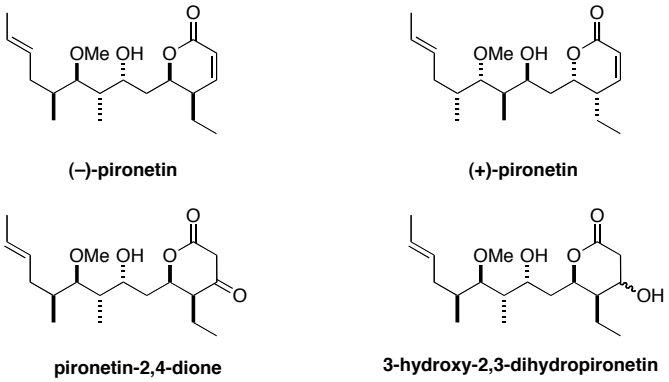

Figure 33. (–)-Pironetin and its analogues

The short and efficient synthesis of (–)-pironetin and its reported potent cytotoxic and microtubule inhibitory properties make it a possible drug candidate. In order to learn more about the mechanism of action of (–)-pironetin, cellular and biochemical evaluation of it and its analogues was performed.

5.1.1 Cellular effects of (–)-pironetin and its analogues as determined by multiparameter immunoflourescence microscopy

This work was performed in Dr. Andreas Vogt's lab in the Department of Pharmacology, School of Medicine, at the University of Pittsburgh. To assess the mitotic effects of (–)-pironetin and its analogues on cells, HeLa cells were treated with indicated concentrations of compounds, the nucleus stained with Hoechst 33342, and incubated with primary antibodies against α-tubulin and phosphorylated histone H3. Fluorescently-labeled secondary antibodies were then added that are conjugated to Cy3 and FITC. Minimum detectable effective concentration (MDEC) values are presented in Table 12. The MDEC values were calculated for nuclear condensation, microtubule mass, and histone H3 phosphorylation.

Table 12. Effects of (–)-pironetin and its analogues on HeLa cells determined using immunofluorescence microscopy

Compound	Nuclear Condensation	Mitotic Index	Microtubule Mass
	MDEC (nM)		
(–)-Pironetin	7.0 ± 1.5	6.2 ± 1.0	7.1 ± 1.6
(+)-Pironetin	> 5000	> 5000	> 5000
Pironetin-2,4-dione	> 10000	> 10000	> 10000
3-Hydroxy-2,3-dihydro-pironetin	242 ± 16	278 ± 46	276 ± 25
Vincristine	2.5 ± 2.0	1.9 ± 1.3	2.5 ± 1.3
Paclitaxel	5.3 ± 5.3	2.82 ± 1.5	4.3 ± 2.7

The values reported are the average ± S.D. of three independent experiments. The proportion of cells undergoing mitosis, the mitotic index, was calculated using the percentage of cells positive for phosphorylated histone H3. The optical antipode of pironetin and pironetin-2,4-dione were inactive in this assay. MDEC values for (–)-Pironetin were comparable to the values for vincristine and paclitaxel. (–)-Pironetin caused increased chromatin condensation and phosphohistone H3 levels. 3-Hydroxy-2,3-dihydropironetin was not as active as (–)-pironetin, but possessed MDEC values < 1 μM.

Fluorescent microscopy images of HeLa cells were obtained after treatment with equipotent concentrations of (–)-pironetin, its analogues, and vincristine. These are presented in Figure 34.

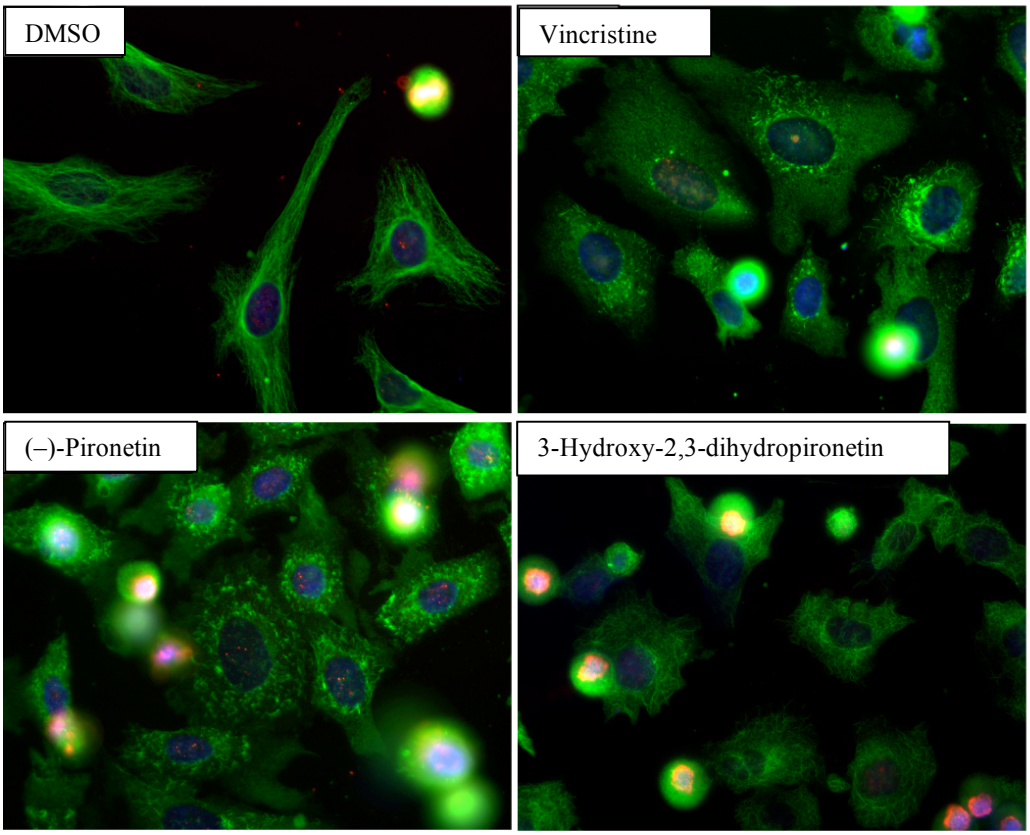

Figure 34. Immunofluorescence images of HeLa cells

Upon treatment with the compounds, there was loss of the normal microtubule network within the cell and the formation of tubulin aggregates. The effects of (–)-pironetin, the 3-hydroxy-analogue, and vincristine on microtubules appear to be very similiar. It is known that vincristine is a potent inhibitor of microtubule polymerization, and it can be extrapolated from the images that (–)-pironetin and its analogue work by the same mechanism.

5.1.2 Antiproliferative effects of (–)-pironetin and its analogues

This work was performed in Dr. Andreas Vogt's lab in the Department of Pharmacology and Chemical Bioligy, School of Medicine, at the University of Pittsburgh. Breast, lung and glioblastoma cells were treated with (–)-pironetin and its analogues for 72 h to determine the antiproliferative activities of the compounds. DC-3F Chinese hamster cell lines rendered resistant to multiple drugs by overexpression of the P-glycoprotein pump were used to assess if (–)-pironetin and its analogues would retain activity in cells containing the ABCB1 transporter. The GI_{50} values were determined as described in Chapter2. Briefly, cells were exposed to MTS and cell number was determined spectrophotometrically at 490 nm minus exposure at 630 nm. The GI_{50} values for (–)-pironetin and its analogues were calculated as an average $\pm$ S.D. of three independent experiments. The fold resistance was calculated from dividing the GI_{50} value in the VCRd5L line by the GI_{50} value in the DC-3F Chinese hamster cell line. (–)-Pironetin gave GI_{50} values in the low nanomolar range for all cell lines tested and maintained activity against the multidrug resistant Chinese hamster cells.

Table 12. Antiproliferative ability of (–)-pironetin and its analogues in various cancer cell lines

Compound	GI_{50} + S.D. [90]						
	MCF-7	T98G	A549	MDA-MB231	DC-3F	VCRd5L	Fold resistance
(–)-Pironetin	5.0 ± 0.2	7.5 ± 1.2	7.5 ± 0.9	4.6 ± 1.2	9.5 + 1.2	31 ± 5	3.2
(+)-Pironetin	47000 ± 3000	30000 ± 3000	> 5000	> 5000	ND		
Pironetin-2,4-dione	> 50000	> 50000	> 10000	> 10000	ND	ND	
3-Hydroxy-2,3-dihydropironetin	370 ± 40	740± 160	179 ± 22	168 ± 65	338 ± 66	1118 ± 56	3.3
Vinblastine	3.5 ± 0.1	< 0.8					
Vincristine	ND	ND	10.8± 2.9	5.5 ± 3.1	19 ± 16	>> 5000	>> 250
Paclitaxel	10.9± 0.2	24.0 ± 9.0	3.5 ± 0.5	1.6 ± 0.9	45 ± 11	2682 ± 109	59

Vincristine and paclitaxel gave low nanomolar GI_{50} values in all cell lines tested except for the multidrug resistant Chinese hamster cell line. There was a greater than 250- and 59-fold increase in the GI_{50} values for vincristine and paclitaxel, respectively. From this information, it seems possible that (–)-pironetin and the vincas differ in the mechanisms through which they interact with cells.

5.1.3 Effects of (–)-pironetin and its analogues on tubulin assembly

To test the hypothesis that (–)-pironetin is mechanistically distinct from the vinca alkaloids in its ability to inhibit tubulin assembly, tubulin polymerization assays were performed as described in Chapter 2. Dr. Raghavan Balachandran performed this work in the Day lab. The MSG system was used to induce polymerization as described in Chapter 2. Briefly, compounds were incubated with 0.8 M MSG pH 6.6, 4% DMSO and 1.0 mg/mL tubulin for 15 min at 30 ^{o}C. The reaction mixture was cooled to 0 ^{o}C, GTP was added to the cuvettes for a final concentration of

400 μM, and tubulin polymerization was followed spectrophotometrically at 350 nm. The results of the experiment are presented in Figure 35.

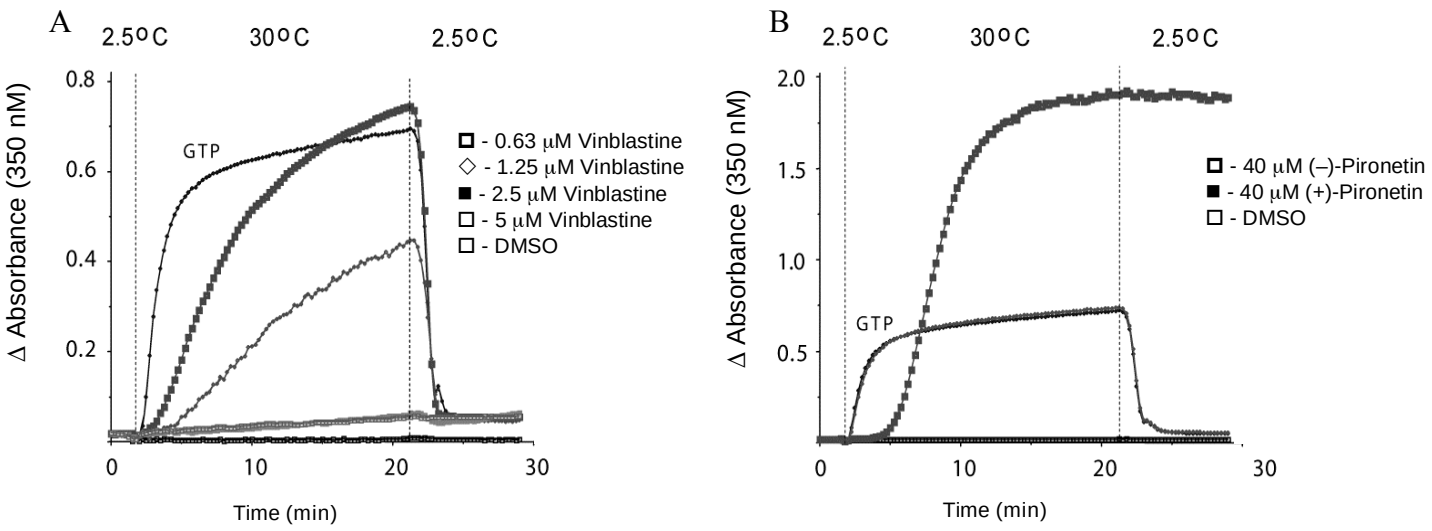

Figure 35. Tubulin polymerization assays comparing concentration dependent assembly in the presence of vinblastine and (–)-pironetin

Panel A in Figure 35 shows tubulin assembly in the presence of indicated concentrations of vinblastine. At a concentration of 5 μM, vinblastine completely inhibited tubulin assembly. Panel B presents the tubulin assembly in the presence of 40 μM (–)-pironetin, which caused the appearance of a sigmoidal curve. The aggregation, which was visualized in the immunofluorescence images of cells, probably corresponds to the increase in polymerization seen in this assay. (–)-Pironetin delayed the onset of assembly, but the aggregation continued until it reached a steady state. The polymer former was stable to cold disassembly. From this assay, it appears that (–)-pironetin is mechanistically different from vinblastine in its ability to

inhibit tubulin polymerization, and may be distinct from any microtubule inhibitor previously characterized.

5.1.4 Inhibition of [^{3}H]vinblastine by (–)-pironetin and its analogues

A competitive inhibition binding assay was performed to assess the ability of these compounds to compete with [^{3}H]vinblastine for its binding site on the tubulin heterodimer. This assay also provided further evidence that (–)-pironetin is mechanistically distinct from the vinca alkaloids. This result was very different from anything obtained with previous microtubule inhibitors. The results of the inhibition assay are shown in Table 13.

Table 13. Competitive inhibition assay utilizing [^{3}H]vinblastine

Test Agent	**% Inhibition of [^{3}H]Vinblastine**
Vincristine	65 ± 2
Vincristine (50 μM)	98 ± 1
Dolastatin 10	61 ± 1
(–)-Pironetin	15 ± 4
(+)-Pironetin	3 ± 7
Pironetin-2,4-dione	3 ± 8
3-Hydroxypironetin	6 ± 7
Colchicine	–11 ± 12

The percent inhibition values are reported as the average ± S.D. of two experiments with each sample processed in duplicate. Vincristine and dolastatin 10 are well known inhibitors of [^{3}H]vinblastine binding, demonstrating their function as positive controls.[44] As shown in Table 13, 5 μM vincristine and dolastatin 10 inhibited the binding of 10 μM [^{3}H]vinblastine to tubulin by 65 ± 2 and 61 ± 1% respectively. (–)-Pironetin inhibited the binding of [^{3}H]vinblastine by 15 ± 4%. Neither the analogues of pironetin nor the antipode showed any appreciable inhibition

binding. Colchicine was used as the negative control and did not compete for [^{3}H]vinblastine for its binding site.

5.2 THE TUBULYSINS

Tubulysins are potent microtubule inhibitors isolated from the myoxbacterial strains *Arthangium gephyra* and *Angiococcus discoformis*.[90, 137, 138] The tubulysins are metabolic peptides with a general sequence of D-methylpipecolate-L-isoleucine-L-tubuvaline-L-tubuphenylalanine. There is considerable structural similiarity between the microtubule destabilizers dolastatin 10 and the hemiasterlins with the tubulysins.

A problem that is often encountered with the use of peptides as potential drug candidates *in vivo* is low bioavailability.[139] The structure of most of the tubulysins contains a labile *N*,*O* acetal functionality. To improve on the stability of the tubulysins but retain biological activity, Wipf *et al.* synthesized N^{14}-desacetoxytubulysin H (WZY-111-63C).[140] In this compound, the *N*,*O* acetal is replaced with an *N*-alkyl group. Two other compounds, WZY-111-64A and WZY-111-64A, were prepared as a means to simplify the synthesis and increase bioavailability. The structures are presented in Figure 36.

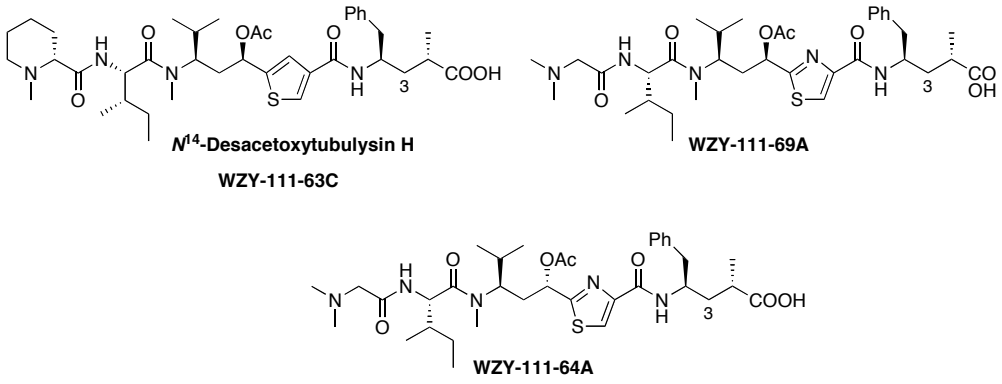

Figure 36. Structural analogues of the tubulysins

Several assays were performed to assess the effect that these changes had on microtubule inhibitor properties and cytotoxic abilities.

5.2.1 Antiproliferative effects of the tubulysins

This work was performed, with my gratitude, by Dr. Raghavan Balachandran in the Day lab. The cytotoxic ability of the tubulysin analogues was assessed in T98 glioblastoma cells. Glioblastoma is the most common and aggressive type of brain tumor.[141] The average GI_{50} values $\pm$ S.D. were determined from four independent experiments. The cells were treated with the compounds and incubated for either 96 h or 72 h. After exposure to MTS the GI_{50} values were determined spectrophotometrically. The results of the experiment are presented in Table 14.

Table 14. Antiproliferative effects of the tubulysin analogues.

Compound	**T98 Glioblastoma cells $GI_{50} \pm$ S.D.**	
	96 h	72 h
N^{14}-desacetoxytubulysin H (WZY-111-63C)	1.6 ± 0.8	4.4 ± 11
WZY-111-64A	400 ± 30	590 ± 1000
WZY-111-69A	350 ± 40	430 ± 130
Paclitaxel	12 ± 7	24 ± 9
Vinblastine	1.0 ± 0.6	8.6 ± 0.9
Dolastatin 10	0.056 ± 0.025	0.1 ± 0.02

The GI_{50} values for N^{14}-desacetoxy tubulysin H (WZY-111-63C) were in the low nanomolar range for both time points. The cytotoxicity of N^{14}-desacetoxy tubulysin H (WZY-111-63C) was comparable to the positive control vinblastine and was more active in this assay than paclitaxel. The other two analogues were not as active and possessed submicromolar GI_{50} values.

5.2.2 The effects of the tubulysins on tubulin assembly

The tubulysins have been reported to be potent inhibitors of microtubule assembly.[90] To determine the ability of the tubulysin analogues to inhibit microtubule assembly, assays were performed with purified tubulin. A tubulin polymerization assay utilizing the MSG system was performed as described in the Materials and Methods section. IC_{50} values were determined for each analogue as previously described. An example of the tubulin polymerization graphs obtained for N^{14}-desacetoxy tubulysin H (WZY-111-63C) are presented in Figure 37.

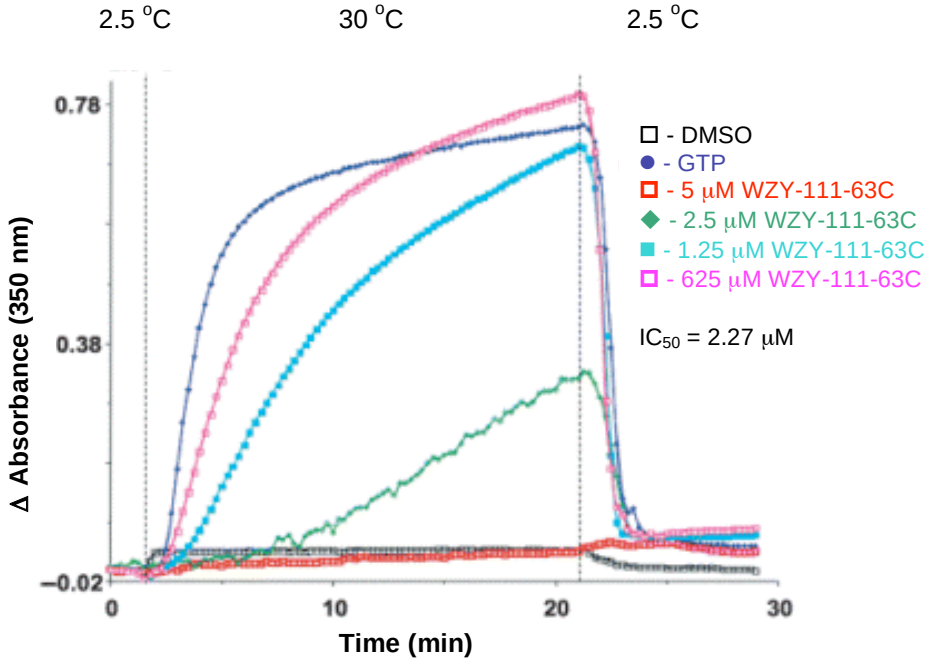

Figure 37. Effects of N^{14}-desacetoxy tubulysin H (WZY-111-63C) on tubulin assembly

The IC_{50} values determined from the tubulin polymerization graphs are presented in Table 15. N^{14}-Desacetoxy-tubulysin H (WZY-111-63C) was the most potent inhibitor of GTP-induced tubulin assembly and was comparable to the positive control values for the known inhibitors vinblastine and dolastatin 10. WZY-111-69A was a potent compound as well with an

IC_{50} value of 3.1 μM. WZY-111-64A had barely an effect on tubulin assembly and had an IC_{50} > 5 μM.

Table 15. Fifty percent tubulin assembly inhibition values for the tubulysin analogues.

Compound	**Tubulin Assembly Inhibition IC_{50} (μM)**
N^{14}-desacetoxytubulysin H (WZY-111-63C)	2.3
WZY-111-64A	>5
WZY-111-69A	3.1
Vinblastine	1.6
Dolastatin 10	1.4

5.2.3 Ability of tubulysin analogues to compete with radiolabeled vinca domain binding agents

The ability of the tubulysin analogues to compete with potent vinca domain binding agents was tested. For the most potent compounds, IC_{50} values were determined by fitting the data to the Hill equation. The percent inhibition values for the assays utilizing [^{3}H]vinblastine and [^{3}H]dolastatin 10 are presented in Table 16. The percent inhibition and IC_{50} values are the average ± S.D. of two experiments with each sample processed in duplicate.

Table 16. Percent Inhibition and IC_{50} values for the vinca domain binding assays.

Compound	**Inhibition of [^{3}H]Vinblastine binding and test agent IC_{50}**	**Inhibition of [^{3}H]Dolastatin 10 binding and test agent IC_{50}**
N^{14}-desacetoxytubulin H	50 ± 4% (5.6 ± 0.5 μM)	31 ± 3% (10 ± 1 μM)
WZY-111-64A	2 ± 5% (>50 μM)	–11 ± 10% (ND)
WZY-111-69A	43 ± 1% (8.8 ± 1.6 μM)	4 ± 3 (64 ± 9 μM)
Dolastatin 10	61 ± 1% (4.6 ± 0.5 μM)	N/A
Vincristine	65 ± 2% (4.4 + 0.7 μM)	21 ± 5% (29 ± 5 μM)
Colchicine	–11 ± 12%	–5 ± 8%

Colchicine was used a negative control and vincristine as a positive control in both assays. Dolastatin 10 was used as a second positive control in the [^{3}H]vinblastine binding assay. The ability of the analogues to inhibit the binding of [^{3}H]vinblastine and [^{3}H]dolastatin 10 into microtubules was in the order N^{14}-desacetoxytubulysin H (WZY-111-63C)>WZY-111-69A>>WZY-111-64A.

The analysis of the binding data for the determination of the IC_{50} for the [^{3}H]vinblastine assay and [^{3}H]dolastatin 10 is presented in Figure 38. The Hill slopes were >1 for all binding sets. The concentration-dependent inhibition binding curves for the [^{3}H]vinblastine assay are shown in Panel A of Figure 38. Vincristine had the lowest IC_{50} at 4.4 $\pm$ 0.7 μM, but the IC_{50} for N^{14}-desacetoxytubulysin H (WZY-111-63C) was comparable, 5.6 $\pm$ 0.5 μM. The IC_{50} for WZY-111-69A was 8.8 $\pm$ 1.6 μM.

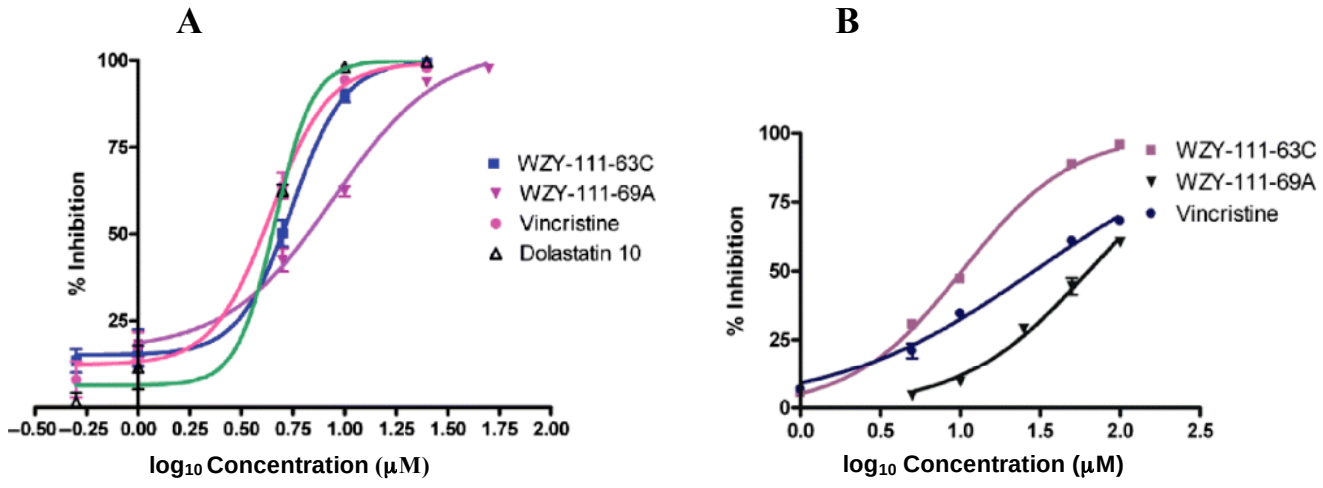

Figure 38. Concentration-dependent inhibition of binding of radiolabeled ligands to bovine brain tubulin

The concentration-dependent inhibition curvers for the [^{3}H]dolastatin 10 binding assay are shown in Figure 38 Panel B. Vincristine was used as the positive control and the calculated IC_{50} was 29 $\pm$ 5 μM. IC_{50} values calculated for N^{14}-desacetoxytubulysin H (WZY-111-63C) and WZY-111-69A were 10 $\pm$ 1 and 64 $\pm$ 9 μM, respectively.

5.3 DISCUSSION

(–)-Pironetin is a small molecule microtubule inhibitor that probably acts by formation of a covalent bond to Lys352.[138] Preparation using the AAC methodology represents a simple synthetic route for the production of (–)-pironetin.[136] From the studies presented here, it is clear that (–)-pironetin is a potent inhibitor of cell proliferation, retains potency against multi-drug resistant cell lines, and differs in its mechanism from traditional microtubule inhibitors.

From the multiparameter cell based immunofluorescence assay, it was clear that (–)-pironetin was an antimitotic agent, and from the immunofluorescence images it was ascertained that it caused tubulin aggregation. This suggested that the compound acts in a mechanism much like the vinca domain binding agents. However, tubulin polymerization and competitive percent inhibition assays with radiolabeled [^{3}H]vinblastine, indicate that (–)-pironetin is a novel microtubule inhibitor.

The (–)-pironetin analogue, 3-hydroxy-2,3-dihydropironetin, was the only analogue examined that possessed any biological activity. Although it was active in the cellular assay, it did not possess any ability to inhibit tubulin assembly (data not shown) or the binding of [^{3}H]vinblastine. One possible explanation for this is that 3-hydroxy-2,3-dihydropironetin is metabolized *in vivo* to an active form, perhaps pironetin. This indicates the possible use of this compound as a prodrug.

The sigmoidal shape of the graphs obtained in the tubulin polymerization graphs is probably due to the aggregation reaction formed in the presence of (–)-pironetin. The delay in the onset of assembly is maybe due to the formation of the covalent linkage, which then causes the aggregation reaction.

(–)-Pironetin is a weak inhibitor of [^{3}H]vinblastine binding. The results presented here for the [^{3}H]vinblastine binding assay coincide with those previously reported by Kondoh *et al.*, although their results suggest a higher percentage of inhibition.[142] This may be due to the differences in the amount of protein, tracer and inhibitor that were used in the two experiments. In the inhibition assay used here, the ratio of tubulin, tracer and inhibitor was 1:1:0.5. The experiment was performed in this ratio because it provided a quick and easy method of comparing the positive controls to the test compounds. This is in comparison to Kondoh's assay, which was performed in the ratio of 1:0.01:10. The 20-fold greater concentration of inhibitor used in Kondoh's assay may account for the discrepancy in the percent inhibition values between the two experiments.

The formation of a covalent bond to Lys352, near the interface of the dimers, places (–)-pironetin in proximity to the nucleotide exchangeable site on β tubulin. The results from the [^{3}H]vinblastine competitive binding assay were in agreement with the proposed mechanism of binding for (–)-pironetin. The covalent linkage of (–)-pironetin to Lys352 should prevent [^{3}H]vinblastine from binding to its site on β tubulin near the exchangeable nucleotide site at the tubulin heterodimer interface. Usui *et al.* have already proposed that this explains the weak inhibition of [^{3}H]vinblastine binding by (–)-pironetin.[135]

The formation of a covalent linkage might be a way of overcoming P-glycoprotein resistance resistance. The formation of a covalent bond between tubulin and compound neutralizes this resistance mechanism because the compound may no longer be actively pumped out of the cell.[49] This mechanism has been reported for the microtubule stabilizer cyclostreptin.[31] Cyclostreptin forms a covalent linkage to Thr 220 and Asn 228 within the paclitaxel binding site on β-tubulin. Unlike paclitaxel, cyclostreptin retains its activity in multi-

drug resistant cell lines, suggesting that a covalent linkage overcomes this resistance.[75] The same mechanism maybe true involving microtubule inhibitors and could represent a future strategy for combating resistance during chemotherapy. Although covalent modifiers are usually not favorable drug candidates, there are examples in clinical use.[143, 144] An example that is used clinically as a chemotherapeutic agent, is the covalent modification of DNA by platinum agents.

Since the isolation and characterization of the tubulysins from myxobacteria, there has been a considerable amount of progress made towards the synthesis of the isolated tubulysins and synthetic analogues.[140, 145-147] This has been due in large part to the discovery that tubulysin A is a powerful cytotoxic agents, a potent microtubule inhibitor, and that there is limited supply from available sources. The limited supply makes it necessary to find synthetic routes, and the pharmacophore through modifications to the tubulysin scallfold.

To make a suitable drug candidate a compound must be bioactive, stable, and bioavailable.[139] Towards this goal, identifying potential labile or reactive groups is important when preparing a molecule to become a drug candidate. Changing these sites often increase bioavailabilty and the half-life of the compound *in vivo*.[148]

Three analogues were synthesized that removed a labile *N*,*O*-acetal functionality in the tubulysin scaffold. The change in this reactive group would hopefully serve to increase bioavailbilty without a loss in activity. N^{14}-desacetoxy-tubulysin H (WZY-111-63C) contained only one modification, which was the replacement of the *N*,*O*-acetal function with an *N*-alkyl group. The WZY-111-69A analogue removed the *N*-methylpipecolate residue and replaced it with an *N*,*N*-dialkylated amino acid. The third analogue, WZY-111-64A, contained all of the previously mentioned modifications and an epimerized stereocenter at C11.

The ability of the tubulysin analogues to inhibit the polymerization of tubulin into microtubules was in the order WZY-111-63C>WZY-111-69A>>WZY-111-64A. The ability of the compounds to inhibit the binding of [^{3}H]vinblastine and [^{3}H]dolastatin 10 mirrored the tubulin polymerization data. From this data, three conclusions were reached: the *N*,*O* acetal at N14 is not necessary for activity; replacement of the D-methylpipecolate residue with the simpler *N*-methylsarcosine reduces the affinity of the compound for the vinca domain binding site but still retains nanomolar potency in cancer cells; and the C11 natural configuration is required for biological activity. This data provided further insight the structure activity relationships for the tubulysins and also supplied important information that may improve the efficacy of tubulysin *in vivo*.

6.0 FUTURE DIRECTIONS

The discovery that 6-*epi*-dictyostatin is a potent analogue of (–)-dictystatin prompted the milligram synthesis of this compound for use in preclinical trials. It has already been tested in mice bearing MDA-MB231 xenografts (Eiseman *et al*., unpublished results). 6-*epi*-Dictyostatin was administered intravenously at a concentration of 20 mg/kg to mice three times every 7th day. Around 14 days mice treated with vehicle or control had to be euthanized due to tumor burden, but mice treated with 6-*epi*-dictyostatin did not have a substantial increase in tumor mass even after 34 days. Paclitaxel at the same concentration and dosing schedule was used as a positive control in this experiment. Animals dosed with paclitaxel had to be euthanized after 24 days due to tumor burden. They were some loss in body weight of animals treated with 6-*epi*-dictyostatin but it was less than 10%.

This first animal study proved that 6-*epi*-dictytostatin is a viable possibility for a future chemotherapeutic agent. Further studies in mice bearing other xenografts will assess the efficacy of this drug against multi-drug resistant and other types of tumors. Specimens of body fluids were taken from the animals after dosing to determine the metabolites of 6-*epi*-dictyostatin formed *in vivo*, and pharmacodynamic and pharmacokinetic parameters will be established in the mouse model for 6-*epi*-dictyostatin.

Combination chemotherapy may become the most effective way to treat cancer. Huang *et al*. have already proven the efficacy of combination of discodermolide and paclitaxel treatment in mice bearing human ovarian cancer cell xenografts.[149] The synergistic effects of peloruside A and laulimalide with other microtubule perturbing agents has already been evaluated.[150] Due to the novel properties of 5HPP-33, it can be hypothesized that a synergistic interaction might exist between it and other microtubule perturbing agents. Chou and Talalay reported the traditional method of reporting synergism, and this will be used to determine the antiproliferative effects of a combination treatment in a variety of cell lines.[151]

It has been established that (–)-pironetin binds to tubulin in a covalent manner through an interaction with Lys352 on α-tubulin.[135] The toxicity aspects of this compound must be determined before use in a clinical setting. Preclinical studies with mice will be performed to determine the efficacy and toxicity of (–)-pironetin.

The (–)-pironetin analogue 3-hydroxy-2,3-dihydropironetin was active in cellular assays but not in assays involving isolated tubulin. A time dependent cellular study must be performed to identify the active species of this compound.

Currently, more tubulysin analogues are being made to increase bioavailability and to reduce synthetic difficulty. These analogues will be tested to determine their antiproliferative effects and microtubule perturbing abilities. From this study, a compound might be chosen for scaled-up synthesis so as to take it into preclinical studies.

APPENDIX A

Spectral and HPLC data for key intermediates and the radiolabeled compound.

6, ^{1}H 600 MHz Bruker, $CDCl_3$

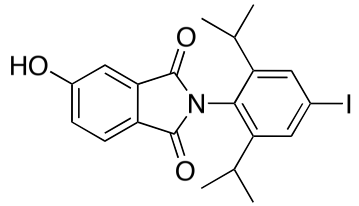

6, ^{13}C, 150 MHz, Bruker, $CDCl_3$

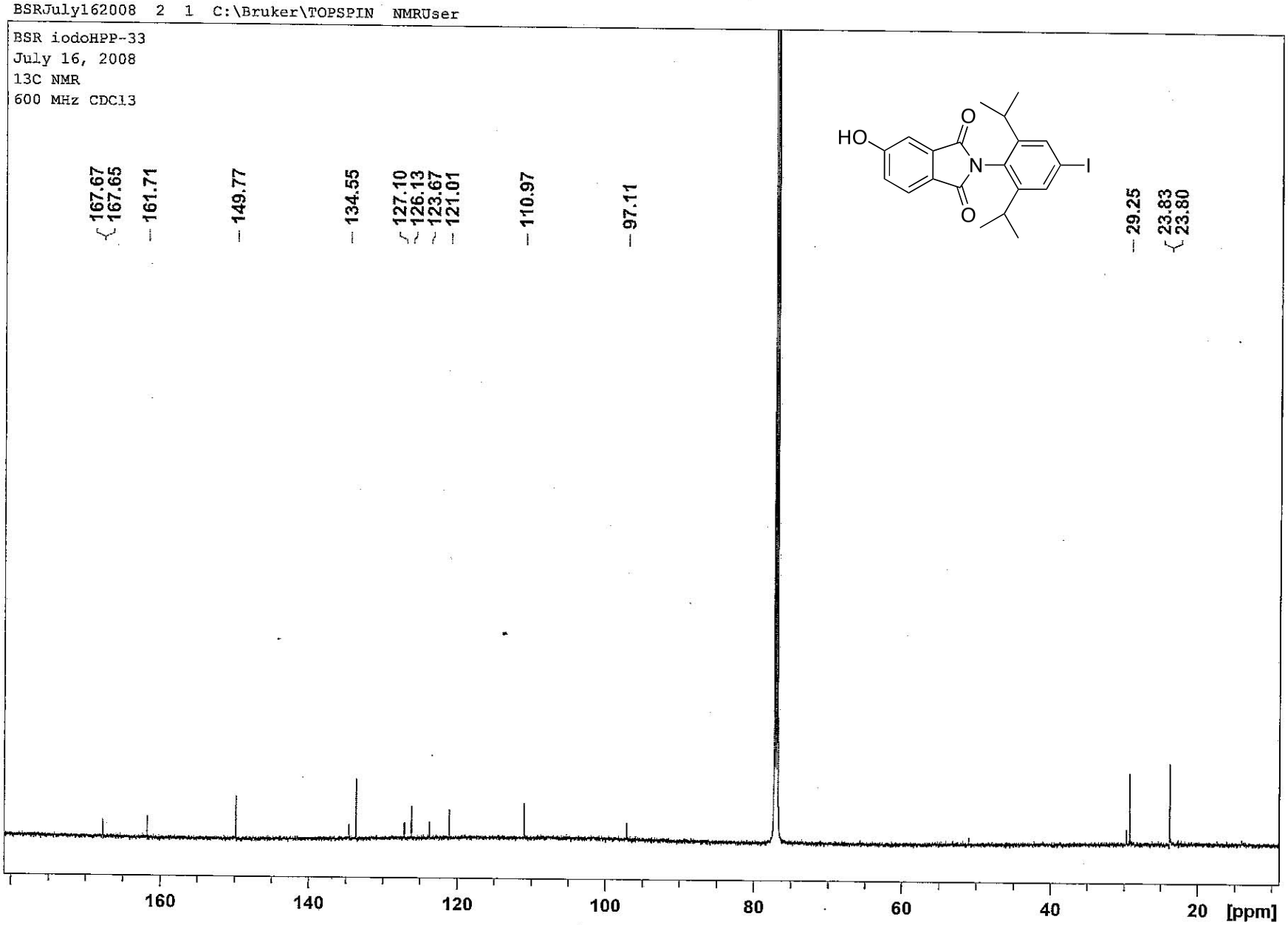

7, HPLC UV Chromatogram, Waters, 254 nm

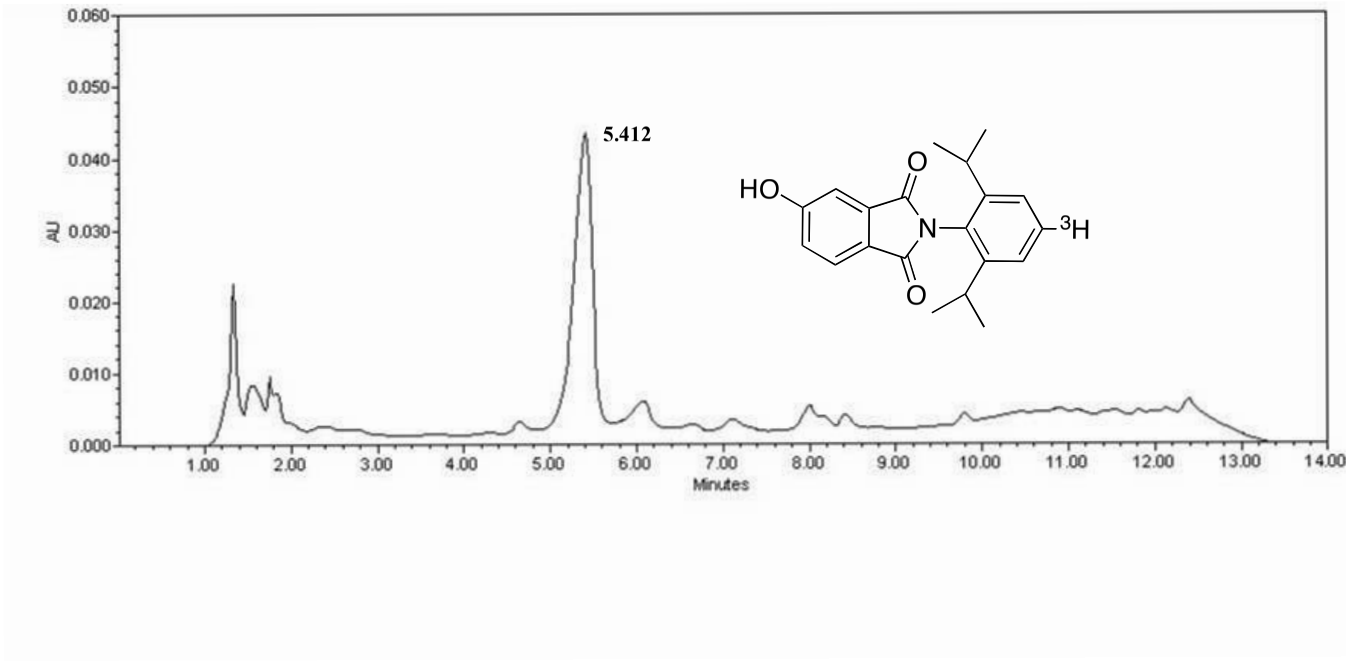

7, Radiochromatogram, Packard Flow Scintillation Analyzer

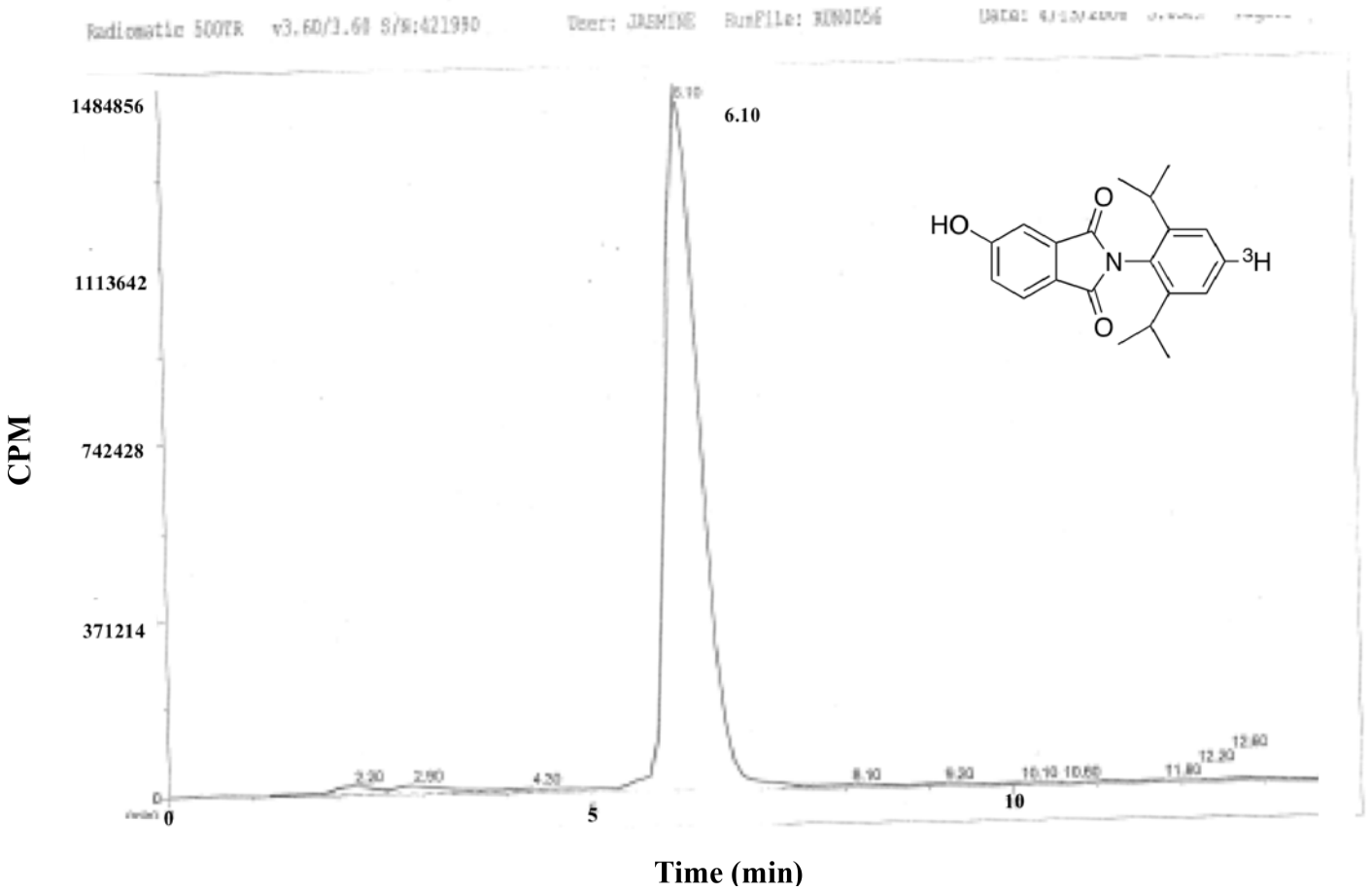

BIBLIOGRAPHY

1. Desai A, Mitchison TJ, (1997). Microtubule polymerization dynamics. *Annu. Rev. Cell Dev. Biol.,* **13**, 83-117.
2. Burns R, (1991). Alpha-, beta-, and gamma-tubulins: Sequence comparisons and structural constraints. *Cell Motil. Cytoskelet.,* **20**, 181-189.
3. Mandelkow E, Schultheiss R, Rapp R, Muller M, Mandelkow E, (1986). On the surface lattice of microtubules: Helix starts, protofilament number, seam, and handedness. *J. Cell Biol.*, **102**, 1067-1073.
4. Nogales E, Wolf SG, Downing KH, (1998). Structure of the alpha beta tubulin dimer by electron crystallography. *Nature*, **391**, 199-203.
5. Allen C, Borisy GG, (1974). Structural polarity and directional growth of microtubules of *Chlamydomonas flagella*. *J. Mol. Biol.*, **90**, 381-402.
6. MacNeal R, Purich DL, (1978). Stoichiometry and role of GTP hydrolysis in bovine neurotubule assembly. *J. Biol. Chem.*, **253**, 4683-4687.
7. Spiegelman B, Penningroth SM, Kirschner MW, (1977). Turnover of tubulin and the N site GTP in chinese hamster ovary cells. *Cell*, **12**, 587-600.
8. Erickson H, Stoffler D, (1996). Protofilaments and rings, two conformations of the tubulin family conserved from bacterial FtsZ to alpha/beta and gamma tubulin. *J. Cell Biol.*, **135**, 5-8.
9. Cassimeris L, Walker RA, Pryer NK, Salmon ED, (1987). Dynamic instability of microtubules. *BioEssays*, **7**, 149-154.
10. Erickson H, O'Brien ET, (1992). Microtubule dynamic instability and GTP hydrolysis. *Annu. Rev. Biophys. Biomol. Struct.*, **21**, 145-166.
11. Mitchison T, Kirschner M, (1984). Dynamic instability of microtubule growth. *Nature*, **312**, 232-237.
12. Walker R, O'Brien ET, Pryer NK, Soboeiro MF, Voter WA, (1988). Dynamic instability of individual microtubules analyzed by video light microscopy: Rate constants and transition frequencies. *J. Cell Biol.*, **107**, 1437-1448.
13. Mitchison T, Salmon ED, (2001). Mitosis: A history of division. *Nat. Cell Biol.*, **3**, E17-E21.
14. Compton D, (2000). Spindle assembly in animal cells. *Annu. Rev. Biochem.*, **69**, 95-114.
15. Wittmann T, Hyman A, Desai A, (2001). The spindle: A dynamic assembly of microtubules and motors. *Nat. Cell Biol.*, **3**, E28-E34.
16. Reider C, Salmon ED, (1998). The vertebrate cell kinetochore and its roles during mitosis. *Trends Cell Biol.*, **8**, 310-318.

17. Field D, Li R, Oegema K, (1999). Cytokinesis in eukaryotes: A mechanistic comparison. *Curr. Opin. Cell Biol.*, **11**, 68-80.
18. Cassimeris L, (1993). Regulation of microtubule dynamic instability. *Cell Motil. Cytoskelet.*, **26**, 275-281.
19. Hyam J, Lloyd CW, (1994). Microtubules. *Wiley-Liss*, New York.
20. Drechsel D, Hyman AA, Cobb MH, Kirschner MW, (1992). Modulation of the dynamic instability of tubulin assembly by the microtubule associated protein tau. *Mol. Biol. Cell,* **3**, 1141-1154.
21. Sze CI, Su M, Pugazhenthi S, Jambal P, Hsu LJ, Heath J, Schultz L, Chang NS, (2004). Down-regulation of WW domain-containing oxireductase induces tau phosphorylation *in vitro*. *J. Biol. Chem.*, **279**, 30498-30506.
22. Amos LA, Schlieper D, (2005). Microtubules and MAPs. *Adv. Protein Chem.*, **71**, 257-298.
23. Cassimeris L, Spittle C, (2001). Regulation of microtubule-associated proteins. *Int. Rev. Cytol.,* **210**, 163-226.
24. Manna T, Thrower D, Miller HP, Curmi P, Wilson L, (2006). Stathmin strongly increases the minus end catastrophe frequency and induces rapid treadmilling of bovine brain microtubules at steady state *in vitro*. *J. Biol. Chem.*, **281**, 2071-2078.
25. Walczak C, Mitchison TJ, Desai A, (1996). XKCM1: A *Xenopus* kinesin-related protein that regulates microtubules dynamics during mitotic spindle assembly. *Cell*, **84**, 37-47.
26. Charbaut E, Curmi PA, Ozon S, Lachkar S, Redeker V, Sobel A, (2001). Stathmin family proteins display specific molecular and tubulin binding properties. *J. Biol. Chem.*, **276**, 16146-16154.
27. Ravelli RBG, Gigant B, Curmi PA, Jourdain I, Lachkar S, Sobel A, Knossow M, (2004). Insight into tubulin regulation from a complex with colchicine and a stathmin-like domain. *Nature*, **428**, 198-202.
28. Sharma N, Bryant J, Wloga D, Donaldson R, Davis RC, Jerka-Dziadosz M, Gaertig J, (2007). Katanin regulates dynamics of microtubules and biogenesis of motile cilia. *J. Cell Biol.*, **178**, 1065-1079.
29. Jordan MA, Wilson, L, (2004). Microtubules as a target for anticancer drugs. *Nature Rev.*, **4**, 253-265.
30. Schiff PB, Fant J, Auste LA, Horwitz SB, (1978). Effects of taxol on cell growth and *in vitro* microtubule assembly. *J. Supramol. Struct.,* **8**, 328.
31. Schiff PB, Fant J, Horwitz SB, (1979). Promotion of microtubule assembly *in vitro* by taxol. *Nature*, **277**, 665-667.
32. Buey RM, Calvo E, Barasoain I, Pineda O, Edler MC, Matesanz R, Cerezo G, Vanderwal CD, Day BW, Sorensen EJ, Lopez JA, Andreu JM, Hamel E, Diaz JF, (2007). Cyclostreptin binds covalently to microtubule pores and lumenal taxoid binding sites. *Nature Chem. Biol.*, **3**, 117-125.
33. Bollag DM, McQueney PA, Zhu J, Hensens O, Koupal L, Liesch J, Goetz M, Lazarides E, Woods CM, (1995). Epothilones, a new class of microtubule-stabilizing agents with a taxol-like mechanism of action. *Cancer Res.*, **55**, 2325-2333.
34. Hamel E, Sackett DL, Vourloumis D, Nicolaou K, (1999). The coral-derived natural products eleutherobin and sarcodictyins A and B: Effects on the assembly of purified tubulin with and without microtubule-associated proteins and binding at the polymer taxoid site. *Biochemistry*, **38**, 5490-5498.

35. Hood KA, West LM, Rouwe B, Northcote PT, Berridge MV, Wakefield SJ, Miller JH, (2002). Peloruside A, a novel antimitotic agent with paclitaxel-like microtubule- stabilizing activity. *Cancer Res.*, **62**, 3356-3360.
36. Kowalski RJ, Giannakakou P, Gunasekera SP, Longley RE, Day BW, Hamel E, (1997). The microtubule-stabilizing agent discodermolide competitively inhibits the binding of paclitaxel (taxol) to tubulin polymers, enhances tubulin nucleation reactions more potently then paclitaxel, and inhibits the growth of paclitaxel-resistant cells. *Mol. Pharmacol.*, **52**, 613-622.
37. West LM, Northcote PT, Battershill CN, (2000). Peloruside A: A potent cytotoxic macrolide isolated from the New Zealand marine sponge Mycale sp. *J. Org. Chem.*, **65**, 445-449.
38. Pryor DE, O'Brate A, Bilcer G, Diaz JF, Wang Y, Wang Y, Kabaki M, Jung MK, Andreu JM, Ghosh AK, Giannakakou P, Hamel E, (2002). The microtubule stabilizing agent laulimalide does not bind in the taxoid site, kills cells resistant to paclitaxel and epothilones, and may not require its epoxide moiety for activity. *Biochemistry*, **41**, 9109-9115.
39. Zhou J, Giannakakou, P, (2005). Targeting microtubules for cancer chemotherapy. *Curr. Med. Chem. Anticancer Agents*, **5**, 65-71.
40. Verdier-Pinard P, Lai JY, Yoo HD, Yu J, Marquez B, Nagle DG, Nambu M, White JD, Falck JR, Gerwick WH, Day BW, Hamel E, (1998). Structure-activity analysis of the interaction of curacin A, the potent colchicine site antimitotic agent, with tubulin and effects of analogs on the growth of MCF-7 breast cancer cells. *Mol. Pharmacol.*, **53**, 62-76.
41. Jordan MA, Thrower D, Wilson L, (1992). Effects of vinblastine, podophyllotoxin and nocodazole on mitotic spindles – implications for the role of microtubule dynamics in mitosis. *J. Cell Sci.*, **102**, 401-416.
42. Lobert S, Ingram JW, Correia JJ, (2007). The thermodynamics of vinca alkaloid-induced tubulin spirals formation. *Biophys. Chem.*, **126**, 50-58.
43. Lobert S, Vulevic B, Correia JJ, (1996). Interaction of vinca alkaloids with tubulin: A comparison of vinblastine, vincristine, and vinorelbine. *Biochemistry*, **35**, 6806-6814.
44. Gupta S, Bhattacharyya B, (2003). Antimicrotubular drugs binding to vinca domain of tubulin. *Mol. Cell. Biochem.*, **253**, 41-47.
45. Hamel E, (1992). Natural-products which interact with tubulin in the vinca domain - maytansine, rhizoxin, phomopsin-A, dolastatin-10 and dolastatin-15 and halichondrin-B. *Pharmacol. Ther.*, **55**, 31-51.
46. Hamel E, Covell DG, (2002). Antimitotic peptides and depsipeptides. *Curr. Med. Chem. Anticancer Agents*, **2**,
47. Lin JH, Yamazaki M, (2003). Clinical relevance of P-glycoprotein in drug therapy. *Drug Metab. Rev.*, **35**, 417-454.
48. Ambudkar S, Kimchi-Sarfaty C, Sauna ZE, Gottesman MM, (2003). P-glycoprotein: From genomics to mechanism. *Oncogene*, **22**, 7468-7485.
49. Baguley BC, Marshall ES, Whittaker JR, Dotchin MC, Nixon J, McCrystal MR, Finlay GJ, Matthews JH, Holdaway KM, van Zijl P, (1995). Resistance mechanisms determining the *in vitro* sensitivity to paclitaxel of tumour cells cultured from patients with ovarian cancer. *Eur. J. Cancer*, **31A**, 230-237.
50. Nooter K, Stoter G, (1996). Molecular mechanisms of multidrug resistance in cancer chemotherapy. *Pathol. Res. Pract.*, **192**, 768-780.
51. Tang S, (2008). Predictive markers of tubulin-targeting agents in breast cancer. *Clin. Breast Cancer*, **8**, S79-S84.

52. Hasegawa S, Miyoshi Y, Egawa C, Ishitobi M, Taguchi T, Tamaki Y, Monden M, Noguchi S, (2003). Prediction of response to docetaxel by quantitative analysis of class I and III beta-tubulin isotype mRNA expression in human breast cancers. *Clin. Cancer Res.*, **9**, 2992-2997.
53. Giannakakou P, Sackett DL, Kang YK, Zhan Z, Buters JT, Fojo T, Poruchynsky MS, (1997). Paclitaxel-resistant human ovarian cancer cells have mutant beta-tubulins that exhibit impaired paclitaxel-driven polymerization. *J. Biol. Chem.*, **272**, 17118-17125.
54. Giannakakou P, Gussio R, Nogales E, Downing KH, Zaharevitz D, Bollbuck B, Poy G, Sackett D, Nicolaou KC, Fojo T, (2000). A common pharmacophore for epothilone and taxanes: Molecular basis for drug resistance conferred by tubulin mutations in human cancer cells. *Proc. Natl. Acad. Sci. USA*, **97**, 2904-2909.
55. Kosynkin DV, Tour, J.M, (2001). Benzyltriethylammonium dichloroiodate/sodium bicarbonate combination as inexpensive, environmentally friendly, and mild iodinating reagent for anilines. *Org Lett*, **3**, 991-992.
56. Hasegawa S, Miyoshi Y, Egawa C, Ishitobi M, Tamaki Y, Monden M, Noguchi S, (2002). Mutational analysis of the class I beta-tubulin gene in human breast cancer. *Int. J. Cancer*, **101**, 46-51.
57. Knox J, Tola RF, Casida JE, (1992). Insectidal thioureas: Preparation of [phenoxy-4-3H]diafenthiuron, the corresponding carbodiimide, and related compounds. *J. Agric. Food Chem.*, **40**, 909-913.
58. Faucher N, Ambroise Y, Cintrat JC, Doris E, Pillon F, Rousseau B, (2002). Highly chemoselective hydrogenolysis of iodoarenes. *J. Org. Chem.*, **67**, 932-934.
59. Shin Y, Fournier JH, Fukui Y, Bruckner AM, Curran DP, (2004). Total synthesis of (–)-dictyostatin: Confirmation of relative and absolute configurations. *Angew. Chem. Int. Ed. Engl.*, **43**, 4634-4637.
60. Fukui Y, Bruckner AM, Shin Y, Balachandran R, Day BW, Curran DP, (2006). Fluorous mixture synthesis of (-)-dictyostatin and three stereoisomers. *Org. Lett.*, **8**, 301-304.
61. Jung WH, Harrison C, Shin Y, Fournier JH, Balachandran R, Raccor BS, Sikorski RP, Vogt A, Curran DP, Day BW, (2007). Total synthesis and biological evaluation of C16 analogs of (–)-dictyostatin. *J. Med. Chem.*, **50**, 2951-2966.
62. Shin Y, Choy N, Turner TR, Balachandran R, Madiraju C, Day BW, Curran DP, (2002). Discodermolide/dictyostatin hybrids: Synthesis and biological evaluation. *Org. Lett.*, **4**, 4443-4446.
63. Shin Y, Fournier JH, Bruckner A, Madiraju C, Balachandran R, Raccor BS, Edler MC, Hamel E, Sikorski RP, Vogt A, Day BW, Curran DP, (2007). Synthesis and biological evaluation of (-)-dictyostatin and stereoisomers. *Tetrahedron*, **63**, 8537-8562.
64. Madiraju C, Edler MC, Hamel E, Raccor BS, Balachandran R, Zhu G, Giuliano KA, Vogt A, Shin Y, Fournier JH, Fukui Y, Bruckner AM, Curran DP, Day BW, (2005). Tubulin assembly, taxoid site binding, and cellular effects of the microtubule-stablilizing agent dictyostatin. *Biochemistry*, **44**, 15053-15063.
65. Skehan P, Storeng R, Scudiero D, Monks A, McMahon J, Vistica D, Warren JT, Bokesch H, Kenney S, Boyd MR, (1990). New colorimetric cytotoxicity assay for anticancer-drug screening. *J. Natl. Cancer Inst.*, **82**, 1107-1112.
66. Li PK, Pandit B, Sackett DL, Hu Z, Zink J, Zhi J, Freeman D, Robey RW, Werbovetz K, Lewis A, Li C, (2006). A thalidomide analogue with *in vitro* antiproliferative, antimitotic, and microtubule-stabilizing activities. *Mol. Cancer Ther.*, **5**, 450-456.

67. Hamel E, Lin CM, (1984). Separation of active tubulin and microtubule-associated proteins by ultracentrifugation and isolation of a component causing the formation of microtubule bundles. *Biochemistry*, **23**, 4173-4184.
68. Bradford MM, (1976). A rapid and sensitive method for the quantitation of microgram quantities of protein utilizing the principle of protein-dye binding. *Anal. Biochem.*, **72**, 248-254.
69. Lowry OH, Rosebrough NJ, Farr AL, Randall RJ, (1951). Protein measurement with the folin phenol reagent. *J. Biol. Chem*, **193**, 265-275.
70. Minguez JM, Kim SY, Guillano KA, Balachandran R, Madiraju C, Day BW, Curran DP, (2003). Synthesis and biological assessment of simplified analogues of the potent microtubule stabilizer (+)-discodermolide. *Bioorg. Med. Chem.* **11**, 3335-3357.
71. Wipf P, Reeves JT, Balachandran R, Day BW, (2002). Synthesis and biological evaluation of structurally highly modified analogues of the antimitotic natural product curacin a. *J. Med. Chem.*, **45**, 1901-1917.
72. Raccor BS, Vogt A, Sikorski RP, Madiraju C, Balachandran R, Montgomery K, Shin Y, Fukui Y, Jung WH, Curran DP, Day BW, (2008). Cell-based and biochemical structure-activity analyses of analogs of the microtubule stabilizer dictyostatin. *Mol. Pharmacol.*, **73**, 718-726.
73. Motulsky H, Christopoulos A, (2003). Fitting models to biological data using linear and nonlinear regression. A practical guide to curve fitting. *GraphPad Software Inc.*, San Diego, CA.
74. Swillens S, (1995). Interpretation of binding curves obtained with high receptor concentrations: Practical aid for computer analysis. *Mol. Pharmacol.*, **47**, 1197-1203.
75. Edler MC, Buey RM, Gussio R, Marcus AI, Vanderwal CD, Sorensen EJ, Diaz JF, Giannakakou P, Hamel E, (2005). Cyclostreptin (FR182877), an antitumor tubulin-polymerizing agent deficient in enhancing tubulin assembly despite its high affinity for the taxoid site. *Biochemistry*, **44**, 11525-11538.
76. Jordan MA, Walker D, de Arruda M, Barlozzari T, Panda D, (1998). Suppression of microtubule dynamics by binding of cemadotin to tubulin: Possible mechanism for its antitumor action. *Biochemistry*, **37**, 17571-17578.
77. ter Haar E, Kowalski RJ, Hamel E, Lin CM, Longley RE, Gunasekera SP, Rosenkranz HS, Day BW, (1996). Discodermolide, a cytotoxic marine agent that stabilizes microtubules more potently than taxol. *Biochemistry*, **35**, 243-250.
78. Bai R, Pettit GR, Hamel E, (1990). Binding of dolastatin 10 to tubulin at a distinct site for peptide antimitotic agents near the exchangeable nucleotide and vinca alkaloid sites. *J. Biol. Chem.*, **265**, 17141-17149.
79. Pettit GR, Cichacz ZA, Gao F, Boyd MR, Schmidt JM, (1994). Isolation and structure of the cancer cell-growth inhibitor dictyostatin-1. *J. Chem. Soc.,Chem. Commun.*, 1111-1112.
80. Buey RM, Diaz F, Andreu JM, O'Brate A, Giannakakou P, Nicolaou KC, Samai PK, Ritzen A, Namato K, (2004). Interaction of epothilone analogs with the paclitaxel binding site: Relationship between binding affinity, microtubule stabilization, and cytotoxicity. *Chem. Biol.*, **11**, 225-236.
81. Paterson I, Gardner NM, (2007). Design, synthesis and biological evaluation of a macrocyclic discodermolide/dictyostatin hybrid. *Chem. Commun. (Camb)*, 49-51.
82. Paterson I, Britton R, Delgado O, Meyer A, Poullennec KG, (2004). Total synthesis and configurational assignment of (–)-dictyostatin, a microtubule-stabilizing macrolide of marine sponge origin. *Angew. Chem. Int. Ed. Eng.l*, **43**, 4629-4633.

83. Shin Y, Fournier JH, Balachandran R, Madiraju C, Raccor BS, Zhu G, Edler MC, Hamel E, Day BW, Curran DP, (2005). Synthesis and biological evaluation of (–)-16-normethyldictyostatin: A potent analogue of (–)-dictyostatin. *Org. Lett.*, **7**, 2873-2876.
84. Paterson I, Gardner NM, Poullennec KG, Wright AE, (2008). Synthesis and biological evaluation of 10,11-dihydrodictyostatin, a potent analogue of the marine anticancer agent dictyostatin. *J. Nat. Prod.*, **71**, 364-369.
85. Hung DT, Nerenberg JB, Schreiber SL, (1996). Syntheses of discodermolides useful for investigating microtubule binding and stabilization. *J. Am. Chem. Soc.*, **118**, 11054-11080.
86. Paterson I, Florence GJ, Gerlach K, Scott JP, Sereinig N, (2001). A practical synthesis of (+)-discodermolide and analogues: Fragment union by complex aldol reactions. *J. Am. Chem Soc.*, **123**, 9535-9544.
87. Paterson I, Gardner NM, Poullennec KG, Wright AE, (2007). Synthesis and biological evaluation of novel analogues of dictyostatin. *Bioorg. Med. Chem. Lett.*, **17**, 2443-2447.
88. Gunasekera SP, Longley RE, Isbrucker RA, (2002). Semisynthetic analogues of the microtubule-stabilizing agent discodermolide: Preparation and biological activity. *J. Nat. Prod.*, **65**, 1830-1837.
89. Smith AB, Freeze BS, LaMarche MJ, Hirose T, Brouard I, Xian M, Sundermann KF, Shaw SJ, Burlingame MA, Horwitz SB, Myles DC, (2005). Design, synthesis, and evaluation of analogues of (+)-14-normethyldiscodermolide. *Org. Lett.*, **7**, 315-318.
90. Sasse F, Steinmetz H, Heil J, Hofle G, Reichenbach H, (2000). Tubulysins, new cytostatic peptides from myxobacteria acting on microtubuli. Production, isolation, physico-chemical and biological properties. *J. Antibiot. (Tokyo)*, **53**, 879-885.
91. Kowalski RJ, Giannakakou P, Hamel E, (1997). Activities of the microtubule-stabilizing agents epothilones A and B with purified tubulin and in cells resistant to paclitaxel (Taxol®). *J. Biol. Chem.*, **272**, 2534-2541.
92. Xia S, Kenesky CS, Rucker PV, Smith AB, Orr GA, Horwitz Su, (2006). A photoaffinity analogue of discodermolide specifically labels a peptide in beta-tubulin. *Biochemistry*, **45**, 11762-11775.
93. Hung DT, Chen J, Schreiber SL, (1996). (+)-Discodermolide binds to microtubules in stoichiometric ratio to tubulin dimers, blocks taxol binding and results in mitotic arrest. *Chem. Biol.*, **3**, 287-293.
94. Smith AB, 3rd, LaMarche MJ, Falcone-Hindley M, (2001). Solution structure of (+)-discodermolide. *Org. Lett.*, **3**, 695-698.
95. Reese M, Sanchez-Pedregal VM, Kubicek K, Meiler J, Blommers MJJ, Griesinger C, Carlomagno T, (2007). Structural basis of the activity of the microtubule-stabilizing agent epothilone A studied by NMR spectroscopy in solution. *Angew. Chem. Int. Ed. Engl.*, **46**, 1864-1868.
96. Padron JA, Carrasco R, Pellon RF, (2002). Molecular descriptor based on a molar refractivity partition using randic-type graph-theoretical invariant. *J. Pharm. Pharmaceut. Sci.*, **5**, 258-265.
97. Canales A, Matesanz R, Gardner NM, Andreu JM, Paterson I, Diaz JF, Jimenez-Barbero J, (2008). The bound conformation of microtubule-stabilizing agents: NMR insights into the bioactive 3D structure of discodermolide and dictyostatin. *Chemistry*, [PMID: 18449868, Epub ahead of print].
98. Hamel E, Vaughns J, Getahun Z, Johnson R, Lin CM, (1995). Interactions of tubulin with guanine nucleotides that have paclitaxel-like effects on tubulin assembly:

2',3'-Dideoxyguanosine 5'-[alpha,beta-methylene]triphoshate, guanosine 5'-[alpha,beta-methylene]triphosphate, and 2'3'-dideoxyguanosine 5'-triphosphate. *Arch. Biochem. Biophys.*, **322**, 486-499.
99. Jimenez-Barbero J, Amat-Guerri F, Snyder JP, (2002). The solid state, solution and tubulin-bound conformations of agents that promote microtubule stabilization. *Curr. Med. Chem. Anticancer Agents*, **2**, 91-122.
100. Sanchez-Pedregal VM, Kubicek K, Meiler J, Lyothier I, Paterson I, Carlomagno T, (2006). The tubulin-bound conformation of discodermolide derived by NMR studies in solution supports a common pharmacophore model for epothilone and discodermolide. *Angew. Chem. Int. Ed. Engl.*, **45**, 7388-7394.
101. Sleijer S, Wim HJ, Stotet G, (2004). Thalidomide in solid tumours: The resurrection of an old drug. *Eur. J. Cancer*, **40**, 2377-2382.
102. Teo SK, Stirling DI, Zeldis JB, (2005). Thalidomide as a novel therapeutic agent: New uses for an old product. *Drug Discov. Today*, **10**, 107-114.
103. Teo SK, Resztak KE, Scheffler MA, Kook KA, Zeldis JB, Stirling DI, Thomas SD, (2002). Thalidomide in the treatment of leprosy. *Microbes Infect.*, **4**, 1193-1202.
104. Folkman J, Rogers MS, (2006). Thalidomide for multiple myeloma. *N. Engl. J. Med.*, **354**, 2389-2390.
105. D'Amato RJ, Loughnan MS, Flynn E, Folkman J, (1994). Thalidomide is an inhibitor of angiogenesis. *Proc. Natl. Acad. Sci. U S A*, **91**, 4082-4085.
106. Shimazawa R, Miyachi H, Takayama H, Kuroda K, Kato F, Kato M, Hashimoto Y, (1999). Antiangiogenic activity of tumor necrosis factor-alpha production regulators derived from thalidomide. *Biol. Pharm. Bull.*, **22**, 224-226.
107. McHugh SM, Rifkin IR, Deighton J, Wilson AB, Lachmann PJ, Lockwood CM, Ewan PW, (1995). The immunosuppressive drug thalidomide induces T helper cell type 2 (Th2) and concomitantly inhibits Th1 cytokine production in mitogen- and antigen-stimulated human peripheral blood mononuclear cell cultures. *Clin. Exp. Immunol.*, **99**, 160-167.
108. Li X, Liu X, Wang J, Wang Z, Jiang W, Reed E, Zhang Y, Liu Y, Li QQ, (2003). Thalidomide down-regulates the expression of VEGF and BFGF in cisplatin-resistant human lung carcinoma cells. *Anticancer Res.*, **23**, 2481-2487.
109. Marriott JB, Dredge K, Dalgleish AG, (2003). Thalidomide derived immunomodulatory drugs (IMiDs) as potential therapeutic agents. *Curr. Drug Targets*, **3**, 181-186.
110. Richardson P, Anderson K, (2004). Immunomodulatory analogs of thalidomide: An emerging new therapy in myeloma. *J. Clin. Oncol.*, **22**, 3212-3214.
111. Hashimoto Y, (1998). Novel biological response modifiers derived from thalidomide. *Curr. Med. Chem.*, **5**, 163-178.
112. Miyachi H, Azuma A, Ogasawara A, Uchimura E, Watanabe N, Kobayashi Y, Kato F, Kato M, Hahimoto H, (1997). Novel biological response modifiers: Phthalimides with tumor necrosis factor-alpha production regulating activity. *J. Med. Chem.*, **40**, 2858-2865.
113. Miyachi H, Ogasawara A, Azuma A, Hashimoto Y, (1997). Tumor necrosis factor-alpha production-inhibiting activity of phthalimide analogues on human leukemia THP-1 cells and a structure-activity relationship study. *Bioorg. Med. Chem.* **5**, 2095-2102.
114. Inatsuki S, Noguchi T, Miyachi H, Oda S, Iguchi T, Kizaki M, Hashimoto Y, Kobayashi H, (2005). Tubulin-polymerization inhibitors derived from thalidomide. *Bioorg. Med. Chem. Lett.*, **15**, 321-325.

115. Ueda K, Cardarelli C, Gottesman MM, Pastan I, (1987). Expression of a full-length cDNA for the human "MDR1" gene confers resistance to colchicine, doxorubicin, and vinblastine. *Proc. Natl. Acad. Sci. U S A*, **84**, 3004-3008.
116. Casazza AM, Fairchild CR, (1996). Paclitaxel (taxol): Mechanisms of resistance. *Cancer Treat. Res.*, **87**, 149-171.
117. Evenson DP, Janca FC, Jost LK, (1987). Effects of the fungicide methyl-benzimidazol-2-yl carbamate (MBC) on mouse germ cells as determined by flow cytometry. *J. Toxicol. Environ. Health*, **20**, 387-399.
118. Juan G, Traganos F, Darzynkiewicz Z, (2001). Methods to identify mitotic cells by flow cytometry. *Methods Cell Biol.*, **63**, 343-354.
119. Gapud EJ, Bai R, Ghosh AK, Hamel E, (2004). Laulimalide and paclitaxel: A comparison of their effects on tubulin assembly and their synergistic action when present simultaneously. *Mol. Pharmacol.*, **66**, 113-121.
120. Hamel E, del Campo AA, Lowe MC, Lin CM, (1981). Interactions of taxol, microtubule-associated proteins, and guanine nucleotides in tubulin polymerization. *J. Biol. Chem.*, **256**, 11887-11894.
121. Grover S, Hamel E, (1994). The magnesium-GTP interaction in microtubule assembly. *Eur. J. Biochem./ FEBS*, **222**, 163-172.
122. Hamel E, del Campo AA, Lowe MC, Waxman PG, Lin CM, (1982). Effects of organic acids on tubulin polymerization and associated guanosine 5'-triphosphate hydrolysis. *Biochemistry*, **21**, 503-509.
123. Bai R, Schwartz RE, Kepler JA, Pettit GR, Hamel E, (1996). Characterization of the interaction of cryptophycin 1 with tubulin: Binding in the vinca domain, competitive inhibition of dolastatin 10 binding, and an unusual aggregation reaction. *Cancer Res.*, **56**, 4398-4406.
124. Watt I, (1997). The principles and practice of electron microscopy. *Cambridge University Press*, Cambridge.
125. Bai R, Pettit GR, Hamel E, (1990). Dolastatin 10, a powerful cytostatic peptide derived from a marine animal. Inhibition of tubulin polymerization mediated through the vinca alkaloid binding domain. *Biochem. Pharmacol.*, **39**, 1941-1949.
126. Jennett RB, Tuma DJ, Sorrell WT, Sorrell MF, (1985). Stabilization of hepatic colchicine-binding activity by organic acids. *Arch. Biochem. Biophys.*, **236**, 304-310.
127. Banerjee AC, Bhattacharyya B, (1979). Colcemid and colchicine binding to tubulin. Similarity and dissimilarity. *FEBS letters*, **99**, 333-336.
128. Tracy TS, (2003). Atypical enzyme kinetics: Their effect on *in vitro-in vivo* pharmacokinetic predictions and drug interactions. *Curr. Drug Metab.*, **4**, 341-346.
129. Na GC, Timasheff SN, (1986). Interaction of vinblastine with calf brain tubulin: Effects of magnesium ions. *Biochemistry*, **25**, 6222-6228.
130. Na GC, Timasheff SN, (1986). Interaction of vinblastine with calf brain tubulin: Multiple equilibria. *Biochemistry*, **25**, 6214-6222.
131. Dahllof B, Billstrom A, Cabral F, Hartley-Asp B, (1993). Estramustine depolymerizes microtubules by binding to tubulin. *Cancer Res.*, **53**, 4573-4581.
132. Burns RG, (1990). Stoichiometry of estramustine phosphate binding to MAP2 measured by the disassembly of chick brain MAP2: Tubulin microtubules. *Cell Motil. Cytoskeleton*, **17**, 167-173.

133. Friden B, Wallin M, (1991). Dependency of microtubule-associated proteins (MAPs) for tubulin stability and assembly; use of estramustine phosphate in the study of microtubules. *Mol. Cell Biochem.*, **105**, 149-158.
134. Kobayashi S, Tsuchiya K, Nishide M, Nishikiori T, Nakagawa T, Shimada N, (1995). Pironetin, a novel plant growth regulator produced by Streptomyces sp. NK10958. III. Biosynthesis. *J. Antibiot. (Tokyo)*, **48**, 893-895.
135. Usui T, Watanabe H, Nakayama H, Tada Y, Kanoh N, Kondoh M, Asao T, Takio K, Watanabe H, Nishikawa K, Kitahara T, Osada H, (2004). The anticancer natural product pironetin selectively targets Lys352 of alpha-tubulin. *Chem. Biol.*, **11**, 799-806.
136. Shen X, Wasmuth AS, Zhao J, Zhu C, Nelson SG, (2006). Catalytic asymmetric assembly of stereodefined propionate units: An enantioselective total synthesis of (-)-pironetin. *J. Am. Chem. Soc.*, **128**, 7438-7439.
137. Kaur G, Hollingshead M, Holbeck S, Schauer-Vukasinovic V, Camalier RF, Domling A, Agarwal S, (2006). Biological evaluation of tubulysin A: A potential anticancer and antiangiogenic natural product. *Biochem. J.*, **396**, 235-242.
138. Khalil MW, Sasse F, Lunsdorf H, Elnakady YA, Reichenbach H, (2006). Mechanism of action of tubulysin, an antimitotic peptide from myxobacteria. *Chembiochem.*, **7**, 678-683.
139. Loffet A, (2002). Peptides as drugs: Is there a market? *J. Pept. Sci.*, **8**, 1-7.
140. Wipf P, Wang Z, (2007). Total synthesis of N14-desacetoxytubulysin H. *Org. Lett.*, **9**, 1605-1607.
141. Asari S, Makabe T, Katayama S, Itoh T, Tsuchida S, Kunishio K, Ohmoto T, (1993). Evaluation of MRI score in the differentiation between glioblastoma multiform and metastatic adenocarcinoma of the brain. *Acta Neurochir. (Wien)*, **122**, 54-59.
142. Kondoh M, Usui, T., Nishikiori, T., Mayumi, T., Osada, H., (1999). Apoptosis induction via microtubule disassembly by an antitumour compound, pironetin. *Biochem. J.*, **340**, 411-416.
143. Brabec V, Kasparkova J, (2005). Modifications of DNA by platinum complexes. Relation to resistance of tumors to platinum antitumor drugs. *Drug Resist. Updat.*, **8**, 131-146.
144. Henness S, Perry CM, (2006). Orlistat: A review of its use in the management of obesity. *Drugs*, **66**, 1625-1656.
145. Peltier HM, McMahon JP, Patterson AW, Ellman JA, (2006). The total synthesis of tubulysin D. *J. Am. Chem. Soc.*, **128**, 16018-16019.
146. Domling A, Beck B, Eichelberger U, Sakamuri S, Menon S, Chen QZ, Lu Y, Wessjohann LA, (2006). Total synthesis of tubulysin U and V. *Angew. Chem. Int. Ed. Engl.*, **45**, 7235-7239.
147. Wipf P, Takada T, Rishel MJ, (2004). Synthesis of the tubuvaline-tubuphenylalanine (Tuv-Tup) fragment of tubulysin. *Org. Lett.*, **6**, 4057-4060.
148. Wang Z, McPherson PA, Raccor BS, Balachandran R, Zhu G, Day BW, Vogt A, Wipf P, (2007). Structure-activity and high-content imaging analyses of novel tubulysins. *Chem. Biol. Drug Des.*, **70**, 75-86.
149. Huang GS, Lopez-Barcons, L, Freeze BS, Smith AB, Goldberg GL, Horwitz SB, McDaid HM, (2006). Potentiation of taxol efficacy by discodermolide in ovarian carcinoma xenograft-bearing mice. *Clin. Cancer Res.*, **12**, 298-304.
150. Hamel E, Day BW, Miller JH, Jung MK, Northcote PT, Ghosh AK, Curran DP, Cushman M, Nicolaou KC, Paterson I, Sorensen EJ, (2006). Synergistic effects of peloruside A and laulimalide with taxoid site drugs, but not with each other, on tubulin assembly. *Mol. Pharmacol.*, **70**, 1555-1564.

151. Chou TC, Talalay P, (1984). Quantitative analysis of dose-effect relationships: The combined effects of multiple drugs or enzyme inhibitors. *Adv. Enzyme Regul.*, **22**, 27-55.